ISSN Print: 2518-4261
ISSN Online: 2518-427X
Vol. 62(4), December 2025

PROCEEDINGS
OF THE PAKISTAN ACADEMY OF SCIENCES:
B. Life and Environmental Sciences

PAKISTAN ACADEMY OF SCIENCES
ISLAMABAD, PAKISTAN

Proceedings of the Pakistan Academy of Sciences: Part B Life and Environmental Sciences

Proceedings of the Pakistan Academy of Sciences: Part B (Life and Environmental Sciences) is the official flagship, the peer-reviewed quarterly journal of the Pakistan Academy of Sciences. This open-access journal publishes original research articles and reviews in the field of Agricultural and Biological Sciences (all), Biochemistry, Genetics and Molecular Biology (all), Environmental Science (all), Health Sciences (all). Authors are not required to be Fellows or Members of the Pakistan Academy of Sciences or citizens of Pakistan. The journal is covered by Print and Online ISSN, indexed in Scopus, and distributed to scientific organizations, institutes and universities throughout the country, by subscription and on an exchange basis.

Annual Subscription: **Pakistan:** Institutions, Rupees 8000/- ; Individuals, Rupees 4000/- (Delivery Charges: Rupees 300/-)
Other Countries: US$ 200.00 (includes air-lifted overseas delivery)

HEC Recognized; Scopus Indexed

Published by **Pakistan Academy of Sciences**, 3 Constitution Avenue, G-5/2, Islamabad, Pakistan
Email: editor@paspk.org; **Tel:** 92-51-9207140; 92-51-920 6770; **Websites:** www.paspk.org/proceedings/; www.ppaspk.org

Printed at **Graphics Point.,** Office 3-A, Wasal Plaza, Fazal-e-Haq Road, Blue Area, Islamabad
Ph: 051-2806257; E-mail: graphicspoint16@gmail.com

PROCEEDINGS OF THE
PAKISTAN ACADEMY OF SCIENCES: PART B
Life and Environmental Sciences

CONTENTS

Volume 62, No. 4, December 2025 **Page**

Submission of Manuscripts: Manuscripts may be submitted as an e-mail attachment at editor@paspk.org or submit online at http://ppaspk.org/index.php/PPASB/about/submissions. Authors must consult the ***Instructions for Authors*** at the end of this issue or at the Website: www.paspk.org/proceedings/ or www.ppaspk.org.

Proceedings of the Pakistan Academy of Sciences: B
Life and Environmental Sciences 62(4): 259-268 (2025)

ISSN (Print): 2518-4261; ISSN (Online): 2518-427X
http://doi.org/10.53560/PPASB(62-4)1125

Pakistan Academy of Sciences

Review Article

X-ray Diffraction Analysis of the Membrane Protein styMdtM from *Salmonella* Typhi†

Aqsa Shaheen[1,2], Anam Tariq[1], Fouzia Ismat[1], Aamir Shehzad[1], and Moazur Rahman[1,3,4]*

[1]Drug Discovery and Structural Biology Group, Health Biotechnology Division, National Institute for Biotechnology and Genetic Engineering (NIBGE), Faisalabad, Pakistan
[2]Department of Biochemistry and Biotechnology, University of Gujrat, Hafiz Hayat Campus, Gujrat, Pakistan
[3]School of Biological Sciences, University of the Punjab, Lahore, Pakistan
[4]Centre of Excellence in Molecular Biology, University of the Punjab, Lahore, Pakistan

Abstract: Structural studies of proteins provide a comprehensive understanding of their functions, and form the basis for designing drugs that can modulate their activity. However, the structural characterization of membrane proteins is often challenging due to their hydrophobic nature. This article highlights key structural and functional aspects of a representative membrane protein, STY4874 – also known as styMdtM, which is an efflux transporter encoded by the genome of *Salmonella* Typhi, the causative agent of typhoid fever in humans. Our structural studies have, so far, been focused on obtaining diffraction-quality crystals of the protein. For this purpose, crystallization trials have been performed using both the wild-type and mutant forms of the protein, in the presence or absence of ligands (substrates or inhibitors). Crystals of the wild-type styMdtM and its thermally stable mutants diffracted anisotropically to resolutions between 4.5 and 8 Å, rendering the collected data not useful for structure solution. On the other hand, crystals of a 13-amino acid deletion mutant isotropically diffracted to 10 Å, fueling our interest in engineering truncated styMdtM mutants for obtaining crystals suitable for diffraction to high resolutions for structure determination. Here, we discuss preliminary findings and key lessons learned from our studies, spanning over a decade.

Keywords: Major Facilitator, Efflux Transporter, styMdtM, STY4874, Membrane Protein, *Salmonella* Typhi.

1. INTRODUCTION

Knowing the three-dimensional (3D) structure of a protein is of paramount importance to understand its functions. Experimental techniques, such as X-ray crystallography, cryo-electron microscopy [1] and nuclear magnetic resonance (NMR) spectroscopy [2], can be used to determine the 3D structure of proteins. Each method has its own advantages and limitations. For example, X-ray crystallography requires the production of well-diffracting crystals, cryo-electron microscopy is most suitable for determining the structure of large proteins or protein complexes, and NMR spectroscopy is generally restricted to smaller proteins because larger proteins produce highly complex and difficult-to-interpret spectra. However, solid-state NMR is increasingly used to resolve membrane protein structures [3, 4]. Among these experimental techniques, X-ray crystallography is still considered the gold standard for solving protein structures. A survey of Protein Data Bank, a repository of experimentally determined macromolecular structures, reveals that it predominantly consists of structures of soluble proteins, whereas membrane proteins constitute less than 2% of all deposited structures. Although membrane proteins generally make up less than half of all proteins encoded by a genome, they are important drug targets because they serve as gateways to the cell. Repositories of membrane

Received: September 2025; Revised: November 2025; Accepted: December 2025
* Corresponding Author: Moazur Rahman <moazur.rahman@fulbrightmail.org>
† This paper was presented in "AASSA-PAS Symposium on Radiation Techniques in Health and Environment" from 18-20 August 2025, held at Islamabad, Pakistan.

proteins have been invaluable in elucidating key physiological aspects of their functions [5]. However, due to their intrinsic hydrophobicity, membrane proteins pose serious challenges for structure determination.

In this study, we highlight the challenges researchers often encounter when undertaking such studies. These challenges are discussed here in the light of key findings from our research work on structural and functional aspects of a representative membrane protein, STY4874 – also known as styMdtM. styMdtM is an efflux transporter encoded by the genome of *Salmonella* Typhi, the causative agent of typhoid fever in humans [6, 7]. styMdtM is an ortholog of the *Escherichia coli* transporters MdtM and MdfA [8]. MdfA serves as a prototype efflux transporter belonging to the major facilitator (MF) superfamily [9-12]. *E. coli* MdfA is the only MF superfamily transporter with a known structure [11, 13].

In our earlier study, the nucleotide sequence encoding styMdtM was cloned into an *Escherichia coli*-based expression vector, and the recombinant vector was transformed into a drug-susceptible strain of *E. coli*. The overexpression of this typhoidal membrane protein in *E. coli* was studied to assess substrate specificity, and it was found that styMdtM could expel structurally diverse substrates out of the cell [14]. Our next aim was to investigate the energy-driven mechanism of this efflux transporter. We found that the transporter used protons as its energy source, and that abolishing the proton gradient stopped its function [14].

Subsequently, we purified the membrane transporter and observed that the purified protein remained structurally stable in the sodium dodecyl maltopyranoside detergent. Further determination of binding constants revealed that the purified styMdtM transporter could bind different substrates with nanomolar affinity [15]. Next, we identified inhibitors of this transporter and found that reserpine could inhibit its function, possibly through competitive binding in the presence of ciprofloxacin [16]. We also identified Asp25 and Arg111 as key residues involved in the function of styMdtM [15]. Mutations involving these residues altered the activity of styMdtM, possibly by inducing structural perturbations in the protein [15]. Moreover, mutational analyses of residues at other positions (Tyr29, Tyr231, Cys185, and Gln294) provided valuable insights into the activity and structural stability of styMdtM [8].

The functionally stable, purified wild-type transporter was characterized using spectroscopic techniques (Fourier-transform infra-red (FTIR) spectroscopy and circular dichroism (CD) spectroscopy). Estimation of the secondary structure content of the purified wild-type styMdtM using the afore-mentioned techniques revealed that the α-helical content was approximately 55% (as estimated using FTIR spectroscopy) and 53% to 69% (as estimated using CD spectroscopy) [15]. The wild-type transporter, its mutant forms and a C-terminal truncated transporter were also subjected to crystallization studies. Preliminary results obtained from crystallization trials and X-ray diffraction studies have been discussed here in detail.

2. MATERIALS AND METHODS

2.1. Expression and Purification of Protein

Proteins (wild-type and mutants) were expressed and purified as described in our earlier reports [8, 15]. The detergent for the solubilization of the wild-type protein was chosen based upon initial detergent screening [8], and 1% (w/v) n-dodecyl-β-D-maltopyranoside (DDM) was used for purification and solubilization. The purified and detergent-solubilized protein was concentrated in the range of 8 to 20 mg/mL with the help of ultracentrifugal membrane filters.

2.2. FTIR and CD Spectroscopies of Protein

The FTIR and CD spectroscopies were performed as described earlier [8, 15]. Briefly, for FTIR, the protein was concentrated by lyophilization, and the spectrum was recorded for 2 to 3 mg/mL of the lyophilized protein sample on Bruker FTIR at wavenumber in the range of 4000 to 500 cm^{-1}. For CD spectroscopy, the detergent-solubilized protein solution at a concentration of 0.02 mg/mL, taken in a 10-mm quartz cell, was used to record the CD spectra in an AVIV Model 400 spectropolarimeter. The CD spectra were recorded in the wavelength ranging from 185 nm to 250 nm. Thermal unfolding was recorded at a wavelength of 222 nm with temperature increments of 1 °C.

2.3. Crystallization Trials

Hanging-drop and sitting-drop vapor-diffusion methods were used for setting up crystallization trials. Initially, a Mosquito Crystal® robot (TTP Labtech) was used to set up crystallization trials in 96-well crystallization plates. Each crystallization droplet consisted of 0.1 µL of the purified protein solution and an equal volume of the reservoir solution, whereas 100 µL of the reservoir buffer was taken in each well.

Later, crystallization trials were set up manually using 24-well crystallization plates, containing 500 µL of the reservoir buffer in each well. The crystallization drop comprised of 0.5 µL of the protein solution and an equal volume of the reservoir buffer. The plates were sealed properly to ensure that a gradual equilibrium could be established between the reservoir buffer and the crystallization drop.

Crystallization conditions were initially screened using commercially available crystallization screening kits from Molecular Dimensions, Hampton Research, and Qiagen [17-19]. In the second phase, buffers with pH values ranging from 4.0 to 8.0 were screened. In the third phase, commercially available detergent and additive screens were tested under conditions that had yielded crystals in initial trials. In the fourth phase, polyethylene glycol (PEG 400) and protein concentrations were systematically screened, with PEG 400 ranging from 27 to 48% (w/v) and protein concentrations ranging from 8 to 20 mg/mL [20]. The incubation temperature for crystallization plates was also changed in an attempt to get good-diffracting crystals (Table 1). For setting up co-crystallization trials, the *Kd* value of the substrate/inhibitor was taken into consideration [15] (Table 1). Substrates were mixed with the purified protein; each mixture was incubated on ice for ~10 min before setting up crystallization drops.

The growth of crystals was monitored after every 24 hrs. For X-ray data collection, crystals were harvested using appropriately sized nylon loops, flash frozen and sent to the Advanced Photon Source (APS) synchrotron at Argonne National Laboratory (Illinois, USA). Data were collected remotely using the 'ADSC software' either on a fixed-energy beamline (12.68 keV), '24-ID-E', or on a variable energy beamline, '21-ID-D'. The energy used in our study on the 21-ID-D beamline was 11.9 keV (https://necat.chem.cornell.edu/) [20]. A crystal-to-detector distance of 0.6 µm was used for data collection.

2.4. Retrieval of AlphaFold Model of the Protein and its Bioinformatics Analysis

The AlphaFold model of the protein was retrieved from the database [21] with the Uniprot ID: Q8XFG0. The structure was analyzed with the help of UCSF Chimera [22].

Table 1. Crystallization conditions employed for wild-type styMdtM in 24-well crystallization plates.

Composition of crystallization droplet	Incubation Temperature (°C)	Composition of reservoir buffer
Only protein (styMdtM; 12-15 mg/mL)	19	100 mM MES (pH 5.5-6.5), PEG 400 (27 - 30%, w/v), 100 mM NaCl, 100 mM Li_2SO_4
styMdtM (12-15 mg/mL) + 500 µM kanamycin/ ciprofloxacin/reserpine/ benzalkonium chloride/norfloxacin		
styMdtM (12-15 mg/mL) + 1 mM gentamycin		
Only protein (styMdtM; 12-15 mg/mL)	4	
Only protein (styMdtM; 8-10 mg/mL)		
styMdtM (12-15 mg/mL) + 500 µM reserpine/berberine		
styMdtM (12-15 mg/mL) + 500 µM reserpine/berberine	25	
styMdtM (12-15 mg/mL) + 500 µM reserpine/berberine	4	100 mM MES (pH 5.5-6.5), PEG 400 (31-34%, w/v), 100 mM NaCl, 100 mM Li_2SO_4

3. RESULTS AND DISCUSSION

3.1. Wild-type styMdtM

Spectroscopic analyses were followed by attempts to crystallize the purified styMdtM for structural studies. Results from crystallization trials revealed that crystals appeared under a variety of buffer conditions, namely MES (2-(N-morpholino) ethanesulfonic acid) at pH 5.5-6.7, Tris (2-Amino-2-hydroxymethyl-propane-1,3-diol) at pH 5.8-7.2, HEPES (2-[4-(2-hydroxyethyl)piperazin-1-yl] ethanesulfonic acid) at pH 6.8-8.2, and MOPS (3-morpholinopropane-1-sulfonic acid) at pH 6.5-7.9. Crystallization was also supported by a range of precipitants and salts, including NaCl, Li_2SO_4, $MgCl_2$, $CaCl_2$, and $(NH_4)_2SO_4$. All positive hits contained PEG 400 in the crystallization mixture. It was observed that protein crystallization was favoured at pH ranging from 5.5 to 6.5, PEG 400 ranging in concentrations from 15 to 30% (w/v), and protein concentrations ranging from 10 to 12 mg/mL [20].

Crystals of styMdtM appeared in different morphologies (Figure 1) but were often fragile due to their high solvent content [23]. Crystal sizes ranged from 10 µm to ~200 µm, with growth continuing over time, and reaching a maximum size after two weeks. Initial data collection from styMdtM crystals showed high mosaicity, which limited diffraction to low resolutions. Anisotropy was also observed in diffraction patterns, indicating non-uniform diffraction in different directions. From initial diffraction experiments, a dataset up to 4.5 Å resolution was obtained. Indexing of this dataset performed with the iMosflm software (7.1.1) allowed calculation of the unit cell parameters of one tetragonal styMdtM crystal: $a = b = 64.3$ Å, $c = 245.4$ Å, $\alpha = \beta = \gamma = 90°$, with space group P4 [8, 15]. However, diffraction was not isotropic, preventing the collection of a complete dataset at a sufficiently high resolution for structure determination. Most crystals diffracted to resolutions ranging from 7 to 9 Å.

For data collection, crystals were rotated by 1° per image, with a total of 180° collected. Due to high mosaicity, diffraction spots from the same lattice planes persisted for more than 1° under diffraction conditions, appearing in multiple consecutive patterns. In addition, styMdtM crystals were highly sensitive to radiation damage (Figure 1), with high-resolution diffraction fading during data collection [8, 20]. These conditions necessitate collection of diffraction data from multiple crystals to obtain a complete dataset. This study also provided preliminary insights into the relationship between crystallization conditions and the diffraction behavior of the wild-type styMdtM transporter.

3.2. Co-crystallization of Wild-type Transporter with Substrates and Inhibitors

Since low resolution and high mosaicity hindered the determination of the protein structure from diffraction data of the wild-type *apo* form of the

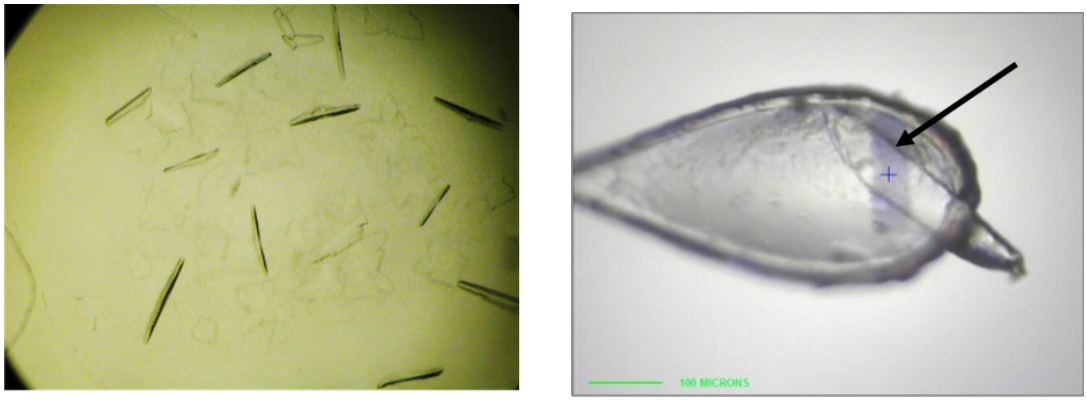

Fig. 1. Morphology of styMdtM crystals; triangular prisms, needlelike, and square plate crystal morphologies were observed for the *apo* and co-crystallized transporter [A]. The arrow points toward the radiation-induced damage in crystal during X-ray data collection [B]. The crystals appeared in the drop after 3 to 4 days of setting crystallization plates. For X-ray data collection, crystals were harvested with a nylon loop and flash frozen in liquid nitrogen.

transporter, co-crystallization of the wild-type styMdtM with substrates/inhibitors was attempted. Co-crystallization trials were carried out in the presence of different substrates (kanamycin, ciprofloxacin, levofloxacin, gentamycin and benzalkonium chloride) and inhibitors (reserpine and berberine), which were added during crystallization [20].

Based on the screening of the *apo* styMdtM protein, optimized crystallization conditions were selected for these co-crystallization trials. Co-crystallization with substrates and inhibitors produced crystals morphologically similar (Figure 1) to those obtained in the initial screenings. Data collection indicated that although the spot intensity had improved, diffraction remained anisotropic [20] (Figure 2(A, B)). Moreover, the resolution could not be improved beyond 7 Å [8, 20]. Therefore, attempts were made to generate structurally stable variants of styMdtM through site-directed mutagenesis.

3.3. Mutant styMdtM

Residues for mutagenesis were selected based on comparative sequence analysis of styMdtM and homologous protein sequences of well-characterized transporters. The sequence analysis revealed that the amino acid sequence of styMdtM shares 39% and 87% identity with *E. coli* MdfA and MdtM, respectively, both of which are well-characterized members of the major facilitator superfamily (MFS) transporters [24-30]. The charged residues, Glu26 and Arg112 in MdfA, as well as the analogous residues Asp22 and Arg108 in MdtM, have been shown to play important roles in recognizing neutral and cationic antimicrobials [24, 31, 32]. To generate a conformationally less-flexible mutant, the corresponding residues in styMdtM − Asp25 and Arg111 − were selected for mutagenesis.

In addition, the AlphaFold model of styMdtM (Figure 3(A)) was used for docking studies, and subsequent analysis identified Tyr29 and Tyr231 as residues of interest for further investigation [8]. Cys185 was also selected due to its location on the outer periphery of the transporter (Figure 3(A, B)), where it may participate in disulfide bridge formation and contribute to oligomerization. Finally, Gln294 was chosen based on its unique position within a shorter helix in the Alphafold model of the protein (Figure 3) [8].

It was hypothesized that mutations of Asp25, Tyr29, Arg111, and Tyr231 in styMdtM to neutral amino acids (e.g., alanine) might increase structural rigidity, allowing the transporter to bind substrates but preventing the conformational changes required for substrate translocation across the membrane. In contrast, mutations at Cys185 and Gln294 were expected to alter the physical properties of the transporter [8], potentially leading to better-diffracting crystals.

The secondary structure content of the purified mutants was initially analyzed using CD spectroscopy, confirming typical α-helical spectra for all mutant transporters. The styMdtM(D25A) mutant showed an α-helical content of ~69% similar to the wild-type, and was therefore selected for crystallization studies. By contrast, the styMdtM(R111A) mutant displayed a

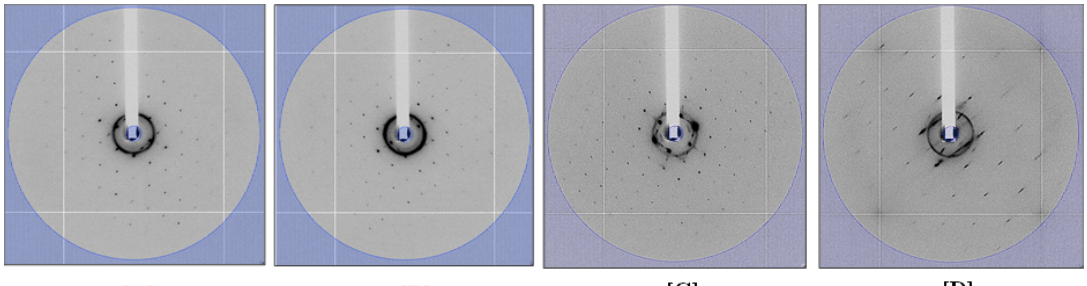

Fig. 2. Representative diffraction patterns; For the co-crystallized styMdtM, a resolution limit of 7.5 Å could be achieved [A & B; where both images are perpendicular to each other]. Diffraction patterns of styMdtM(D25A) co-crystallized with gentamicin showed spots well resolved in one direction [C], but a streaky pattern in the perpendicular direction [D]. This data was collected remotely using 'ADSC software' on 24-ID-E or 21-ID-D beamlines at the Advanced Photon Source (APS) synchrotron at Argonne National Laboratory (Illinois, USA).

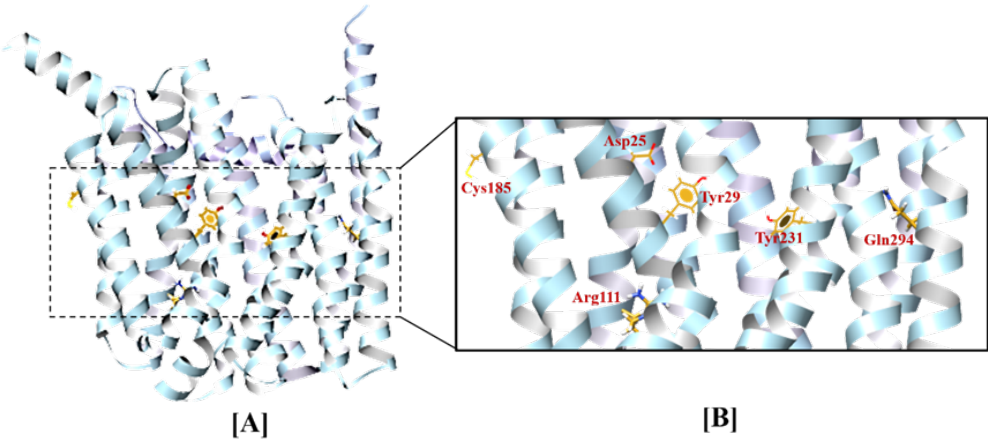

Fig. 3. AlphaFold model of styMdtM [A] (Uniprot ID: Q8XFG0): Targeted residues are indicated [B]. The transporter comprises of 12 transmembrane helices [A] and targeted residues are lying at different helices [B] within that part of transporter that is immersed in the membrane. The structure was visualized with the help of UCSF-Chimera [22].

significantly higher α-helical content (~95%) [15], and was excluded from further analysis. The styMdtM(C185A) and styMdtM(C185L) mutants each exhibited ~74% α-helical content. Since both had comparable functional and physical properties, styMdtM(C185A) was chosen for conducting crystallization trials [8]. The calculated α-helical content for styMdtM(Y29A), styMdtM(Q294A), and styMdtM(Y231A) mutants was ~78%, ~79%, and ~80%, respectively [8].

Prior to conducting crystallization trials, styMdtM mutants were characterized for thermal stability using biophysical techniques. Thermal stability measurements showed that the wild-type styMdtM had a *Tm* of 52 °C [8, 15]. The D25A mutation did not affect the thermal stability, as determined by CD spectroscopy [15]. Among the other mutants, C185A/L and Y231A exhibited *Tm* values within ± 2 °C of the wild-type. The Y29A mutant displayed an increased *Tm* of 56.5 °C, indicating enhanced stability [8]. In contrast, the Q294A mutant showed a reduced *Tm* of 47.27 °C, suggesting decreased stability; therefore, this mutant was not selected for crystallization trials [8].

Crystallization drops of the mutant transporters (D25A, Y29A, C185A, and Y231A) were set under conditions optimized for the wild-type transporter, and crystals were obtained under all tested conditions [8, 20]. Co-crystallization was also attempted, producing crystals of varying morphologies similar to those observed for the wild-type [8, 20]. The diffraction patterns of the styMdtM(D25A) mutant co-crystallized with gentamicin showed spots that were well-resolved in one direction, but poorly resolved in the perpendicular direction, resulting in streaked patterns (Figure 2(C, D)). The presence of diffuse and streaky patterns in the diffraction image is suggestive of lattice disorder. Moreover, the diffraction was anisotropic [20]. Similar observations were made for the other mutant transporters, most of which diffracted in the range of ~6-8 Å [8], thereby limiting the utility of the diffraction data for structure determination.

It must be noted here that the only MFS transporter with a known structure i.e., MdfA is resolved in its singly, doubly and triply mutated forms, including MdfA(Q131R) [13], MdfA(Q131R/L339E) [33], MdfA(I239T/G354E) [9], and MdfA(E26T/D34M/A150E) [10]. All of these resolved strcutures are in susbstrate-bound states. Since membrane transporters are highly flexible with continuous switiching of conformational states during loading of substrate from one side of memebrane and its unloading on the other side, this phenomenon likely makes it difficult to capture any single conformational state of the wild-type transporter in its *apo* form. In future, such a strategy of generating doubly and triply mutated forms of the styMdtM transporter can also be adopted to improve the quality of diffracting crystals.

3.4. Truncated styMdtM

Crystallization is still considered more of an art than a science [34], although some governing principles such as changes in Gibbs free energy

are taken into account. Crystal lattice formation involves changes in the enthalpy and entropy of the participating molecules (i.e., solvent and protein) [35]. In most cases, enthalpy changes are negligible [36-38], while, entropic factors dominate [39-41]. Entropy is particularly influenced by the presence of intrinsically unstructured elements, such as flexible termini or loops, especially in regions involved in protein-protein contacts during lattice formation [42]. To increase the likelihood of generating well-diffracting crystals, the target protein should therefore contain as few intrinsically unstructured fragments as possible such as solvent-exposed long loops at N- or C-termini [42].

Previous studies on polytopic inner membrane proteins of the MF superfamily have shown that deletion of the C-terminal cytoplasmic tail has a minimal impact on transporter functionality [27]. For example, in *E. coli* MFS transporters, such as LacY (lactose permease) and MelB (melibiose permease), the C-terminus is not essential for function [43-45]. Consistent with these findings, we attempted to improve crystallization of styMdtM by reducing its intrinsically unstructured elements through truncation of the C-terminal region. Notably, in *E. coli* MdfA (61% similar to styMdtM), deletion of the C-terminal loop does not significantly affect the multidrug resistance phenotype [27].

Accordingly, two deletion constructs were generated in parallel for styMdtM: one lacking 9 amino acids and the other lacking 13 amino acids at the C- terminus [20]. Both truncated proteins were subjected to crystallization trials under conditions optimized for the wild-type transporter. The construct with a 13- amino acid deletion yielded cubic crystals (Figure 4(A, B)) that diffracted isotropically to ~10 Å (Figure 4(C, D)) [8, 20]. Efforts to obtain better-diffracting crystals from this construct are ongoing.

4. CONCLUSIONS

This work provides preliminary insights into crystallization and X-ray diffraction of a multidrug efflux transporter, styMdtM, from *Salmonella* Typhi. So far, structure determination has not been achieved because of the resolution limit (~7.5 Å). However, along the structure determination way, the study has provided valuable insights into the function of this transporter and its analogs, contributing to the broader goal of structure elucidation. The ultimate aim of the structure determination endeavor always remains to elucidate the structural basis of the function. Importantly, recent advances in structure prediction using deep learning methods [46] offer a valuable alternative when experimentally determined structures are unavailable. However, these deep learning-based methods are trained on experimentally determined structures, and where such data exist, they can be used to more accurately predict transporter structures in different conformational states, thereby capturing the full transport cycle. For MFS transporters, each transport cycle comprises of at least 6 conformational states including two occluded states (empty and loaded), two inward facing (open and occluded), and two outward facing (open and occluded) states [47]. Currently, the only available structure for the close homologue of the styMdtM transporter is for an *E.*

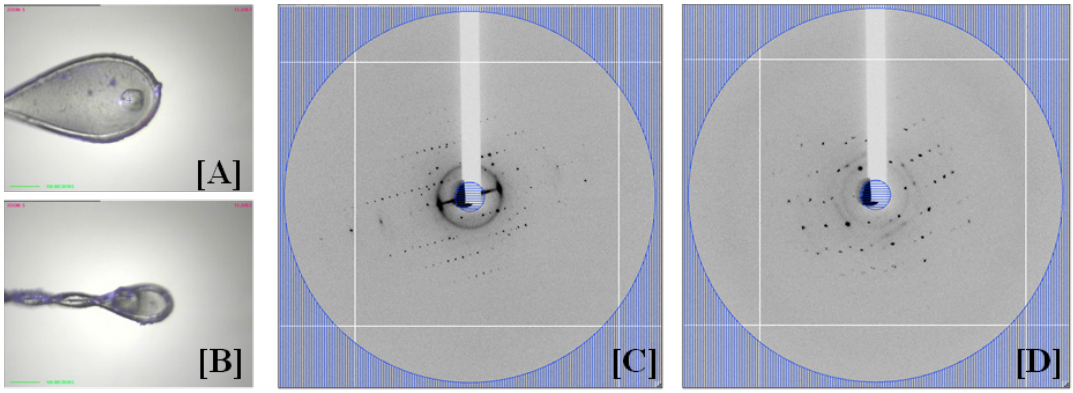

Fig. 4. Cubic crystals of truncated styMdtM [A and B] and their isotropic diffraction pattern with a resolution limit of 10Å [C and D]. The truncated transporter had a deletion of 13 amino acids (i.e., V_{398}RQHEAAELAAEK$_{410}$) from the C-terminus of the transporter.

coli MdfA mutant in inward-occluded and occluded (loaded with ligands) conformations. Following this training module, the Alphafold structure of the styMdtM also appears to be nearly in the inward-occluded conformation. However, as mentioned above, capturing the full transport cycle calls for further experimental determination of structures in other conformations.

The future work on the transporter under study may involve optimization of conditions for the growth of crystals, thereby minimizing anisotropic effects, generating doubly mutant forms of the transporter and whereby needed triply mutated forms to induce conformational locking. The co-crystallization of the transporter with a soluble protein can also be followed to improve the quality of the crystals. To minimize the radiation-induced damage, the X-ray exposure time can be minimized as well as the intensity of the beam can be reduced. This will also be helpful in addressing the issue of the presence of streaky patterns in diffraction images.

5. ACKNOWLEDGEMENTS

This work was funded by Higher Education Commission, Pakistan (NRPU grant No. 20-1504 to M.R., SRGP grant No.1197 to A.S., IRSIP fellowships to A.S. at Harvard Medical School, Boston, and to A.T. at the University of Michigan, Ann Arbor), and the Fulbright Scholar Program (to M.R. at Harvard Medical School, Boston).

6. CONFLICT OF INTEREST

The authors declare they have no conflict of interest.

7. REFERENCES

1. J. Garcia-Nafria, and C.G. Tate. Cryo-Electron Microscopy: Moving Beyond X-Ray Crystal Structures for Drug Receptors and Drug Development. *Annual Review of Pharmacology & Toxicology* 60: 51-71 (2020).
2. J.A. Purslow, B. Khatiwada, M.J. Bayro, and V. Venditti. NMR Methods for Structural Characterization of Protein-Protein Complexes. *Fronteiers in Molecular Bioscience* 7: 9 (2020).
3. H. Xie, Y. Zhao, W. Zhao, Y. Chen, M. Liu, and J. Yang. Solid-state NMR structure determination of a membrane protein in E. coli cellular inner membrane. *Scientific Advancement* 9(44): eadh4168 (2023).
4. S. Narasimhan, C. Pinto, A. Lucini Paioni, J. van der Zwan, G.E. Folkers, and M. Baldus. Characterizing proteins in a native bacterial environment using solid-state NMR spectroscopy. *Nature Protocol* 16(2): 893-918 (2021).
5. F. Li, P.F. Egea, A.J. Vecchio, I. Asial, M. Gupta, J. Paulino, R. Bajaj, M.S. Dickinson, S. Ferguson-Miller, B.C. Monk, and R.M. Stroud. Highlighting membrane protein structure and function: A celebration of the Protein Data Bank. *Journal of Biological Chemistry* 296: 100557 (2021).
6. Q. Ain, M. Tahir, A. Sadaqat, A. Ayub, A.B. Awan, M. Wajid, A. Ali, M. Iqbal, A. Haque, and Y. Sarwar. First Detection of Extensively Drug-Resistant Salmonella Typhi Isolates Harboring VIM and GES Genes for Carbapenem Resistance from Faisalabad, Pakistan. *Microbial Drug Resistance* 28(12): 1087-1098 (2022).
7. J. Akram, A.S. Khan, H.A. Khan, S.A. Gilani, S.J. Akram, F.J. Ahmad, and R. Mehboob. Extensively Drug-Resistant (XDR) Typhoid: Evolution, Prevention, and Its Management. *Biomedical Research International* 2020: 6432580 (2020).
8. A. Shaheen, A. Tariq, F. Ismat, H. Naveed, R. De Zorzi, M. Iqbal, P. Storici, O. Mirza, T. Walz, and M. Rahman. Identification of additional mechanistically important residues in the multidrug transporter styMdtM of Salmonella Typhi. *Journal of Biomolecular Structure & Dynamics* 42(21): 11641-11650 (2024).
9. H.H. Wu, J. Symersky, and M. Lu. Structure of an engineered multidrug transporter MdfA reveals the molecular basis for substrate recognition. *Communication Biology* 2: 210 (2019).
10. H.H. Wu, J. Symersky, and M. Lu. Structure and mechanism of a redesigned multidrug transporter from the Major Facilitator Superfamily. *Scientific Report* 10(1): 3949 (2020).
11. E.H. Yardeni, T. Bahrenberg, R.A. Stein, S. Mishra, E. Zomot, B. Graham, K.L. Tuck, T. Huber, E. Bibi, H.S. McHaourab, and D. Goldfarb. Probing the solution structure of the E. coli multidrug transporter MdfA using DEER distance measurements with nitroxide and Gd(III) spin labels. *Scientific Report* 9(1): 12528 (2019).
12. E.H. Yardeni, S. Mishra, R.A. Stein, E. Bibi, and H.S. McHaourab. The Multidrug Transporter MdfA Deviates from the Canonical Model of Alternating Access of MFS Transporters. *Journal of Molecular Biology* 432(20): 5665-5680 (2020).
13. K.O. Alegre, S. Paul, P. Labarbuta, and C.J. Law. Insight into determinants of substrate binding and

transport in a multidrug efflux protein. *Scientific Report* 6: 22833 (2016).
14. A. Shaheen, F. Ismat, M. Iqbal, A. Haque, R. De Zorzi, O. Mirza, T. Walz, and M. Rahman. Characterization of putative multidrug resistance transporters of the major facilitator-superfamily expressed in *Salmonella* Typhi. *Journal of Infection & Chemotherapy* 21(5): 357-362 (2015).
15. A. Shaheen, F. Ismat, M. Iqbal, A. Haque, Z. Ul-Haq, O. Mirza, R. De Zorzi, T. Walz, and M. Rahman. Characterization of the multidrug efflux transporter styMdtM from *Salmonella enterica* serovar Typhi. *Proteins* 89(9): 1193-1204 (2021).
16. A. Tariq, M. Sana, A. Shaheen, F. Ismat, S. Mahboob, W. Rauf, O. Mirza, M. Iqbal, and M. Rahman. Restraining the multidrug efflux transporter STY4874 of *Salmonella* Typhi by reserpine and plant extracts. *Letters in Applied Microbiology* 69(3): 161-167 (2019).
17. S. Iwata (Ed.). Methods and results in crystallization of membrane proteins. *International University Line La Jolla*, *California* (2003).
18. M.B. Khan, G. Sponder, B. Sjoblom, S. Svidova, R.J. Schweyen, O. Carugo, and K. Djinovic-Carugo. Structural and functional characterization of the N-terminal domain of the yeast Mg^{2+} channel Mrs2. *Acta. Crystallographica, Section D: Biological Crystallography* 69(Pt 9): 1653-1664 (2013).
19. A. McPherson. A comparison of salts for the crystallization of macromolecules. *Protein Science* 10(2): 418-422 (2001).
20. A. Shaheen. Characterization of efflux pumps conferring multidrug resistance in *Salmonella enterica* serovar Typhi. Ph.D. Thesis. *Pakistan Institute of Engineering and Applied Sciences, Islamabad, Pakistan* (2016).
21. M. Varadi, S. Anyango, M. Deshpande, S. Nair, C. Natassia, G. Yordanova, D. Yuan, O. Stroe, G. Wood, A. Laydon, A. Zidek, T. Green, K. Tunyasuvunakool, S. Petersen, J. Jumper, E. Clancy, R. Green, A. Vora, M. Lutfi, M. Figurnov, A. Cowie, N. Hobbs, P. Kohli, G. Kleywegt, E. Birney, D. Hassabis, and S. Velankar. AlphaFold Protein Structure Database: massively expanding the structural coverage of protein-sequence space with high-accuracy models. *Nucleic Acids Research* 50(D1): D439-D444 (2022).
22. E.F. Pettersen, T.D. Goddard, C.C. Huang, G.S. Couch, D.M. Greenblatt, E.C. Meng, and T.E. Ferrin. UCSF Chimera-a visualization system for exploratory research and analysis. *Journal of Computational Chemistry* 25(13): 1605-1612 (2004).
23. R.M. Bill, P.J. Henderson, S. Iwata, E.R. Kunji, H. Michel, R. Neutze, S. Newstead, B. Poolman, C.G. Tate, and H. Vogel. Overcoming barriers to membrane protein structure determination. *Nature Biotechnology* 29(4): 335-340 (2011).
24. S.R. Holdsworth and C.J. Law. Functional and biochemical characterisation of the *Escherichia coli* major facilitator superfamily multidrug transporter MdtM. *Biochimie* 94(6): 1334-1346 (2012).
25. S.R. Holdsworth and C.J. Law. The major facilitator superfamily transporter MdtM contributes to the intrinsic resistance of *Escherichia coli* to quaternary ammonium compounds. *Journal of Antimicrobial Chemotherapy* 68(4): 831-839 (2013).
26. S.R. Holdsworth and C.J. Law. Multidrug resistance protein MdtM adds to the repertoire of antiporters involved in alkaline pH homeostasis in *Escherichia coli*. *BMC Microbiology* 13: 113 (2013).
27. J. Adler and E. Bibi. Membrane topology of the multidrug transporter MdfA: complementary gene fusion studies reveal a nonessential C-terminal domain. *Journal of Bacteriology* 184(12): 3313-3320 (2002).
28. J. Adler and E. Bibi. Determinants of substrate recognition by the *Escherichia coli* multidrug transporter MdfA identified on both sides of the membrane. *Journal of Biological Chemistry* 279(10): 8957-8965 (2004).
29. J. Adler and E. Bibi. Promiscuity in the geometry of electrostatic interactions between the *Escherichia coli* multidrug resistance transporter MdfA and cationic substrates. *Journal of Biological Chemistry* 280(4): 2721-2729 (2005).
30. J. Adler, O. Lewinson, and E. Bibi. Role of a conserved membrane-embedded acidic residue in the multidrug transporter MdfA. *Biochemistry* 43(2): 518-525 (2004).
31. R. Edgar and E. Bibi. A single membrane-embedded negative charge is critical for recognizing positively charged drugs by the *Escherichia coli* multidrug resistance protein MdfA. *EMBO Journal* 18(4): 822-832 (1999).
32. N. Sigal, E. Vardy, S. Molshanski-Mor, A. Eitan, Y. Pilpel, S. Schuldiner, and E. Bibi. 3D model of the *Escherichia coli* multidrug transporter MdfA reveals an essential membrane-embedded positive charge. *Biochemistry* 44(45): 14870-14880 (2005).
33. E. Zomot, E.H. Yardeni, A.V. Vargiu, H.K. Tam, G. Malloci, V.K. Ramaswamy, M. Perach, P. Ruggerone, K.M. Pos, and E. Bibi. A New Critical Conformational Determinant of Multidrug Efflux by

an MFS Transporter. *Journal of Molecular Biology* 430(9): 1368-1385 (2018).
34. M. Levantino, B.A. Yorke, D.C. Monteiro, M. Cammarata, and A.R. Pearson. Using synchrotrons and XFELs for time-resolved X-ray crystallography and solution scattering experiments on biomolecules. *Current Opinion in Structural Biology* 35: 41-48 (2015).
35. J.D. Gunton, A. Shiryayev, and D.L. Pagan (Eds.). Protein condensation: kinetic pathways to crystallization and disease. *Cambridge University Press* (2007).
36. S.T. Yau, D.N. Petsev, B.R. Thomas, and P.G. Vekilov. Molecular-level thermodynamic and kinetic parameters for the self-assembly of apoferritin molecules into crystals. *Journal of Molecular Biology* 303(5): 667-678 (2000).
37. D.N. Petsev, B.R. Thomas, S.T. Yau, D. Tsekova, C. Nanev, W.W. Wilson, and P.G. Vekilov. Temperature-independent solubility and interactions between apoferritin monomers and dimers in solution. *Journal of Crystal Growth* 232(1): 21-29 (2001).
38. O. Gliko, N. Neumaier, W. Pan, I. Haase, M. Fischer, A. Bacher, S. Weinkauf, and P.G. Vekilov. A metastable prerequisite for the growth of lumazine synthase crystals. *Journal of the American Chemical Society* 127(10): 3433-3438 (2005).
39. P.G. Vekilov, A. Feeling-Taylor, S.T. Yau, and D. Petsev. Solvent entropy contribution to the free energy of protein crystallization. *Acta Crystallography Section D: Biological Crystallography* 58(10): 1611-1616 (2002).
40. Z.S. Derewenda and P.G. Vekilov. Entropy and surface engineering in protein crystallization. *Acta Crystallography Section D: Biological Crystallography* 62(1): 116-124 (2006).
41. P.G. Vekilov. Solvent entropy effects in the formation of protein solid phases. *Methods in Enzymology* 368: 84-105 (2003).
42. Z.S. Derewenda. Application of protein engineering to enhance crystallizability and improve crystal properties. *Acta Crystallography Section D: Biological Crystallography* 66(5): 604-615 (2010).
43. M.C. Botfield and T.H. Wilson. Carboxyl-terminal truncations of the melibiose carrier of *Escherichia coli*. *Journal of Biological Chemistry* 264(20): 11643-11648 (1989).
44. P.D. Roepe, R.I. Zbar, H.K. Sarkar, and H.R. Kaback. A five-residue sequence near the carboxyl terminus of the polytopic membrane protein lac permease is required for stability within the membrane. *Proceedings of National Academy of Science USA.* 86(11): 3992-3996 (1989).
45. K. Sato, M.H. Sato, A. Yamaguchi, and M. Yoshida. Tetracycline/H^+ antiporter was degraded rapidly in *Escherichia coli* cells when truncated at last transmembrane helix and this degradation was protected by overproduced GroEL/ES. *Biochemical and Biophysical Research Communication* 202(1): 258-264 (1994).
46. J. Jumper, R. Evans, A. Pritzel, T. Green, M. Figurnov, O. Ronneberger, K. Tunyasuvunakool, R. Bates, A. Zidek, A. Potapenko, A. Bridgland, C. Meyer, S.A.A. Kohl, A.J. Ballard, A. Cowie, B. Romera-Paredes, S. Nikolov, R. Jain, J. Adler, T. Back, S. Petersen, D. Reiman, E. Clancy, M. Zielinski, M. Steinegger, M. Pacholska, T. Berghammer, S. Bodenstein, D. Silver, O. Vinyals, A.W. Senior, K. Kavukcuoglu, P. Kohli, and D. Hassabis. Highly accurate protein structure prediction with AlphaFold. *Nature* 596(7873): 583-589 (2021).
47. D. Drew, R.A. North, K. Nagarathinam, and M. Tanabe. Structures and General Transport Mechanisms by the Major Facilitator Superfamily (MFS). *Chemical Reviews* 121(9): 5289-5335 (2021).

Proceedings of the Pakistan Academy of Sciences: B
Life and Environmental Sciences 62(4): 269-281 (2025)

ISSN (Print): 2518-4261; ISSN (Online): 2518-427X
http://doi.org/10.53560/PPASB(62-4)1089

Pakistan Academy of Sciences

Research Article

Micropropagation of Date Palm (*Phoenix dactylifera* L.) Cultivar Gulistan Using Immature Inflorescence Explants

Najamuddin Solangi[1*], Mushtaque Ahmed Jatoi[1], Adel Ahmed Abul-Soad[2], Ameer Ahmed Mirbahar[1], Abdul Aziz Mirani[1], and Ghulam Sarwar Markhand[1]

[1]Date Palm Research Institute, Shah Abdul Latif University, Khairpur, Sindh, Pakistan
[2]Horticulture Research Institute, Agricultural Research Center, Cairo, Egypt

Abstract: Current study described micropropagation of commercial date palm cultivar Gulistan through juvenile inflorescence explants. Immature spathes (20 cm in length) were excised before emergence from leaf axils in the crown at particular time i.e. early of February. For sterilization, the undissected spathes were dipped in NaOCl solution (40%) for 10 minutes on laminar air flow hood. Medium used for callus formation in the inflorescence explants was consisted of 0.1 mg/L 2,4-D, 0.1 mg/L IAA, 5.0 mg/L NAA induced significantly highest callus (87%) in primary explants. Highest somatic embryogenesis (84%) was obtained on the medium contained 0.1 mg/L NAA, 0.1 mg/L Kinetin. Shoot induction and multiplication (91%) was recorded on the medium consisted of 0.1 mg/L NAA, 0.05 mg/L BA. Leaves number (4.1), leaves length (17 cm), roots number (4.0), roots length (7 cm) were recorded as significantly highest on the medium consisted of 0.1 mg/L NAA. Trimming of embryonic root at 1-2 mm distance from plantlets' base produced 3-4 adventitious roots. *In vitro* hardening supported to choose healthy plantlets which survived well in greenhouse. Plantlets' survival percentage in greenhouse after 1M (88%) as significantly highest was recorded on the soil mixture contained peatmoss, river sand, perlite (1:1:¼ v/v). 46 cm long plantlets produced 4 small fronds/compound leaves, were cultivated in open field. Fruiting in trees started after three years of cultivation in open field. Introduction of elite date palm cultivars like Gulistan via micropropagation will be an addition to the existing cultivars in the area.

Keywords: Micropropagation, Somatic Embryogenesis, Plantlet Regeneration, *In vitro* Hardening, Acclimatization.

1. INTRODUCTION

Date palm (*Phoenix dactylifera* L.) a member of family Arecaceae is dioecious and diploid (2n = 36), contains vast number of varieties cultivated in arid and semi-arid regions in the world [1-3]. Date palm is titled as ''Tree of Life" due to its worldwide occurrence in Oasis and arid areas [4, 5]. Date palm yields up to 40-50 years; however, it may reach to 150 years age in certain conditions [6]. Dates contain vitamins, sugars, minerals, and various compounds used in the pharmaceutical industry for medicines' production [7-10]. Date palm generates considerable chances for the peoples living in rural areas, earning source for the date growers, increases income and is a good source of food [11]. Generally, the traditional propagation methods of date palm are by seeds and offshoots, but are labour intensive and time consuming. Commercially valued date palms are hindered via seed propagation due to heterozygous nature of the plants [12]. Generally, the date palm propagated via seeds either become male or female, and also produce inferior quality fruits, slow growth (8-10 years up to fruiting). Offshoot-grown date palm yields true-to-type fruits but show slow growth up to fruiting [13]. A date palm tree produces only 10-20 offshoots in whole life, its low survival in the field (50% mortality rate), and threat of Red Palm Weevil, Bayoud and Bayoud like diseases; such as, sudden decline disease [4, 14]. Keeping in view, the current scenario of date palm cultivation and production, the tissue culture is an additional possible way to multiply the selected local and exotic cultivars in a shortest

Received: September 2024; Revised: October 2025; Accepted: December 2025
* Corresponding Author: Najamuddin Solangi <najamsolangi@gmail.com>

time and space under controlled environmental conditions [2, 14, 15]. Simultaneously, the tissue culture-derived plants of date palm remain free from pests and diseases compared to the date palms propagated via traditional propagation methods. Micropropagation is suitable means of date palm propagation in contrast to seeds and offshoots, which can fulfil the requirement of date palm plants for large scale cultivation [16].

Additionally, the micropropagation is widely applied for the rapid production of the plant material [17]. Explants of the offshoots and inflorescences of the date palms have been used largely. Inflorescence based micropropagation proved as an efficient way for producing huge number of plants in a shortest time and space without sacrificing the whole tree; instead, a single inflorescence is excised from the tree without harm. Micropropagation is also a means for multiplication of the male or female recalcitrants of commercially important date palm cultivars [18]. A complete tree of date palm is utilized to obtain meristematic shoot tip explants, whereas, the tree remains un-damaged during excision of a spathe.

Several workers [19-26] utilized inflorescences of female date palms as an alternative to shoot tip explants; and found as a potential explant for *in vitro* culture compared to male inflorescence regarding induction of somatic embryos [22, 27]. Low somaclonal variation was observed in previous studies in the date palm plants derived from juvenile inflorescences [1, 28, 29]. Plant regeneration protocols of date palm through somatic embryogenesis were established through several studies [30-32]. Recently, inflorescence explants of date palm have been used widely in tissue culture [2, 15, 26, 33]. Commercial date palm cultivars in Pakistan are a few, simultaneously attacked by pests and diseases. Gulistan cultivar is a commercial semi-dry cultivar originally belongs to Dera Ismail Khan, Khyberpakhtunkhwa, Pakistan.

In this study micropropagation of commercial date palm cultivar Gulistan is an addition to existing cultivars in the area. Lot of work have been conducted on the micropropagation of several date palms in the world, but most of the studies were restricted to acclimatization stage, or if transferred in the open field produced fruits indistinguishable to the mother tree, or the trees were completely infertile due to irreversible genetic variations. On the contrary, this study described successful micropropagation of date palm produced fruits similar to mother palms; hence this study distinguishes to previously conducted studies on micropropagation of other date palm cultivars.

Present study designed to optimize stage-wise procedures for *in vitro* propagation of date palm via inflorescence explants, somatic embryogenesis, acclimatization of plantlets on various soil mixtures, transfer of plants in open field, and finally to check fruit quality are key objectives. Established tissue culture protocols of date palm by the current study will be applicable to micropropagate the other varieties and cultivars on commercial level growing in the world.

2. MATERIALS AND METHODS

2.1. Excision of Spathes and Explant Preparation

Spathes were collected from Orchard of Date Palm Research Institute, Shah Abdul Latif University, Khairpur located at latitude 27.490418˚ N, longitude 68.761593˚ E. Annual rainfall average of Khairpur is 87.6 mm and temperature (50 ˚C) in July. 20 cm long spathes were excised from the tree during first week of February in 2006; grown in the district Khairpur, Pakistan. Any residual particles on spathes' surface were removed with cotton. Later, spathes shifted to the laboratory, kept in closed ice box (4 ℃) to save from desiccation. Washing of spathes was carried out with tap water inside the laboratory. Further sterilization of spathes was carried out in culture room with NaOCl (40%) with 4-5 drops of tween-twenty for 10 min. After sterilization process, the spathe's cover was excised vertically with scalpel from both sides, keeping the inflorescence bunch intact.

After excision of both sides, the spathe was dissected horizontally to remove spathe cover entirely. Spikelets of 2-3 cm isolated from bunch and cultured directly on initiation media (kept vertically in culture tubes on the medium in a way the lower side of explant touched the medium); whereas, long spikelets were excised into 2-3 cm. Callus cultures were incubated under dark up to 7-9 months. Somatic embryos were induced under complete dark, and were multiplied under photoperiod 16/8 hours. Shoots (10 cm long) were shifted to elongation and rooting media for further

growth. After 1-2 subcultures, roots of the long plantlets were cut at 1-2 mm distance from plantlet's rooting area for production of multiple roots.

2.2. Media Preparation and Culture Conditions

Initiation medium was based on MS micronutrients, B5 macronutrients, sucrose 30 g/L, agar 2.2 g/L, gelrite 1.4 g/L, MS vitamins, KH_2PO_4 170 mg/L, glutamine 100 mg/L, adenine sulphate 40 mg/L, 2,4-Dichlorophenoxyacetic Acid (2,4-D) (0.1 mg/L), Indole-3-Acetic Acid (IAA) (0.1 mg/L), Naphthalene Acetic Acid (NAA) (5.0 mg/L) (M1). Initiation medium was based on 2,4-D 0.2 mg/L, IAA 0.1 mg/L, NAA 5.0 mg/L (M2). Maturation medium was based on Activated Charcoal (AC) 1.5 g/L, 2,4-D (5.0 mg/L), 2-Isopentenyladenine (2iP) (1.0 mg/L). Differentiation medium was consisted of full MS, NAA (0.1-0.2 mg/L) and Kinetin (0.1-0.2 mg/L). Multiplication medium was based on NAA (0.1-0.2 mg/L) and 6-Benzylaminopurine (BA) (0.05 mg/L). Rooting media were consisted of MS (¼), calcium pantothenate (0.1 mg/L), AC (3 g/L), NAA 0.1 mg/L (M1); Indole-3-Butyric Acid (IBA) 0.1 mg/L (M2), NAA 0.2 mg/L (M3), IBA 0.2 mg/L (M4). Initiation and differentiation were carried out under full dark (24 °C); while the rooted plantlets were grown under photoperiod (16/8 hours), temperature (27 °C). Multiplication and rooting were achieved under photoperiod 16/8 hours (fluorescent light intensity at 40-60 µmol m^{-2} s^{-1}). Light intensity during elongation and rooting stages was 160 µmol m^{-2} s^{-1}. At initiation stage, subculturing was carried out after every three weeks; while at multiplication and rooting stages; subculturing was done after every four weeks. pH of the media was fixed at 5.7 at all *in vitro* growth stages. Medium was dispensed either in 150 × 25 mm tubes or in 350 ml jars utilized for *in vitro* cultures. 20 ml medium dispensed in each culture tube or 25 ml medium dispensed per jar. Sterilization of the media was done by autoclave (Mitsubishi, Japan) for 15 min at 121 °C.

2.3. *In vitro* Hardening

In vitro hardening was performed inside laboratory during June, 2008 for 2-3 days before shifting the plantlets in the greenhouse. Plantlets used for *in vitro* hardening were consisted of 2-3 roots and 3-4 leaves. Liquid medium was used for *in vitro* hardening consisted of ½ MS, 15 g/L sucrose. Small holes were made in the cape of culture vessels for movement of gases in and out of the culture tubes 1-2 hours prior to transfer the plantlets in greenhouse.

2.4. Acclimatization

20 cm long plants with four simple leaves and adventive roots were transplanted in greenhouse during June, 2008. Plantlets directly exposed to greenhouse environment by removing the cap of the culture tubes for 1-2 hours prior to shift on soil mixture. Later, the plantlets taken out of vessels to remove gel from roots with sterilized water. Systemic fungicide (Carbendazim) solution (3 g/L) was used for washing the plantlets before shifting in 19 × 13 cm plastic bags on various mixtures of peatmoss, river sand, perlite (1:1:¼), (1:2:¼), (1:3:¼), (1:4:¼). Humidity was maintained to 85-90% inside the tunnel in the greenhouse for few weeks. Ventilation of the tunnel was carried out after a week for 10 min. After one month, the plantlets were exposed to the environment of greenhouse and the tunnel/polyethylene cover was removed completely. At this stage no any fertilizer was applied to the plants. One and half years old plants were shifted in 41.5 × 21 cm bags on soil mixtures used during acclimatization, and left for two and half years (up to end of 2010) until formation of compound leaves (3-4 per plant), and capable to grow well in open field environment. Plants' survival percentages were recorded subsequently at one and three months' interval.

2.5. Open Field Transfer

Plants about 46 cm long with maximum 4 fronds/compound leaves were cultivated in open field to evaluate true-to-typeness of tree and fruit. Fruiting in the plants started after two years of plantations in the field i.e. in the year 2012. NPK fertilizer was applied to the plants in the field as per need according to the age of the tree.

2.6. Statistical Analysis

Three spathes were obtained from cultivar Gulistan yielded total 150 explants. One explant per culture tube was cultured on initiation media. Completely Randomized Design was performed; whereas, the ANOVA and LSD tests were performed at $p < 0.05$ according to Steel and Torrie [34].

3. RESULTS AND DISCUSSION

3.1. Callus Formation in Primary Explants

2,4-D is one of the important plant growth regulators (PGRs) induces callus in immature inflorescence explants. In this study different auxins and their concentrations induced callus in the floral bud explants (Figure 1(a)) during third week of the initial culture (Figure 1(b)). About 120 out of 150 explants (on both treatments used during initiation stage) formed callus in the floral buds. Data in Table 1 show significantly highest callus formation (87%) in floral buds on the medium contained 2,4-D 0.1 mg/L, IAA 0.1 mg/L, NAA 5.0 mg/L. On the contrary, callus formation was decreased significantly (55%) on the medium contained 2,4-D 0.2 mg/L, IAA 0.1 mg/L, NAA 5.0 mg/L. Inflorescence explants can induce better callus using 2,4-D up to 0.5 mg/L [26]; however, in the current study three auxins were used in order to induce callus in the floral bud explants. Increase in 2,4-D (0.2 mg/L) decreased callus induction percentage in primary explants. 2,4-D concentrations i.e. 0.5 mg/L, 2iP 3.0 mg/L induced maximum callus; but further increase in 2,4-D to 1.0 mg/L showed vitrification [2]. Until maturation stage i.e. 7-9 months (induction of globular embryos) (Figure 1(c)); the cultures were retained on initiation media. Later, the callus cultures (7-9 months old) shifted to maturation medium contained 2,4-D (5.0 mg/L), 2iP (1.0 mg/L) for a single subculture. 2,4-D occurrence in calli initiation media exhibited positive effect on explants to induce highest callus, but higher 2,4-D levels may sometimes bring variations in plants; therefore 2,4-D in the media should be excluded once the calli is formed and matured. 2.4-D might bring permanent genetic variations at callus stage which may persist throughout the whole life making whole the cycle useless. Medium contained 2,4-D (100 mg/L), 2iP (3.0 mg/L) and AC (3 g/L) was used for propagating the date palm *in vitr*o from shoot tip [30]. Several workers [26, 35] reported the 2,4-D a major callus inducing PGR in primary explants. Al-Khayri [36] obtained callus in shoot tip explants on the medium comprised of 2,4-D (100 mg/L), 2iP (3.0 mg/L), AC (1.5 g/L). Badawy *et al*. [37] described the medium for callus formation in date palm cv. Sewi consisted of 2,4-D (100 mg/L), 2iP (3 mg/L). Auxins disrupt the normal development leading to callus induction in primary explants

Table 1. Influence of various combinations of PGRs on callus induction in spikelet explants of cv. Gulistan.

PGRs (mg/L)	Callus (%)
0.1 2,4-D + 0.1 IAA + 5.0 NAA	87±0.5[a]
0.2 2,4-D + 0.1 IAA + 5.0 NAA	55±0.2[b]
LSD (0.05)	**0.000*** **

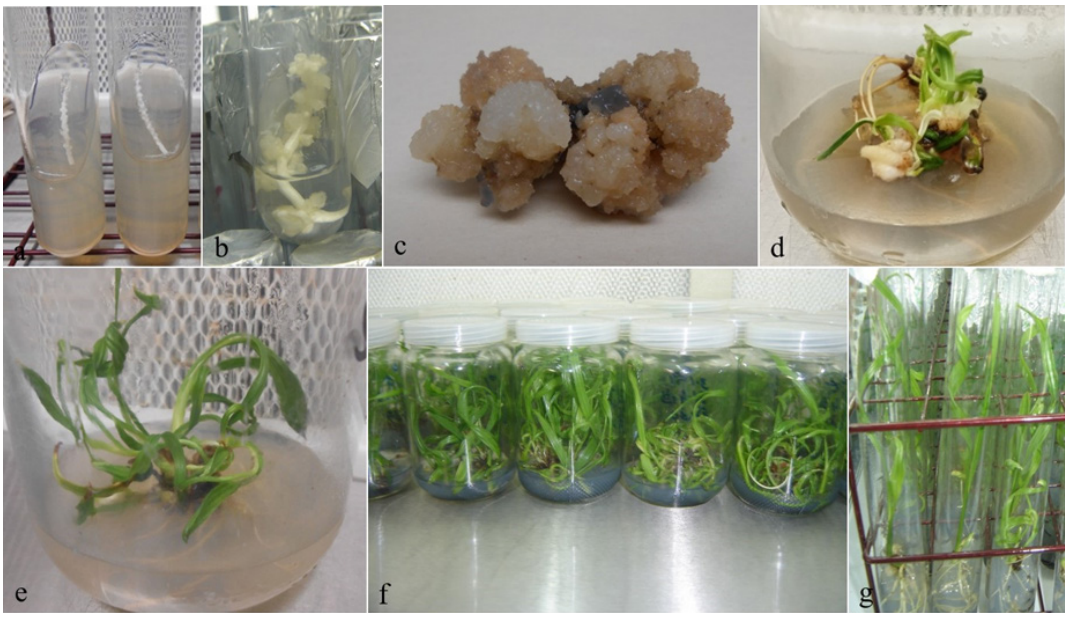

Fig. 1. (a) Inflorescence explants, (b) Callus formation in inflorescence explants, (c) Maturation stage of callus prior to differentiation, (d) Somatic embryogenesis and germination, (e) Small shoot clusters\, (f) Long plantlets in jars before separation, and (g) Isolated plantlets in culture vessels with healthy shoot and root ready for transfer in greenhouse.

[2, 38, 39]. Callus cultures should be retained on 2,4-D contained medium until appearance of small globular structures in the callus, indicates maturation stage of the callus. Several workers [15, 40, 41] studied callus induction behavior of soft, semi-dry or dry cultivars in inflorescence explants. Age of the spathe and explant size had the positive role in callus induction in the spikelet explants. 2-3 cm long explants can be easily submerged in the nutrient medium for callus induction. Any part of the explant away from the nutrient medium undergoes necrosis. Juvenile inflorescence explants used in the present study obtained from 20 cm long spathes excised during 1st week of February, 2006 induced significantly highest callus.

Previous studies used juvenile inflorescence explants obtained from spathes (15 cm long) obtained during early of February [42] formed calli in bulk in the primary explants. Several workers [43-45] observed that in date palm calli induction was supported by explants' age and PGRs' types. Most workers observed that the 2,4-D is an effective PGR among auxins regarding callus formation in initial explants [46-48].

3.2. Somatic Embryogenesis

Data in Table 2 exhibit significantly highest ($p < 0.000$) somatic embryogenesis (84% of the callus cultures obtained during initiation stage) on the medium containing NAA (0.1 mg/L), Kinetin (0.1 mg/L). Contrary, the lowest percentage of embryos (51%) was achieved on the medium containing NAA (0.2 mg/L), Kinetin (0.2 mg/L). Use of 2,4-D in the media was restricted up to maturation in callus, i.e., calli ready to produce embryos; however, the continued occurrence of 2,4-D in the media also retard somatic embryogenesis. Formation of somatic embryos require low 2,4-D concentration in the media or sometimes complete exclusion of 2,4-D. 2,4-D should be added up to the appearance of rounded structures in the callus cultures i.e. start of the differentiation stage [2, 26]. Embryogenic calli in inflorescence explants was also noted within six weeks on PGRs contained media [15]. Embryogenic callus cultures were declined gradually due to prolong subculture on the media consisted of 2,4-D under full dark. Shifting of callus on the media lacking 2,4-D retarded normal proliferation of callus under light. Furthermore, embryogenic clusters produced from friable callus under light developed into somatic embryos. Green photosynthetic leaves produced in plantlets upon germination (Figure 1(d)). 2,4-D concentrations i.e. 1.5, 5 and 10 (mg/L) also used for somatic embryogenesis in the callus [49-52]. Genotypic effects influence somatic embryogenesis which may take few to several months in different cultivars [46, 53].

3.3. Proliferation and Germination of Somatic Embryos

Data in Table 3 indicate that highest germination (91%) of somatic embryos achieved on medium consisted of NAA (0.1 mg/L), BA (0.05 mg/L) (Figure (1d)). Contrary, the lowest germination (57%) of somatic embryos was recorded on the medium contained NAA (0.2 mg/L), BA (0.05 mg/L). Increase in NAA concentration to 0.2 mg/L significantly decreased the multiplication of somatic embryos. Individual shoots formed after germination of somatic embryos were isolated and shifted on rooting media for elongation of shoot/root. Embryos exhibited highest multiplication and germination under light. Steward *et al*. [54] described the need of auxin in the medium until initiation of somatic embryos; whereas, complete removal of auxins from the media supports embryo maturation. Cytokinins bring maturation of somatic embryos [55], followed by cotyledon development [56]. Likewise, in this study the procedures were exploited for maturation of embryos at proper

Table 2. Influence of various combinations of PGRs on somatic embryogenesis in callus of cv. Gulistan.

PGRs (mg/L)	Embryogenesis (%)
0.1 NAA + 0.1 Kinetin	84±1.1[a]
0.2 NAA + 0.1 Kinetin	51±2.1[b]
LSD (0.05)	**0.000*** **

Table 3. Influence of various combinations of PGRs on somatic embryos germination in cv. Gulistan.

PGRs (mg/L)	Germination (%)
0.1 NAA + 0.05 BA	91±0.5[a]
0.2 NAA + 0.05 BA	57±2.2[b]
LSD (0.05)	**0.000*** **

growth stage. Two types of somatic embryos were recognized such as repeated i.e. cluster of embryos and non-repeated i.e. single embryos [2, 42]. Germination of somatic embryos (repeated and non-repeated) resulted in formation of green shoots with roots (Figure 1(d)). Up on germination, covering of embryos opens vertically, results in the emergence of shoot and root. After 1-2 subcultures on the multiplication medium, the plantlets were shifted on shoots and roots elongation medium (Figure 1(e-f)). Previous studies also observed germination of single and clustered embryos [15, 26, 42]. A comprehensive study conducted on micropropagation of date palm via floral bud explants [14]. However, in this study several combinations of PGRs used at each *in vitro* growth stages differ greatly to those of Solangi *et al*. [2].

3.4. Shoot Elongation and Rooting

Data in Table 4 describe highest response of NAA than IBA for shoot and root growth (Figure 1(g)). Total number of plantlets produced during elongation stage was 1100. About 100 plantlets were contaminated or died due to poor rooting, whereas remaining 1000 plantlets were survived after root trimming process. Results revealed that significantly highest ($p < 0.000$) leaves number (4.1), leaves length (17 cm), roots number (4.0) and roots length (7.2 cm) were achieved on the medium containing ¼ MS, calcium pantothenate (0.1 mg/L), AC (3 g/L), NAA (0.1 mg/L). Leaves number (3.2), leaves length (11 cm), roots number (3.1) and roots length (5.0 cm) were achieved on the medium contained ¼ MS, calcium pantothenate (0.1 mg/L), AC (3 g/L), IBA (0.1 mg/L). NAA and IBA (0.2 mg/L) induced lowest leaves and roots number. NAA and IBA (0.1 mg/L) have been widely exploited in the rooting media for date palm and other plants. 0.1 mg/L BA, 0.1 mg/L NAA significantly enhanced leaves and roots growth [14]. Several workers [15, 42] used BA 0.05 mg/L, NAA 0.1 mg/L for shoots and roots elongation in date palm. El-Sharabasy *et al*. [57] observed positive effect of 0.1 mg/L NAA on shoot length of cv. Zaghlool and cv. Sewi than IBA and IAA. Healthy root formation was acquired on the medium consisted of NAA (0.1 mg/L) [58]. Tisserat [59] also acquired adventive roots through re-culturing of isolated plantlets on the medium comprised of NAA (0.1 mg/L). Omar [60] obtained healthy plants of date palm by transferring small shoots on the medium comprised of NAA (0.1 mg/L) for improved rooting, and BA (0.01 mg/L) for improved shoot. NAA is widely used PGR for the rooting in date palm [35, 59, 61, 62], and several other plant species.

3.5. Root Trimming

Better survival of plants in greenhouse at acclimatization stage was based on the healthy roots developed during *in vitro* growth. In this way, the embryonic roots were cut at 1-2 mm distance to lower side of 10 cm plantlets to induce multiple roots in each plantlet (Figure 2(a)). Multiple healthy roots enhance survival percentage of plants during acclimatization. Plantlets acquired after germination of somatic embryos consisted of single embryonic root (Figure 2(b)). Several studies [14, 15, 62, 64] exploited root trimming for formation of healthy adventive roots in each plantlet. Root trimming is the means of getting higher survivability of plants in greenhouse. Solangi *et al*. [14, 26] achieved healthy growth and maximum survival of plantlets in greenhouse. Plantlets with untrimmed roots showed weak growth in the greenhouse compared to the plantlets with multiple roots developed via root trimming at proper growth stage.

3.6. *In vitro* Hardening

In vitro hardening was performed few days before to transfer the plantlets in greenhouse. Liquid nutrient medium consisted of ½ MS and 15 g/L sucrose was used for *in vitro* hardening. An opening was made in the cap of culture tube for gaseous movement just

Table 4. Influence of various combinations of NAA and IBA on shoot and root formation and elongation in cv. Gulistan.

PGRs (mg/L)	Cv. Gulistan			
	Leaves number	Leaves length (cm)	Roots number	Roots length (cm)
0.1 NAA	4.1±0.58[a]	17±3.10[a]	4.0±1.00[a]	7.2±2.00[a]
0.1 IBA	3.2±0.45[ab]	11±0.42[b]	3.1±0.58[ab]	5.0±1.14[b]
0.2 NAA	2.2±0.51[b]	9±1.12[c]	2.2±0.44[b]	2.3±0.46[b]
0.2 IBA	2.1±0.43[b]	8±1.16[c]	1.1±0.34[c]	2.1±0.58[b]
LSD (0.05)	0.03**	0.002**	0.04**	0.05**

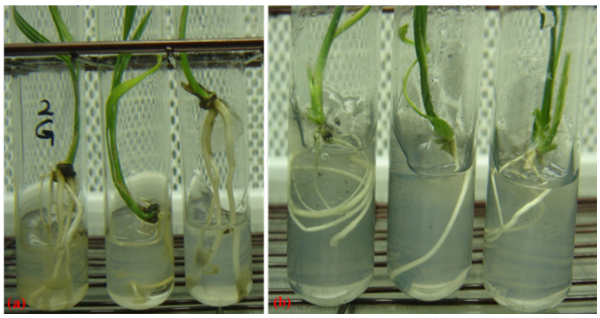

Fig. 2. (a) Multiple roots produced at the base of date palm plantlets after trimming the embryonic root, (b) Single root developed in plantlets with untrimmed embryonic roots.

one hour prior to shifting the plants in greenhouse. Number of *in vitro* hardened plants was 1000. *In vitro* hardening helps to bring changes in the physiological nature of plants from heterotrophic to autotrophic [14, 42]. *In vitro* hardening helped to isolate healthier plantlets able for acclimatization. More than 85% survivability of plantlets was acquired in greenhouse. Poorly developed plantlets turned into wilted leaves via *in vitro* hardening; such plantlets were recognized easily, and isolated before acclimatization. Hassan *et al*. [63] suggested hardening *in vitro* to choose healthy plantlets prior to acclimatization. *In vitro* hardening is an important final stage of *in vitro* growth [64]. *In vitro* hardening was also performed for many other crops [65]. This technique helps to adapt plantlets' physiology and anatomical features well suited to *ex vitro* environment to ensure maximum survival rate in greenhouse.

3.7. Plantlets' Survival in Greenhouse

Adaptation of *in vitro* grown plants in varied environmental conditions is called acclimatization [14, 42]. Plants develop varied physiology and anatomy grown under high humidity, low gaseous exchange, which needs to reverse to their normal structures by maintaining the humidity in the greenhouse during acclimatization [14, 42]. Number of plantlets acclimatized in the greenhouse was 980, which was 1000 before *in vitro* hardening. Only 20 plantlets showed wilted leaves during *in vitro* hardening and discarded before acclimatization. Table 5 shows highest survival (88% and 80%) of plantlets after 1M and 3M respectively on soil mixture contained peatmoss, river sand, perlite (1:1:¼). Gradual decrease was noted regarding survival of plantlets in greenhouse on soil mixture consisted of peatmoss, river sand, perlite (1:2:¼) (77% and 71% after 1M and 3M respectively). Results showed significantly highest values at $p < 0.000$ after 1M and 3M. Further decrease in the survival rate of the plants was noted on soil consisted of peatmoss, river sand, perlite (1:3:¼) and peatmoss, river sand, perlite (1:4:¼). Results showed that river sand is not rich in nutrients as peatmoss; however, river sand provides good aeration to the roots but deficient in nutrients compared to peatmoss. Peatmoss contains essential elements such as potassium, phosphorus, nitrogen, iron, magnesium, calcium etc. Peatmoss does not fulfil all nutrient requirements of the plants which always fulfilled with fertilizers when plants rooted in soil mixtures and start growing after acclimatization. Results revealed that total mortality rate of plants in greenhouse was 20% in 3 months on a soil mixture contained peatmoss, river sand, perlite (1:1:¼) and no more plants were died until shifting in the open field. On the contrary, significantly highest plant mortality rate (45%) was noted on a soil mixture contained peatmoss, river sand, perlite (1:4:¼) after 3 months. Phenomenon indicated that higher ratios of river sand were not suitable for acclimatization of date palm. Peatmoss should always be added with river sand, but the ratio of river sand should not increase to peatmoss ratio; however, peatmoss ratio can be increased; whereas, the perlite always should be in little amount. Perlite is a light weight porous volcanic glass used as a soil conditioner to improve drainage and aeration in the

Table 5. Influence of various mixtures of Peatmoss, River sand, Perlite on plantlets' survival in greenhouse cv. Gulistan.

Soil Mixtures			**Cv. Gulistan**	
Peatmoss	**River sand**	**Perlite**	**1 Month**	**3 Months**
1	1	½	88±1.3^{a}	80±2.2^{a}
1	2	½	77±0.5^{b}	71±0.2^{b}
1	3	½	65±0.4^{c}	60±1.2^{c}
1	4	½	60±2.1^{c}	54±2.2^{d}
LSD (0.05)			0.000***	0.000***

plants. It is created by heating volcanic glass, which causes it to expand. Perlite is pH neutral and helps to prevent soil compaction while creating air pockets for root growth. It also enhances water retention. In previous studies [63, 66, 67] low survival (25-30%) in date palm plants was obtained during acclimatization due to improper soil mixtures. Kurup *et al*. [68] noted 60% survival of plants on a soil mixture contained peatmoss and vermiculite (2:1) in cv. Kheneizi. Othmani *et al*. [51] obtained survival (60%) in date palm cultivar Boufeggous and 80% in cultivar Deglet Nour. 72-84% survival rate of date palm plants was obtained by Al-Khayri [48] in cultivars Nabout Saif and Khasab. Solangi *et al*. [14] recorded survival (92%) of plants on soil mixture contained peatmoss and river sand (3:1). Various studies [69, 70] used a soil mixture of peatmoss and vermiculite (1:1) for growing 12 cm plantlets in greenhouse.

Plantlets of date palm successfully acclimatized and established in the greenhouse (Figure (3a)). One and half year old plantlets in greenhouse with a compound leaf were transferred into 41.5 × 21 cm plastic bags (Figure (3b)). Two and half years old plantlets in greenhouse with four compound leaves (Figure (3c)) transferred in field showed 100% survival due to well established roots at base of plants grown in greenhouse. Fertilizer (NPK) was applied to plants in greenhouse and in open field according to the age of plants. Several studies [14, 15] applied 3 g/L NPK on six months old plants in greenhouse; whereas, 20 g/L NPK applied to two and half years old plants.

3.8. Vegetative Growth and true-to-type Fruiting of Date Palm in the Open Field Conditions

Plants grown in greenhouse up to two and half years produced 3-4 compound leaves and adventitious roots (Figure (3c)) were shifted in the open field for further vegetative growth and fruiting (Figure (3d)). Fruits of cv. Gulistan were similar morphologically to the fruits as in their native place (Dera Ismail Khan, Khyberpakhtunkhwa, Pakistan). Date palm cv. Gulistan started fruiting after three years of cultivation in the field (Figure 3(e-f)). Quality of ripened dates of the tissue cultured plants was also similar to the dates grown in their native place (Figure 3(g)). However, phenotypic abnormalities i.e. twisted inflorescence, fertilization failure, dwarf plants, bastard offshoots, ceased flowering, multiple carpels [71], were rarely noted after two years of cultivation in the open field, and were reversible. Mirani *et al*. [28, 29] observed epigenetic variations which were reversible to normal phenotypes after two years of cultivation in the field. Additionally, the variations like dwarf plants reverted to normal phenotypes were reported by Gurevich *et al*. [72]. Several workers [73-76] observed the epigenetic variations in tissue cultured plants of date palm reverted to normal phenotypes. Climate and soil conditions of Khairpur, Pakistan were suitable for growing date palm cultivars grown in other provinces of Pakistan. Mirani *et al*. [28, 29] conducted detailed study on somaclonal variations in tissue cultured date palm cvs. Gulistan, Dedhi, Kashuwari. Mirani *et al*. [28] conducted study on reversion of phenotypic variations in tissue cultured

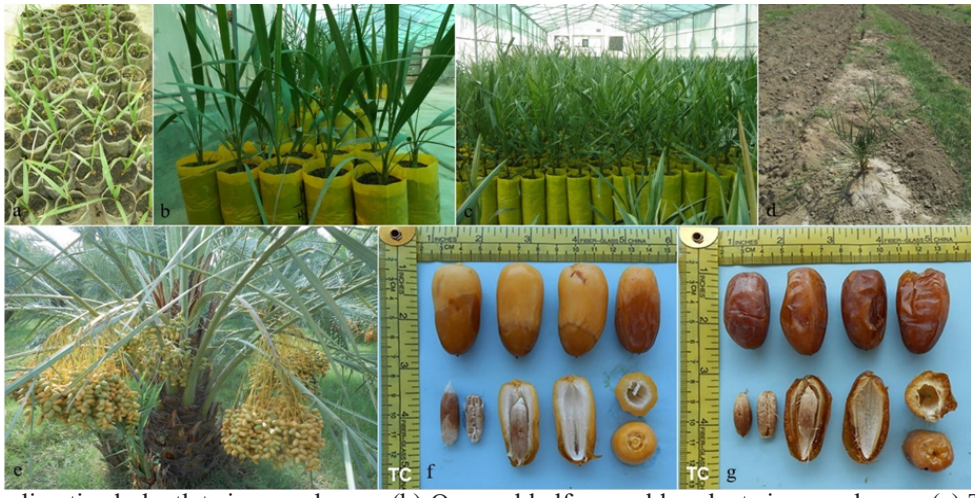

Fig. 3. (a) Acclimatized plantlets in greenhouse, (b) One and half year older plants in greenhouse, (c) Two and half years older plants in greenhouse, (d) Plants growing in the open field, (e) Date palm cv. Gulistan with true-to-type fruits, (f) Rutab stage dates of TC derived cv. Gulistan, (g) Tamar stage dates of TC derived cv. Gulistan.

date palm, and observed that phenotypic variations occurred in tissue cultured plants were epigenetic variations (reversible variations). Solangi *et al*. [77] conducted comparative study on field performance of tissue cultured and offshoot-grown date palm cvs. Gulistan, Kashuwari, Dedhi, and observed that tissue cultured plants produced true-to-type fruits. Date Palm Research Institute, Shah Abdul Latif University, Khairpur witnessed to micropropagate around 2400 plants of date palm cvs. Gulistan, Kashuwari, Dedhi, Samany and Bertamoda, which were distributed among the active growers, belong to different areas of Pakistan produced true-to-type fruits. However, still there is need to have a tissue culture laboratory for production of huge number of plants for commercialization. Tissue culture is expensive; consume high cost; but simultaneously huge number of elite and rare plant species can be propagated within shortest time and space. In this study true-to-type fruits were obtained, which were also confirmed by genetic studies conducted by Mirani *et al*. [29].

4. CONCLUSIONS

Commercially valued date palm cultivar Gulistan was successfully micropropagated through immature inflorescence explants. PGRs exhibited significant role in promoting the growth in each *in vitro* growth stage. Improved germination and multiplication of somatic embryos were obtained, led to shoot formation and rooting. Growth of shoots and roots improved on the media comprised of NAA or IBA. 3-4 adventive roots produced per plantlet by trimming the embryonic root. *In vitro* hardening helped to change slowly from heterotrophic mode of nutrition to autotrophic (to obtain food by photosynthesis). In greenhouse plantlets showed better survival rate on the soil mixtures contained equal ratios of peatmoss and river sand. 100% plants survived in open field due to well-formed roots. Normal tree growth (except reversible changes) and true-to-type fruits were noted showed similar colour, size, shape and taste. Results obtained in this study can be applied to micropropagate elite date palm cultivars grown in Pakistan and around the world.

5. CONFLICT OF INTEREST

The authors declare no conflict of interest.

6. ACKNOWLEDGMENT

Authors acknowledge HEC's financial assistance for the project at Date Palm Research Institute, Shah Abdul Latif University, Khairpur, Pakistan.

7. REFERENCES

1. A.A. Mirani, M.A. Jatoi, L. Bux, C.H. Teo, A.I. Kabiita, J.A. Harikrishna, G.S. Markhand, T. Jatt, N. Solangi, and S. Abro. Genetic stability analysis of tissue culture derived date palm cv. Dedhi plants using IRAP markers. *Acta Ecologica Sinica* 42(1): 76-81 (2022).
2. N. Solangi, A.A. Abul-Soad, G.S. Markhand, M.A. Jatoi, T. Jatt, and A.A. Mirani. Comparison among different auxins and cytokinins to induce date palm (*Phoenix dactylifera* L.) somatic embryogenesis from floral buds. *Pakistan Journal of Botany* 52(4): 1243-1249 (2020).
3. N. Solangi, M.A. Jatoi, N. Tunio, A.A. Mirani, A.A. Abul-Soad, and G.S. Markhand. Fruit Morphological and Biochemical Characterization of Three Saudi Arabian Date Palm (*Phoenix dactylifera* L.) Cultivars Grown in District Khairpur, Pakistan. *Proceedings of the Pakistan Academy of Sciences: B. Life and Environmental Sciences* 61(1): 11-20 (2024).
4. A.A. Abul-Soad, S.M. Jain, and M.A. Jatoi. Biodiversity and conservation of date palm. In: Biodiversity and conservation of woody plants. M.R. Ahuja and S.M. Jain (Eds.). *Sustainable Development and Biodiversity; No. 17. Springer Cham* pp. 313-353 (2017).
5. M.T. Rashid, B. Safdar, M.A. Jatoi, N. Solangi, A. Wali, N. Ali, and K. Liu. Structure, rheology, and tribology of date fruit paste procured from different date palm cultivars. *Journal of Food Process Engineering* 44: e13891 (2021).
6. C.T. Chao and R.R. Krueger. The date palm (*Phoenix dactylifera* L.): overview of biology, uses, and cultivation. *Horticultural Science* 42(5): 1077-1082 (2007).
7. P.K. Vayalil. Date fruits (*Phoenix dactylifera* Linn): an emerging medicinal food. *Critical Reviews in Food Science and Nutrition* 52(3): 249-271 (2012).
8. J. Ahmed, F.M. Al-Jasass, and M. Siddiq. Date fruit composition and nutrition. M. Siddiq, S.M. Aleid, and A.A. Kader (Eds.). In: Dates: postharvest science, processing technology and health benefits, (First Edition). *Wiley, Chichester, United Kingdom* pp. 261-283 (2013).

9. R. Omran, Z.M. Al-Taee, H.O. Hashim, and M.J. Al-Jassani. Preventive effects of *Phoenix dactylifera* polyphenols against 7,12-dimethylbenz (a) anthracene-induced mammary cancer. *Asian Journal of Pharmaceutical and Clinical Research* 10(7): 172-181 (2017).
10. C. Selmani, D. Chabane, and N. Bouguedoura. Ethnobotanical survey of *Phoenix dactylifera* L. pollen used for the treatment of infertility problems in Algerian oases. *African Journal of Traditional, Complementary and Alternative Medicines* 14(3): 175-186 (2017).
11. K. Rajmohan. Date palm tissue culture: A pathway to rural development. In: Date Palm Biotechnology. S.M. Jain, J.M. Al-Khayri, and D.V. Johnson (Eds.). *Springer, Dordrecht* pp. 29-45 (2011).
12. B. Tisserat. Factors involved in the production of plantlets from date palm callus cultures. *Euphytica* 31: 201-214 (1982).
13. N. Al-Khalifah and E. Askari. Growth abnormalities associated with micropropagation of date palm. In: Date palm biotechnology. S.M. Jain, J.M. Al-Khayri and D.V. Johnson (Eds.). *Springer, Dordrecht, Heidelberg, London, New York* pp. 205-219 (2011).
14. N. Solangi, M.A. Jatoi, G.S. Markhand, A.A. Abul-Soad, M.A. Solangi, T. Jatt, A.A. Mirbahar, and A.A. Mirani. Optimizing Tissue Culture Protocol for *In Vitro* Shoot and Root Development and Acclimatization of Date Palm (*Phoenix dactylifera* L.) Plantlets. *Erwerbs-Obstbau* 64: 97-106 (2022).
15. A.A. Abul-Soad and J.M. Al-Khayri. Date palm somatic embryogenesis from inflorescence explant. In: Step Wise Protocols for Somatic Embryogenesis of Important Woody Plants. S.M. Jain and P. Gupta (Eds.). *Springer Cham* pp. 329-347 (2018).
16. M.M. Saker and H.A. Moursi. Molecular Characterization of Egyptian date palm cultivars: RAPD fingerprints. *Arab Journal of Biotechnology* 2(1): 71-78 (1999).
17. J. Janick (Ed.). Horticultural Science. *W.H. Freeman and Company, San Francisco* (1979).
18. A.A. Abul-Soad and S.M. Mahdi. Commercial production of tissue culture date palm (*Phoenix dactylifera* L.) by inflorescence technique. *Journal of Genetic Engineering and Biotechnology* 8(2): 39-44 (2010).
19. D.A. De Mason. The occurrence and structure of apparently bisexual flowers in the date palm, *Phoenix dactylifera* L. (Arecaceae). *Botanical Journal of the Linnean Society* 81(4): 283-292 (1980).
20. D.R. Sharma, R. Kumari, and J.B. Chowdhury. *In vitro* culture of female Date Palm (*Phoenix dactylifera* L.) tissues. *Euphytica* 29: 169-174 (1980).
21. S. Bhaskaran and R. Smith. Somatic embryogenesis from shoot tip and immature inflorescence of *Phoenix dactylifera* L cv. Barhee. *Plant Cell Report* 12: 22-25 (1982).
22. J.M. Al-Khayri. Micropropagation of Date Palm *Phoenix dactylifera* L. In: Protocols for Micropropagation of Woody Trees and Fruits. S.M. Jain and H. Haggman (Eds.). *Springer, Berlin, Germany* pp. 509-526 (2007).
23. L. Abahmane. Micropropagation of date palm (*Phoenix dactylifera* L.) selected genotypes from inflorescence tissues by using somatic embryogenesis technique. *Acta Horticulturae* 882: 827-832 (2010).
24. N. Nimavat and P. Parikh. Innovations in Date palm (*Phoenix dactylifera* L.) micropropagation: Detailed review of in vitro culture methods and plant growth regulator applications. *Plant Cell Tissue and Organ Culture* 159: 6 (2024). https://doi.org/10.1007/s11240-024-02866-7.
25. L. Abahmane. Recent achievements in date palm (*Phoenix dactylifera* L.) micropropagation from inflorescence tissue. *Emirates Journal of Food and Agriculture* 25(11): 863-874 (2013).
26. N. Solangi, M.A. Jatoi, A.A. Abul-Soad, A.A. Mirani, M.A. Solangi, and G.S. Markhand. Factors influencing somatic embryogenesis and plantlet regeneration of date palm using immature floral buds. *Sarhad Journal of Agriculture* 39(2): 323-331 (2023).
27. A. Zaid, A.A. Al-Kaabi, and B. El-Korchi. Large scale in vitro propagation of rare and unique male date palm (*Phoenix dactylifera* L.). *Acta Horticulturae* 736: 243-254 (2007). https://doi.org/10.17660/ActaHortic.2007.736.22
28. A.A. Mirani, C.H. Teo, A.A. Abul-Soad, G.S. Markhand, T. Jatt, A.A. Mirbahar, and N. Solangi. Phenotypic reversion of somaclonal variants derived from inflorescence of date palm (*Phoenix dactylifera* L.) in the open field trials. *Sarhad Journal of Agriculture* 35(3): 719-726 (2019).
29. A.A. Mirani, C.H. Teo, G.S. Markhand, A.A. Abul-Soad, and J.A. Harikrishna. Detection of somaclonal variations in tissue cultured date palm (*Phoenix dactylifera* L.) using transposable element-based markers. *Plant Cell, Tissue and Organ Culture* 141(1): 119-130 (2020).
30. B. Tisserat. Propagation of date palm (*Phoenix dactylifera* L.) *in vitro*. *Journal of Experimental Botany* 30: 1275-1283 (1979).

31. A. Othmani, C. Bayoudh, N. Drira, and M. Trifi. In vitro Cloning of Date Palm *Phoenix Dactylifera* L., Cv. Deglet Bey by Using Embryogenic Suspension and Temporary Immersion Bioreactor (TIB). *Biotechnology and Biotechnological Equipment* 23(2): 1181-1188 (2009).
32. M.S. Omar, M.K. Hameed, and M.S. Al-Rawi. Micropropagation of date palm (*Phoenix dactylifera* L.). In: High-Tech and Micropropagation II. Biotechnology in agriculture and forestry. Volume 18. Y.P.S. Bajaj (Ed.). *Springer-Verlag, Berlin, Heidelberg* pp. 471-492 (1992). https://doi.org/10.1007/978-3-642-76422-6_25.
33. M.A. Abohatem, A. Ba-Asher, and M. Al-Duais. In vitro germination of date palm somatic embryos and conversion into plants under dark culture conditions: novel protocol to reducing the time and production costs. *Discover Plants* 1(1): 40 (2024).
34. O. Heinisch. Steel, R.G.D. and J.H. Torrie: Principles and Procedures of Statistics (With special Reference to the Biological Sciences). *Biometrical Journal* 4(3): 207-208 (1962). https://doi.org/10.1002/bimj.19620040313.
35. A.M.A. Ali, A.A. Qahtan, J.M. Al-Khayri, and H.S. Ghazzawy. Effect of low 2,4-D concentration on enhancing indirect embryogenesis and genetic stability in date palm (*Phoenix dactylifera* L.). *Scientific Reports* 15: 43865 (2025).
36. J.M. Al-Khayri. Somatic Embryogenesis of Date Palm (*Phoenix dactylifera* L.) from Shoot Tip Explants. In: Step Wise Protocols for Somatic Embryogenesis of Important Woody Plants, Forestry Sciences. S.M. Jain and P. Gupta (Eds.). *Springer, Cham* pp. 231-244 (2018).
37. E.M. Badawy, A.M.A. Habib, A. El Bana, and G.M. Yosry. Propagation of date palm (*Phoenix dactylifera* L.) plants by using tissue culture technique. *Arab Journal of Biotechnology* 8: 343-354 (2005).
38. C. Eeuwens and J. Blake. Culture of coconut and date palm tissue with a view to vegetative propagation. *Acta Horticulturae* 78: 277-286 (1977).
39. A.A. Abul-Soad. Influence of inflorescence explant age and 2,4-D incubation period on somatic embryogenesis of date palm. *Emirates Journal of Food and Agriculture* 24(5): 434-443 (2012).
40. M. Laaguidi, R. Meziani, and K. Sellam. In vitro culture of date palm: a review of challenges and solutions for managing endophytic bacteria contamination. *Vegetos* (2025). https://doi.org/10.1007/s42535-025-01287-x.
41. C.J. Eeuwens. Mineral requirements for growth and callus initiation of tissue explants excised from mature coconut palms (Cocosnucifera) and cultured *in vitro*. *Physiologia Plantarum* 36(1): 23-28 (1978).
42. A.A. Abul-Soad. Micropropagation of date palm using inflorescence explants. In: Date Palm Biotechnology. S.M. Jain, J.M. Al-Khayri, and D.V. Johnson (Eds.). *Springer Dordrecht* pp. 91-117 (2011). https://doi.org/10.1007/978-94-007-1318-5.
43. N. Drira and A. Benbadis. Multiplication végétative du palmierdattier (*Phoenix dactylifera* L.) par réversion en culture *in vitro*d'ébauchesflorales de piedsfemelles. *Journal of Plant Physiology* 119: 227-235 (1985).
44. L. Fki, R. Masmoudi, N. Drira, and A. Rival. An optimized protocol for plant regeneration from embryogenic suspension cultures of date palm, *Phoenix dactylifera* L., cv. Deglet Nour. *Plant Cell Report* 21: 517-524 (2003).
45. M. Mazri and R. Meziani. Micropropagation of date palm: a review. *Cell and Developmental Biology* 4(3): 160 (2015).
46. P. Eshraghi, R. Zarghami, and M. Mirabdulbaghi. Somatic embryogenesis in two Iranian date palm cultivars. *African Journal of Biotechnology* 4(11): 1309-1312 (2005).
47. J.M. Al-Khayri. Date Palm (*Phoenix dactylifera* L.). In: Protocols of somatic embryogenesis in woody plants. S.M. Jain and P.K. Gupta (Eds.). *Springer, Dordrecht* pp. 309-319 (2005). https://doi.org/10.1007/1-4020-2985-3_25.
48. J.M. Al-Khayri. Somatic embryogenesis of date palm (*Phoenix dactylifera* L.) improved by coconut water. *Biotechnology* 9(4): 477-484 (2010).
49. I. El-Hadrami and M. Baaziz. Somatic embryogenesis and analysis of peroxidases in *Phoenix dactylifera* L. *Biologia Plantarum* 37(2): 197-203 (1995).
50. J. Aslam, S.A. Khan, A.J. Cheruth, A. Mujib, M.P. Sharma, and P.S. Srivastava. Somatic embryogenesis, scanning electron microscopy, histology and biochemical analysis at different developing stages of embryogenesis in six date palm (*Phoenix dactylifera* L.) cultivars. *Saudi Journal of Biological Sciences* 18: 369-380 (2011).
51. A. Othmani, C. Bayoudh, N. Drira, and M. Trifi. Somatic embryogenesis and plant regeneration in date palm *Phoenix dactylifera* L., cv. Boufeggous is significantly improved by fine chopping and partial desiccation of embryogenic callus. *Plant Cell, Tissue and Organ Culture* 97: 71-79 (2009).
52. A. Othmani, C. Bayoudh, N. Drira, and M. Trifi. *In vitro* cloning of date palm *Phoenix dactylifera*

L. cv. Deglet Bey using embryogenesis suspension and temporary immersion bioreactor (TIB). *Biotechnology & Biotechnological Equipment* 23(2): 1181-1188 (2009).
53. M.H. Hassan and R.A. Taha. Callogenesis, somatic embryogenesis and regeneration of date palm (*Phoenix dactylifera* L.) cultivars affected by carbohydrate sources. *International Journal of Agricultural Research* 7: 231-242 (2012).
54. F.C. Steward, A.E. Kent, and M.O. Mapes. Growth and organization in cultured cells: sequential and synergestic effects of growth regulating substances. *Annals of the New York Academy of Sciences* 144: 326-334 (1967).
55. T. Fujimura and A. Komamine. Effects of various growth regulators on the embryogenesis in a carrot cell suspension culture. *Plant Science Letters* 5(6): 359-364 (1975).
56. P.V. Ammirato and F.V. Steward. Some effects of the environment on the development of embryos from cultured free cells. *Botanical Gazette* 132(2): 149-158 (1971). https://doi.org/10.1086/336573
57. S.F. El-Sharabasy, H.A. Bosila, and I.A. Ibrahim. Micropropagation studies on Zaghlool and Sewi cvs. of date palm (*Phoenix dactylifera* L.): III. Plantlet acclimatization. *Proceedings of the Second International Conference on Date Palm, Al Ain, UAE* (2001).
58. A. Zaid and B. Tisserat. *In vitro* shoot tip differentiation in *Phoenix dactylifera* L. *Date Palm Journal* 2(2): 163-182 (1983).
59. B. Tisserat. Propagation of date palm by shoot tip cultures. *Horticultural Science* 19: 230-231 (1984).
60. M.S. Omar. *In vitro* response of various date palm explants. *Date Palm Journal* 2: 371-389 (1988).
61. K.W. Al-Maari and A.S. Al-Ghamdi. Micropropagation of five date palm cultivars through *in vitro* axillary buds' proliferation. *Journal of Agricultural Science* 13: 55-71 (1997).
62. A.A. Abul-Soad and M.A. Jatoi. Factors affecting *in vitro* rooting of date palm (*Phoenix dactylifera* L.). *Pakistan Journal of Agricultural Science* 51: 467-474 (2014).
63. M.M. Hassan, I.A. Ibrahim, N.M. Fathy, M.K.H. Ebrahim, and E. Komor. Protocol for Micropropagated Date Palm Acclimatization: Effect of Micropropagated Plantlet Type, Soil Composition, and Acclimatization Season. *International Journal of Fruit Science* 14(2): 225-233 (2014).
64. M.F. Gabr and M.M. Abd-Alla. Micropropagation of *Phoenix dactylifera* L. var. karama. *New York Science Journal* 3(12): 64-69 (2010).
65. T. Kozai, M. Hayashii, Y. Hirosawa, T. Kodama, and I. Watanabe. Environmental control for acclimatization of *in vitro* cultured plantlets (1) Development of acclimatization unit for accelerating the plantlet growth and test cultivation. *Journal of Agricultural Meteorology* 42(4): 349-358 (1987).
66. M. Mohammed, M. Munir, and H.S. Ghazzawy. Design and Evaluation of a Smart Ex Vitro Acclimatization System for Tissue Culture Plantlets. *Agronomy* 13(1): 78 (2023).
67. S.T. Hussein and E.B. Mohamed. Micropropagation of some Egyptian date palm dry cultivars 1-maturation of somatic embryos. *Arab Journal of Biotechnology* 10(2): 333-340 (2007).
68. S.S. Kurup, M.A. Aly, G. Lekshmi, and N.H. Tawfik. Rapid *in vitro* regeneration of date palm (*Phoenix dactylifera* L.) cv. Kheneizi using tender leaf explant. *Emirates Journal of Food and Agriculture* 26: 539-544 (2014).
69. B. Tisserat (Ed.). Date palm tissue culture. Volume 17. Advances in Agricultural Technology. Western Series. *U.S. Department of Agriculture, Science and Education Administration, USA* (1981).
70. A.M. Abdelghaffar, S.S. Soliman, T.A. Ismail, A.M. Alzohairy, A.A.H.A. Latef, K. Alharbi, J.M. Al-Khayri, N.I.M. Aljuwayzi, D.A. El-Moneim, and A.A. Hassanin. *In Vitro* Propagation of Three Date Palm (*Phoenix dactylifera* L.) Varieties Using Immature Female Inflorescences. *Plants* 12(3): 644 (2023).
71. A.A. Abul-Soad, S.M. Mahdi, and G.S. Markhand. Date Palm Status and Perspective in Pakistan. In: Date Palm Genetic Resources and Utilization. J.M. Al-Khayri, S.M. Jain, and D.V. Johnson (Eds.). *Springer Dordrecht* pp. 153-205 (2015).
72. V. Gurevich, U. Lavi, and Y. Cohen. Genetic variation in date palms propagated from offshoots and tissue culture. *Journal of the American Society of Horticultural Science* 130: 46-53 (2005).
73. I. Pinker, Y.M. Ibraheem, and M.H. Böhme. Propagation of some date palm cultivars by using tissue culture methods. *Acta Horticulturae* 839: 71-77 (2009).
74. S. Alavipour, E. Khaleghi, N. Moallemi, K. Mehdikhanlou, and A. Trohi. Heteromorphism of normal and abnormal flowers of date palm cv. Barhee and comparison of green and red Ghanami pollens as dominant pollens. *South African Journal of Botany* 163: 541-551 (2023).
75. Y. Cohen, R. Kochinsky, and E. Tripler. Flower abnormalities cause abnormal fruit setting in tissue culture-propa*gated date palm (Phoenix*

dactylifera L.). *Journal of Horticultural Science and Biotechnology* 79(6): 1007-1013 (2004).

76. Y. Cohen. Molecular detection of somaclonal variation in date palm. In: Date Palm Biotechnology. S.M. Jain, J.M. Al-Khayri, and D.V. Johnson (Eds.). *Springer, Dordrecht* pp. 221-235 (2011). https://doi.org/10.1007/978-94-007-1318-5_11.
77. N. Solangi, A.A. Mirani, M.A. Jatoi, A.A. Abul-Soad, L.B. Bhanbhro, G.S. Markhand, M. Hedayat, and G. Abdi. Field evaluation of tissue culture-derived and offshoot-grown date palm cultivars: a comparative analysis of vegetative and fruit attributes. *Frontiers in Plant Science* 16: 1516983 (2025).

Proceedings of the Pakistan Academy of Sciences: B
Life and Environmental Sciences 62(4): 283-294 (2025)

ISSN (Print): 2518-4261; ISSN (Online): 2518-427X
http://doi.org/10.53560/PPASB(62-4)1121

Pakistan Academy of Sciences

Research Article

Effect of Humic Acid Levels on the Production of Gladiolus Cultivars

Ahmad Naeem[1†], Noor Ul Amin[1], Hamza Ali[2†*], Masood Ahmad[1*], Abdul Mateen Khattak[1], Amna Shafi[3], Ateeq Ur Rehman[1], and Habib Ur Rehman[4]

[1]Department of Horticulture, Faculty of Crop Production Sciences, The University of Agriculture Peshawar, 25120, Pakistan

[2]State Key Laboratory for Crop Stress Resistance and High-Efficiency Production, College of Horticulture, Northwest A&F University, Yangling, Shaanxi 712100, China

[3]Agriculture Research Institute Tarnab, Peshawar, Pakistan

[4]Muhammad Nawaz Shareef University of Agriculture, Multan, Pakistan

Abstract: Gladiolus is a valuable ornamental crop, widely cultivated for its aesthetic appeal and commercial demand. However, its growth and flowering performance are often hindered by poor soil fertility and suboptimal nutrient management, which needs to be optimized for its commercial production under the agroclimatic conditions of Peshawar, Pakistan. Humic acid is a natural organic substance and is known to enhance soil properties and improve plant growth. Therefore, this experiment was conducted under RCBD split plot arrangement to evaluate the different humic acid levels and their influence on five different gladiolus cultivars. Results indicated that both humic acid and cultivars significantly influenced vegetative and reproductive attributes. The humic acid at the rate of 4 kg ha^{-1} treatment was most effective, resulting in improved emergence, number of leaves, leaf area, spike emergence, 1st floret opening, florets per spike, field flower persistence, vase life, corm weight, and number of cormels. Enhanced performance was attributed to better nutrient uptake, chlorophyll synthesis, hormonal balance, and source–sink relationships under humic acid supplementation. Among cultivars, 'White Prosperity' showed superior vegetative growth and cormel production, while 'Priscilla' had longer vase life and heavier corms, indicating genetic differences in nutrient use and reproductive efficiency. The results show that humic acid not only promotes vegetative growth but also accelerates floral initiation, increases floret production, delays senescence, and enhances postharvest quality. It is concluded that humic acid at the rate of 4 kg ha^{-1}, in cultivars White Prosperity and Priscilla, was optimal for commercial gladiolus cultivation under Peshawar's agro-climatic conditions.

Keywords: Bulbous Crops, Flowering, Gladiolus, Humic Acid, Vase Life.

1. INTRODUCTION

Gladiolus (*Gladiolus Grandiflorus* L.) is a popularly grown bulbous ornamental which is a member of the Iridaceae family. It is indigenous to South Africa, but now grows in many countries because of its exquisite beauty, long petal spikes, and their great variation in colors. About 260 species and nearly 1,000 cultivars have been identified with the genus with about 120 being cultivated as cut flowers [1]. The other cultivars are normally used in decoration of the garden, sales and display, and used in making seasonal flower displays. Gladiolus can also be called the "Queen of bulbous flowers" since it has a lovely look and excellent performance as a cut flower [2]. Its plant is popular due to its long shelf life after harvest and its beauty in decorative pots, in bouquet and flowers arrangements. The demand of gladiolus cultivation has increased tremendously in different states worldwide, the leading producers

Received: August 2025; Revised: November 2025; Accepted: December 2025
* Corresponding Authors: Hamza Ali and Masood Ahmad <hamzaali@nwafu.edu.cn; masoodhort@aup.edu.pk>
† These authors have contributed equally

of gladiolus are the United States, followed by Netherlands, Italy, and Brazil etc. [3]. It has got a large export value particularly in Europe in the winter seasons where people use it a lot in its indoor decoration and landscaping [4]. Gladiolus has the potential to generate handsome revenue in cut flowers trade [5].

In order to increase growth, quality and commercial value of gladiolus careful nutrient management is necessary. Humic acid is one of the numerous types of organic amendments that are becoming of great significance due to its capability to enhance soil health and plant performance. Humic acid is a polymeric organic compound in nature, which increases nutrient adsorption, raises the activity of microorganisms, and improved the soil properties [6]. It improves soil fertility due to the fact that it forms chelates with applicable nutrients making them more readily available to the plants [7]. Humic acid enhances the capacity to absorb water and aerate the soils as well as drain the soils and also makes plants withstand environmental stress [8]. It encourages early germination, strong vegetative development and effective flowering. Also, Humic acid minimizes the use of synthetic fertilizers thus enhancing sustainable farming. Soils contain large quantities of humic substances such as fulvic and humic acids that are very vital in the developmental stages of plants [9]. Application of Humic acid can induce relevant and significant physiological processes in plants that include a rise in respiration, enhanced photosynthesis, enhanced root growth, and more chlorophyll synthesis [10]. Such advances are especially valuable to ornamental crops such as gladiolus, where marketability depends on plant aesthetics, flower size and duration. The climate in Khyber Pakhtunkhwa, Pakistan, is favorable to the gladiolus production, but most of the available cultivars are poor in performance and do not meet the required characteristics in the global market [11]. A rising interest in comparing local and introduced cultivars is aimed at establishing cultivars that perform better. Moreover, the effect of organic amendments like humic acid on gladiolus in the agro-climatic conditions of Peshawar can help in enhancing the quality of flowers, its yield and its market value.

Current research was aimed to test the performances of the various gladiolus cultivars to evaluate the best levels of humic acid in enhancing various growth, yield and quality attributes of gladiolus under the agro-climatic environment of Peshawar. The objectives of the study were to determine the interaction between levels of humic acid and gladiolus cultivars on the general plant performance in order to be able to recommend the best cultivar-nutrient combination that can be used in commercial production of gladiolus flowers in the area.

2. MATERIALS AND METHODS

2.1. Experimental Design and Factors

This study was conducted at the Ornamental Horticulture Nursery, The University of Agriculture Peshawar. It was performed following the randomized complete block design with split plot arrangement. Main plots were consisted of four humic acid concentrations, i.e., 0, 2, 4, and 6 kg ha^{-1} whereas five cultivars, i.e., White Prosperity, Priscilla, Advance Red, Purple Flora, and Green Star were assigned to sub plots. There was a total of twenty treatments replicated three times.

2.2. Planting of Corms

The experimental site was thoroughly prepared before planting. Gladiolus corms were arranged from a reliable seed company in Islamabad. A basal dose of Nitrogen, Phosphorus, and Potassium at the rate of 100:75:75 kg ha^{-1} was applied before planting, with nitrogen supplied in two split doses, the first at the time of planting and the second at the three-leaf stage. Urea, di-ammonium phosphate (DAP), and sulphate of potash (SOP) were used as sources of nitrogen, phosphorus, and potassium, respectively. Humic acid was also applied in two split doses: the first at planting and the second at the three-leaf stage. Corms were planted with a spacing of 30 cm between plants and 60 cm between rows, at a depth of 6 cm. All cultural practices, including irrigation, weeding, and hoeing, were carried out uniformly across treatments. Additionally, soil-based application of humic acid was performed 15 days before corm planting.

2.3. Soil Analysis

Before the application of humic acid and planting of corms, soil samples were collected from the field

at three depths (0-15 cm, 15-30 cm, and 30-45 cm). These samples were analyzed in the laboratory of the Department of Soil and Environmental Science, The University of Agriculture, Peshawar, to determine soil pH, electrical conductivity (EC), organic matter (OM), nitrogen, phosphorus, and potassium contents. These results are presented in Table 1, that gives the insights into the existing field conditions.

2.4. Cultural Practices

Weeds were removed from the field as needed throughout the cropping period. Irrigation was carried out on a weekly basis from January to August. Bamboo sticks were used for staking when necessary to support taller plants that could not stand upright on their own. For data collection, five plants were randomly selected and tagged from each subplot.

2.5. Attributes Studied

To evaluate the growth, flowering, and corm yield of gladiolus, various morphological and reproductive parameters were recorded during the experiment. Days to emergence of plants were calculated by noting the days from plantation of corms till the emergence of 50% plants in every treatment and replication and its mean was computed. The number of leaves per plant was determined by counting the total number of leaves on five randomly selected plants per treatment and calculating the mean. For leaf area (cm^2), mature leaves from five randomly selected plants were measured using a leaf area meter, and the mean was computed. Days to spike emergence were recorded by counting the number of days from planting to the appearance of flower spike in each treatment, with averages taken across replications.

The days to first floret opening were calculated by recording the time taken from planting until the first floret opened on three randomly selected plants, and the average was determined. The number of florets per spike was counted from five randomly selected plants per plot, and the average value was used for analysis. Spike length (cm) was measured using a meter rod from the internode just above the fourth leaf up to the tip of the spike on five randomly selected plants, and the results were averaged. Field flower persistency was assessed by noting the number of days from the opening of the first floret until the fading of the last floret on selected spikes, with the average calculated accordingly.

To evaluate postharvest performance, vase life (days) was measured by harvesting spikes at the color-showing stage, placing them in distilled water at room temperature, and recording the duration until it lost its decorative value. For corm yield assessment, corm weight (g) was recorded using a digital balance after harvesting, and mean values were calculated for each treatment. The size of the corms (cm) was measured using vernier caliper, and average dimensions were determined for each treatment. Lastly, the number of cormels per plant was obtained by counting all the cormels produced per plant in each plot and computing the mean [11].

2.6. Statistical Analysis

The analysis of variance (ANOVA) was analyzed for the collected data using Statistix 8.1 using a RCBD design with split plot arrangement, and treatment means were compared using the Least Significant Difference (LSD) test at a 5% level of significance [12]. The bar graphs were made using sigma plot 15.0, the PCA, correlation matrix and heatmap were built with R-studio.

Table 1. Soil analysis of the experimental area.

Property	Soil Depth		
	0-15 cm	15-30 cm	30-45 cm
pH	7.86	8.19	8.24
EC (ds m^{-1})	0.23	0.19	0.14
Soil Organic Matter (%)	0.78	0.61	0.42
AB–DTPA extractable N (mg kg^{-1})	0.15	0.12	0.09
AB–DTPA extractable P (mg kg^{-1})	5.34	5.10	4.32
AB–DTPA extractable K (mg kg^{-1})	73.2	68.4	66.1

3. RESULTS

The statistical analysis revealed that humic acid levels and gladiolus cultivars had significantly affected days to plant emergence, whereas their interaction was found to be non-significant (Figure 1(A)). Among the humic acid treatments, the earliest plant emergence (14.3 days) was recorded in plots treated with humic acid at 6 kg ha^{-1}, followed by 4 kg ha^{-1} (14.9 days) and 2 kg ha^{-1} (16.6 days). The maximum days to emergence (17.1) were recorded in the control (untreated) plots. Regarding cultivars, the minimum number of days to emergence was observed in Priscilla (13.5), followed by White Prosperity (13.9) and Advance Red (16.3), while the highest emergence duration (18.4 days) was noted in Green Star.

There was significant variation in number of leaves in response to humic acid and cultivars, but their interaction was found to be non-significant (Figure 1(B)). The max no. of leaves per plant (8.5) were recorded in plots supplied with 4 kg ha^{-1} humic acid, followed by 6 kg ha^{-1} (8.0) and 2 kg ha^{-1} (7.6), whereas the lowest (7.0) was noted in control plots. Among cultivars, White Prosperity produced highest no. of leaves per plant (8.5), followed by Priscilla (8.3) and Green Star (7.7), whereas Advance Red resulted in least no. of leaves (7.1).

The leaf area per plant was significantly affected by both humic acid levels and cultivars, though their interaction remained non-significant (Figure 1(C)). Maximum leaf area (290 cm²) was observed when the gladiolus cultivars were

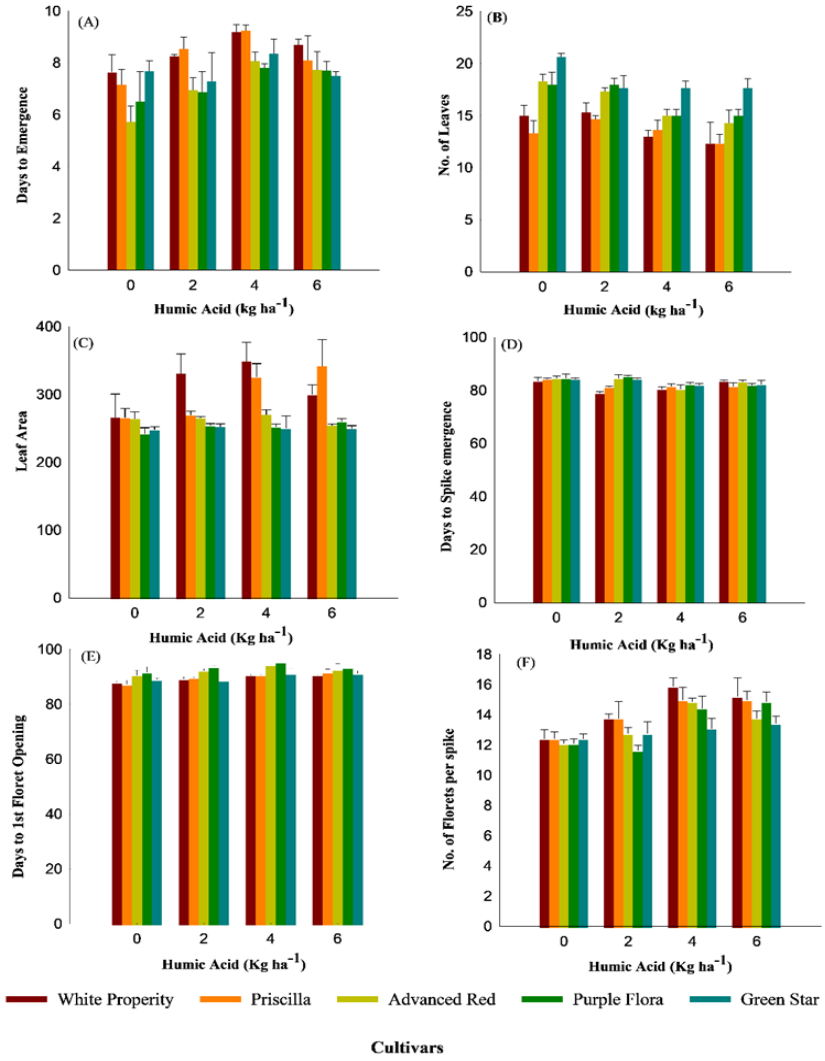

Fig. 1. Effect of humic acid on different gladiolus cultivars, (A) Days to Emergence, (B) No. of Leaves, (C) Leaf Area, (D) Days to spike emergence, (E) Days to floret opening, and (F) No. of florets per spike.

supplied with humic acid @ 4 kg ha^{-1} while the least was recorded in control. Among cultivars, the maximum leaf area was recorded in White Prosperity (312.1 cm^2), followed by Priscilla (301.2 cm^2) and Advance Red (264.2 cm^2), while Green Star produced the minimum leaf area (250.6 cm^2). The spike emergence was significantly influenced by humic acid levels, cultivars, and their interaction (Figure 1(D)). Plots treated with 4 kg ha^{-1} humic acid recorded the earliest spike emergence (70.7 days), followed by 6 kg ha^{-1} (73.5 days) and 2 kg ha^{-1} (74.7 days), while control plots took the longest (75.6 days). Among cultivars, White Prosperity produced the earliest spikes (69.9 days), followed by Priscilla (71.0 days) and Purple Flora (74.7 days), while the highest days to emergence (76.7) was noted in Green Star.

For days to first floret opening, significant effects were observed for humic acid and cultivar, but not for their interaction (Figure 1(E)). Plots treated with 4 kg ha^{-1} humic acid showed the earliest floret opening (76.0 days), followed by 6 kg ha^{-1} (78.7 days) and 2 kg ha^{-1} (79.5 days). The maximum days to floret opening (82.6) were recorded in the control. Among cultivars, White Prosperity opened first (76.9 days), followed by Advance Red (77.6 days), Purple Flora (79.9 days), and Priscilla (80.2 days), with Green Star that took maximum days (81.5) to first floret opening.

The number of florets per spike was greatly influenced by both humic acid levels and cultivars, while their interaction remained non-significant (Figure 1(F)). Maximum florets per spike (14.7) was observed at 4 kg ha^{-1}, followed by 6 kg ha^{-1} (14.5) and 2 kg ha^{-1} (13.0), with the control resulted in least no. of florets per spike (12.30). Among cultivars, White Prosperity produced the highest number of florets (14.3), followed by Priscilla (14.1), Advance Red (13.4), and Purple Flora (13.3), with Green Star recording the minimum (12.9).

Spike length was significantly affected by humic acid levels, cultivars, and their interaction (Figure 2(A)). The longest spike (66.3 cm) was produced with 4 kg ha^{-1} humic acid, followed by 6 kg ha^{-1} (66.2 cm) and 2 kg ha^{-1} (60.4 cm), while the control had the shortest spikes. Among cultivars, White Prosperity produced the longest spikes (67.0 cm), followed by Priscilla (63.2 cm) and Advance Red (62.5 cm), with Purple Flora producing the shortest (60.1 cm). Notably, the maximum spike length (71.5 cm) was recorded from the interaction in gladiolus cv. White Prosperity that received 4 kg ha^{-1} humic acid.

Vase life of gladiolus cultivars was significantly influenced by the different levels of humic acid and cultivars, whereas their interaction was non-significant (Figure 2(B)). The longest vase life (9.3 days) was recorded cut flowers of plants treated with 4 kg ha^{-1} humic acid, followed by 6 kg ha^{-1} (8.4 days) and 2 kg ha^{-1} (7.5 days), while the control showed the shortest (6.1 days). Among cultivars, Advance Red had the longest vase life (9.9 days), followed by White Prosperity (8.4), Priscilla (7.8), and Purple Flora (6.7), with Green Star exhibiting the shortest vase life (6.3 days).

The analysis also indicated that both humic acid and cultivars had a significant effect on field flower persistency, though their interaction was non-significant (Figure 2(C)). The longest field persistency (12.5 days) was observed in plants that received humic acid @ 4 kg ha^{-1}, followed by 6 kg ha^{-1} (11.6 days) and 2 kg ha^{-1} (10.4 days), while the control exhibited the shortest duration. Among cultivars, White Prosperity showed the highest persistency (12.3 days), followed by Priscilla (12.0 days) and Advance Red (10.2 days), while the lowest (8.8 days) was noted for Green Star.

In case of corm weight, there was significant variation in corm weight due to humic acid levels and cultivars, but their interaction was not significant (Figure 2(D)). The heaviest corms were obtained from plots supplied with 4 kg ha^{-1} humic acid (20.7 g), followed by 6 kg ha^{-1} (19.2 g) and 2 kg ha^{-1} (17.4 g), while the control plots that received no humic acid had the lowest weight (13.8 g). Priscilla had the heaviest corms (22.2 g) followed by White Prosperity (18.9 g) and Purple Flora (18.0 g) whereas Green Star produced the lightest corms (14.7 g).

The largest corms (4.3 cm) were obtained at 4 kg ha^{-1} humic acid, followed by 6 kg ha^{-1} (3.9 cm) and 2 kg ha^{-1} (3.7 cm), while the smallest corms were found in control plots (Figure 2(E)). Among cultivars, Priscilla produced the largest corms (4.3 cm), followed by White Prosperity (3.9 cm) and Purple Flora (3.7 cm), while Green Star recorded the smallest corms (3.0 cm).

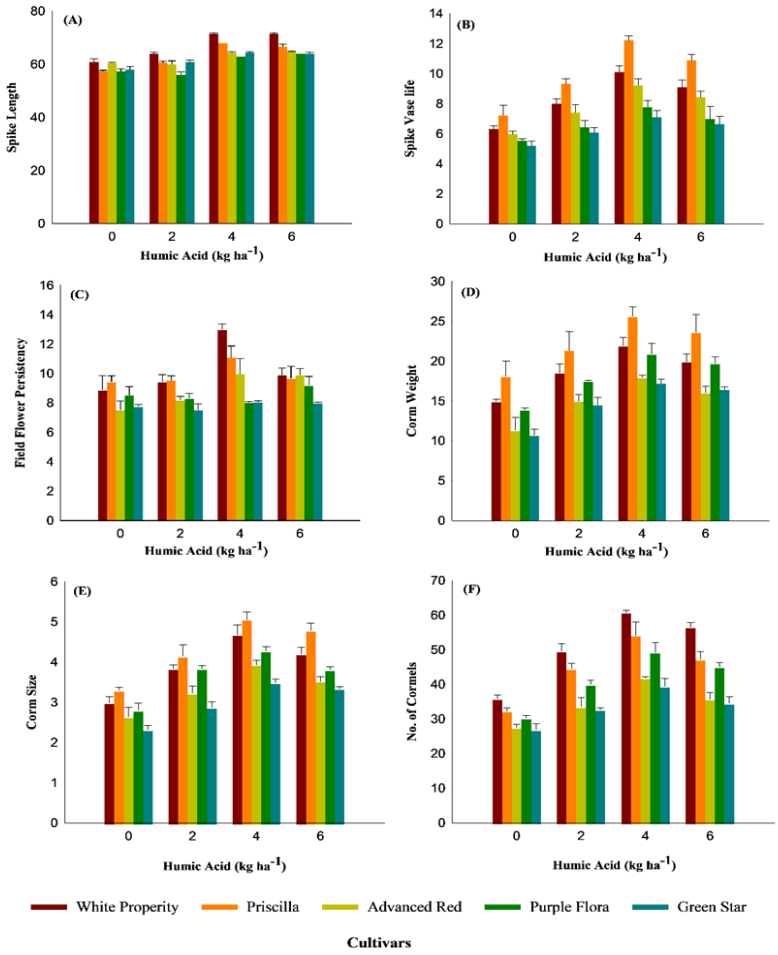

Fig. 2. Effect of humic acid on different gladiolus cultivars, (A) Spike Length, (B) Spike Vase life, (C) Field Flower Persistency, (D) Corm weight, (E) Corm Size, and (F) No. of Cormels.

Lastly, humic acid and cultivars had a significant effect on the number of cormels per plant but the interaction was not significant (Figure 2(F)). Plots treated with 4 kg ha^{-1} had the highest cormels (49.1) and were followed by 6 kg ha^{-1} (43.9), 2 kg ha^{-1} (40.1) and the lowest number (30.6) was recorded in the control. White Prosperity recorded the highest number of cormels (50.7), however least no. of cormels (33.5) were noted in Green Star.

3.1. Principal Component Analysis

The principal component analysis (PCA) was conducted to reduce dimensionality and identify the most influential traits contributing to overall variation among the genotypes (Figure 3(A)). The first principal component (PC1) accounted for 55.9% of the total variance, while the second principal component (PC2) explained an additional 9.6%, making the cumulative contribution of the first two components 65.5%.

The PCA biplot revealed that traits such as corm weight (CW), corm size (CS), number of cormels per plant (NOC), spike length (SL), and number of florets per spike (NOF) were strongly associated with PC1, indicating their dominant role in explaining variability. Conversely, days to first floret opening (DFO) contributed more significantly to PC2. The quality of representation (cos^2) indicated by the color gradient revealed that DFO, CW, and CS were well represented in the two-dimensional space. The accompanying scree plot illustrated a sharp decline in explained variance after the first component, supporting the selection of PC1 and PC2 for interpretation and trait analysis (Figure 3(B)).

The Pearson correlation analysis elucidated the strength and direction of relationships among vegetative, phenological, reproductive, and yield-related traits in gladiolus (Figure 4. Strong and highly significant positive correlations were

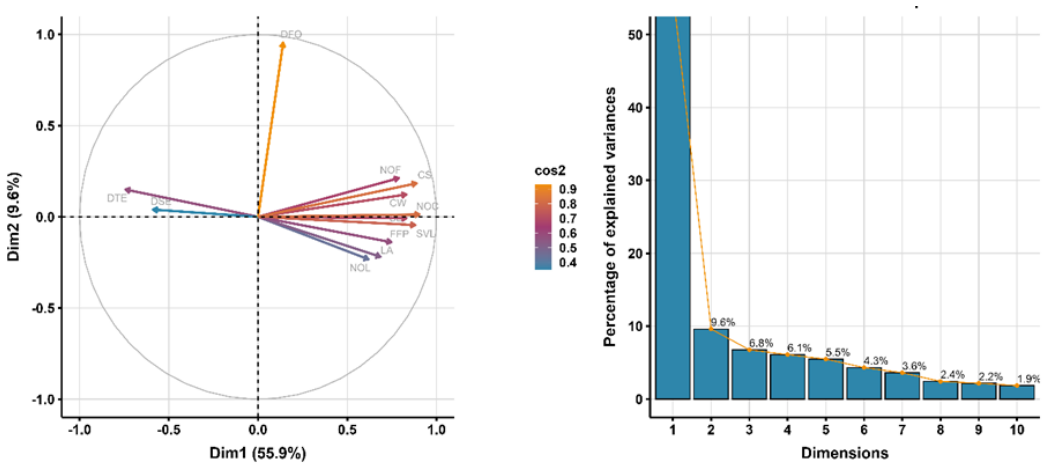

Fig. 3. Principal component analysis (A) and scree plot (B) of the studied attributes of gladiolus.

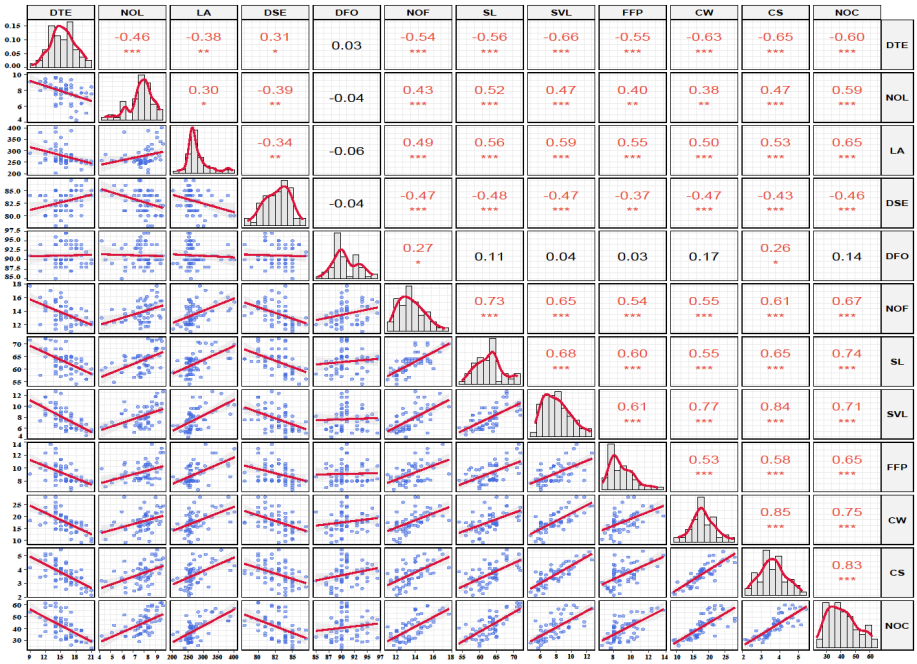

Fig. 4. Correlation matrix of the studied attributes of the gladiolus.

observed among floral and yield attributes, indicating their coordinated contribution to overall plant performance. In particular, corm weight (CW) was positively and significantly correlated with corm size (CS; r = 0.85), number of cormels (NOC; r = 0.75), and spike length (SL; r = 0.65), suggesting that plants producing larger and heavier corms also express superior floral traits.

Conversely, phenological traits such as days to plant emergence (DTE), days to spike emergence (DSE), and days to first floret opening (DFO) exhibited negative correlations with most reproductive and yield-related attributes, indicating that earlier developmental progression favors enhanced flowering and corm productivity. These negative associations, particularly between DTE and CW or SL, were visually represented by red shades in the heatmap, highlighting the inverse relationship between delayed phenology and reproductive performance. Moderate positive correlations were also observed among vegetative traits, including number of leaves per plant (NOL), leaf area (LA), field flower persistency (FFP), and spike vase life (SVL), reflecting their indirect yet meaningful contribution to floral longevity and yield.

The correlation heatmap (Figure 5) provided an intuitive visualization of these relationships by integrating correlation strength and significance through color intensity and symbol size. Strong positive associations among CW, CS, SL, number of florets (NOF), and NOC were depicted by large, dark blue circles, reinforcing patterns observed in the correlation matrix. In contrast, traits such as DFO exhibited several non-significant associations, marked by 'X' symbols, suggesting that their variation may be regulated by different or more independent factors. Overall, the heatmap effectively complements the correlation matrix and PCA results by visually confirming key trait interrelationships that are critical for targeted breeding and selection programs.

4. DISCUSSION

Humic acid is a well-known organic fertilizer that is very effective in the early emergence of gladiolus plants as it as soil conditioner and helps to improve soil structure, lower soil pH, and raise the availability of nutrients [13]. It enhances root development and metabolic activity, which increases the release of stored energy in corms, and hence increase the rate of emergence [14, 15]. Furthermore, soil consisting of humic acid is more porous, which makes sprouting more favorable [16]. The variability in days to emergence among different cultivars might be due to the differences in their genetic constitution, which influences their physiological responses in the prevailing soil and environmental conditions [17]. Our findings are in line with that of Rizwan *et al.* [18], they also reported significant differences in plant emergence in gladiolus cultivars grown in Peshawar condition. The positive effect of humic acid application on the number of leaves per plant is due to enhanced absorption of essential nutrients such as nitrogen, potassium, and trace elements [19]. They are essential nutrients having directly or indirectly a role in the biosynthesis of chlorophyll and cellular metabolism as well as continuous leaf formation [20]. The increase in nutrient availability causes a more vigorous shoot meristem encouraging growth in the leaves [21]. Our results are in agreement with that of Baldotto and Baldotto [22]; they also reported significant increase in no. of leaves in plants treated with humic acid. The variation in the number of leaves in the cultivars also depend on how efficiently they used the available nutrients and control their growth [19]. Likewise, Nasir *et al.* [11] also reported a significant variation in leaves no. among gladiolus cultivars grown under the agro-climatic conditions of Peshawar.

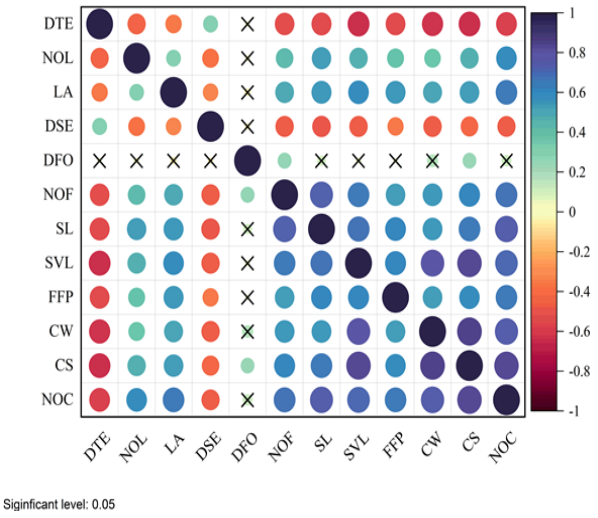

Fig. 5. Heat map of the studied attributes of gladiolus.

Being acidic in nature and a good soil conditioner, humic acid may cause better absorption of other essential plant nutrients such as nitrogen, potassium, and trace elements for improved vegetative growth [23]. The increased nutrient uptake causes an increase in the activity of the shoot meristem that stimulate the development of leaves [24]. Humic acid is also reported to improve shoot formation due to enhanced uptake of nutrients and development of chlorophyll and other pigmented compounds [25]. Humic acid improves the hormonal balance of the plants and increases cell division, and expansion, resulting in larger leaf area [10].

The earlier emergence of spike on treatment with humic acids suggests an accelerated shift in growth between vegetative and reproductive growth. Hormonal balance, and in particular gibberellins and cytokinins can regulate and stimulate flower bud initiation in plants raised on the soil with optimum level of humic substances [26]. Better root systems also facilitate the acquisition of nutrients which facilitates the development of reproductive organs [27]. This interaction between the level of humic acid and cultivars was significant and these findings indicated that there were some cultivars that are more sensitive to hormones or efficient in resource allocation in terms of being grown in

enriched conditions. Early floret opening is usually observed due to better physiological condition and optimal water and nutrient supply [28]. Humic acid helps in enhanced root development, which makes it easy to absorb nutrients, leading to fast growth of flowers [29]. Optimum concentrations of the humic acid improve flowering due to reduced stress and more allocation of resources to the reproductive organs with improved source-sink relationship [30].

Enhanced florets per spike in response to humic acid might be due to the enhanced photosynthesis and production of energy. The increase in availability of nutrients, in particular phosphorus and potassium, by the presence of humic acid favors the development of the floral meristem and floret differentiation [31]. It also stimulates hormonal messages that control flowering [32]. Variability occurred because cultivars differed in the intrinsic genetic ability to transform nutrients into reproductive output in the form of floret production [33]. Humic acid enhanced spike elongation considerably, due to the enhanced nutrient and water base uptake and regulated auxins that initiate cell elongation [14]. With a better soil, the vascular system grows stronger and internode grows big [34]. The profound interaction between humic acid and cultivar indicates that some genotypes including the White Prosperity are more responsive to such favorable growth conditions and hence exhibited taller spikes. Our results are similar as those of Hassan *et al.* [14] they also reported significant increase in spike length of gladiolus cv. White prosperity.

The higher persistency of field flowers is associated with better retention of reducing and non-reducing sugars and also due to the osmotic balance [35], and provision of humic acid to the plants. Producing better nutrient retention and stress tolerance, humic acid delays senescence and preserves cell integrity of floral tissues [36]. Such genotypes as 'White Prosperity' are less liable to be discolored in the fields as they have better quality metabolic and structural stability. The prolonged vase life on the use of humic acid is probably through increased calcium and other building nutritious intake which makes the cell walls stronger and less prone to oxidative stress [37]. Humic acid also plays a role in hormonal balance to slow down the process of senescence and maintain color and shape of petals [38]. Similarly, humic acid has significant role in calcium uptake of the plants that enhances the membrane stability and increase vase life in cut flowers of tuberose [39]. Changes in the cell structure, rate of transpiration, and post-harvest metabolism can explain variation in the vase life among cultivars.

Higher photosynthetic efficiency and nutrient transport result in greater biomass distribution of plants to corm development [36]. Higher corm weight of the cultivars probably indicates an increased sink strength and shows capacity to allocate biomass with the best possible growing settings [40]. The increased size of the corm can be attributed to increase of nutrient accessibility and hormonal activity that causes division and expansion of cells under the humic acid treatment [14]. The presence of more essential nutrients such as phosphorus and potassium due to the presence of humic acid contributes towards the growth of the corms [40]. Humic acid improves the calcium use efficiency of the plants which ameliorate the weight of corms in gladiolus thereby results in significant increase in corm production per unit area [41, 42]. The variation between different cultivars can be attributed to genotypic differences where some cultivars are more vigorously growing [43]. Humic acid caused a significant improvement in vegetative attributes such as number of leaves and leaf area (Figure 1(B and C)), resulted in healthy plants with enhanced nutrient uptake [44] and hence resulted in better production of cormels in gladiolus.

5. CONCLUSIONS

Applying humic acid at a rate of 4 kg ha^{-1} enhanced the vegetative and reproductive traits of gladiolus. It significantly improved almost all the measured vegetative and reproductive parameters. Among cultivars, White Prosperity showed improvements in spike length, leaf area, number of florets, number of cormels, and field flower persistence, while Priscilla demonstrated better vase life, corm size, and corm weight. Therefore, humic acid at 4 kg ha^{-1} is recommended for better performance of gladiolus while cultivars White prosperity and Pricilla could be grown for better flowers and corm production under the agro-climatic conditions of Peshawar.

6. CONFLICT OF INTEREST

The authors have declared no conflict of interest.

7. REFERENCES

1. M. Kumar, V. Chaudhary, U. Sirohi, J. Singh, M.K. Yadav, S. Prakash, A. Kumar, V. Kumar, V. Pal, C. Chauhan, and K. Kaushik. In Vitro Propagation Journey of Ornamental Gladiolus (*Gladiolus Species*): a systematic review analysis based on more than 50 years Research. *Horticulturae* 10(2): 148 (2024).
2. A. Javaid, R.K. Pandey, A.H. Shah, P. Bakshi, I.T. Nazki, N. Kaushal, G. Chand, S. Dogra, R. Kumar, A.K. Singh, and A. Singh. Response of *Gladiolus grandiflorus* varieties to planting date: effects on growth, flowering, and vase life. *BMC Plant Biology* 25(1): 481 (2025).
3. M. Bala and F. Sala. Comparative analysis of some Gladiolus varieties in relation to vegetative indices and floral quality parameters. *Scientific Papers Series Management, Economic Engineering in Agriculture and Rural Development* 21(3): 159-166. (2021).
4. N. Devrani, P. Kakkar, A. Sahu, and C. Tiwari. Global trends in floriculture. In: Floriculture and Landscaping Chronicles: A Collaborative Insights. A. Burud, S.M. Kolur, D.R. Karthik, D.L. Kumar, D. Yadav, and N. Kaushal (Eds.) *Stella International Publication, Haryana, India* pp. 190-221 (2023).
5. M. Ahmad and A. Rab. Calcium effects on post-harvest attributes and vase life of gladiolus using different methods of application. *Pakistan Journal of Botany* 52(1):167-179 (2020).
6. K. Ampong, M.S. Thilakaranthna, and L.Y. Gorim. Understanding the role of humic acids on crop performance and soil health. *Frontiers in Agronomy* 4: 848621 (2022).
7. R.E. Pettit. Organic matter, humus, humate, humic acid, fulvic acid and humin: their importance in soil fertility and plant health. *CTI Research* 10: 1-7 (2004). https://earthwiseagriculture.net/wp-content/uploads/2018/02/ORGANICMATTERPettit.pdf.
8. F. Nabi, A. Sarfaraz, R. Kama, R. Kanwal, and H. Li. Structure-based function of humic acid in abiotic stress alleviation in plants: a review. *Plants* 14(13): 1916 (2025).
9. J. Tiwari, A.L. Ramanathan, K. Bauddh, and J. Korstad. Humic substances: Structure, function and benefits for agroecosystems-A review. *Pedosphere* 33(2): 237-249 (2023).
10. Q. Chen, Z. Qu, G. Ma, W. Wang, J. Dai, M. Zhang, Z. Wei, and Z. Liu. Humic acid modulates growth, photosynthesis, hormone and osmolytes system of maize under drought conditions. *Agricultural Water Management* 263:107447 (2022).
11. S. Nasir, M. Ahmad, H. Ali, S. Jabin, A. Khan, M. Ullah, A. Bano, H.A. Khan, A. Khan, and A. Ullah. Performance of Gladiolus Cultivars on Morphological Traits and Corm Production under the Agro-Climatic Conditions of Peshawar-Pakistan. *Indus Journal of Bioscience Research* 3(1): 58-63 (2025).
12. H. Ali, M. Ahmad, S. Jabin, R.Z. Muqarrab, I. Ahmad, M.A. Khan, M. Khan, I. Khalil, A. Basit, M. Kamal, and M. Ahmad. Influence of willow bark extracts and application times on the production of Roselle. *Plant Protection* 8(4): 671-677 (2024).
13. R.S. Nada, M.N. Soliman, M.M. Zarad, M.H. Sheta, S. Ullah, A.I. Abdel-Gawad, A.H. Ghoneim, and A.A. Elateeq. Effect of Organic Fertilizer and Plant Growth-Promoting Microbes on Growth, Flowering, and Oleanolic Acid Content in *Calendula officinalis* under Greenhouse Conditions. *Egyptian Journal of Soil Science* 64(3): 815-831 (2024).
14. M. Hassan, S.A. Shaaban, R.A. El Ziat, and K.A. Khaled. Laser-induced changes in the gene expression, growth and development of gladiolus grandiflorus cv.“White prosperity”. *Scientific Reports* 14(1): 6257 (2024).
15. K. Decsi, M. Ahmed, R. Rizk, D. Abdul-Hamid, and Z. Tóth. Analysis of plant physiological parameters and gene transcriptional changes under the influence of humic acid and humic acid–amino acid combinations in maize. *International Journal of Molecular Sciences* 25(24): 13280 (2024).
16. P. Bhatt and V.K. Singh. Effect of humic acid on soil properties and crop production-A review. *Indian Journal of Agricultural Sciences* 92(12): 1423-1430 (2022).
17. R. Motzo and F. Giunta. The effect of breeding on the phenology of Italian durum wheats: from landraces to modern cultivars. *European Journal of Agronomy* 26(4) 462-470 (2007).
18. M. Rizwan, M. Ahmad, A.M. Khattak, A. Mohammad, F. Ali, G. Nabi, S. Ayaz, and N. Ayaz. Influence of organic potash on the vegetative attributes and corm production of gladiolus cultivars. *Bioscience Research* 18(4): 3326-3333. (2021).
19. K.S. Karthika, I. Rashmi, and M.S. Parvathi. Biological functions, uptake and transport of essential nutrients in relation to plant growth. In: Plant Nutrients and Abiotic Stress Tolerance. M. Hasanuzzaman, M. Fujita, K. Nahar, B. Hawrylak-Nowak, and H. Oku (Eds.). *Springer Nature Singapore* pp. 1-49. (2018).
20. H.M. Fan, X.W. Wang, X. Sun, Y.Y. Li, X.Z. Sun,

and C.S. Zheng. Effects of humic acid derived from sediments on growth, photosynthesis and chloroplast ultrastructure in chrysanthemum. *Scientia Horticulturae* 177: 118-123 (2014).
21. J.A.H. Murray, A. Jones, C. Godin, and J. Traas. Systems analysis of shoot apical meristem growth and development: integrating hormonal and mechanical signaling. *The Plant Cell* 24(10): 3907-3919 (2012).
22. M.A. Baldotto and L.E.B. Baldotto. Gladiolus development in response to bulb treatment with different concentrations of humic acids. *Revista Ceres* 60: 138-142 (2013).
23. Z. Rengel and P.M. Damon. Crops and genotypes differ in efficiency of potassium uptake and use. *Physiologia Plantarum* 133(4): 624-636 (2008).
24. S.K. Verma, P.K. Sahu, K. Kumar, G. Pal, S.K. Gond, R.N. Kharwar, and J.F. White. Endophyte roles in nutrient acquisition, root system architecture development and oxidative stress tolerance. *Journal of Applied Microbiology* 131(5): 2161-2177 (2021).
25. A.C. Souza, F.L. Olivares, L.E.P. Peres, A. Piccolo, and L.P. Canellas. Plant hormone crosstalk mediated by humic acids. *Chemical and Biological Technologies in Agriculture* 9(1): 29 (2022).
26. M. Babarabie, H. Zarei, S. Badeli, A. Danyaei, and F. Ghobadi. Humic acid and folic acid application improve marketable traits of cut tuberose (*Polianthes tuberosa*). *Journal of Plant Physiology and Breeding* 10(1): 85-91 (2020).
27. S. Proietti, V. Scariot, S. De Pascale, and R. Paradiso. Flowering mechanisms and environmental stimuli for flower transition: bases for production scheduling in greenhouse floriculture. *Plants* 11(3): 432 (2022).
28. S.Q. Zhang, L. Yuan, Z.A. Lin, Y.T. Li, S.W. Hu, and B.Q. Zhao. Advances in humic acid for promoting plant growth and its mechanism. *Journal of Plant Nutrition and Fertilizers* 23(4): 1065-1076 (2017).
29. A. El-Naggar and G.F.M. Imhmd. Influence of humic acid and mineral nutrition on the growth, yield of flowers and the chemical constituents of Rosa hybrida L. *Scientific Journal of Flowers and Ornamental Plants* 10(1): 17-26 (2023).
30. O.A. Ali. Role of humic substances and compost tea in improvement of endogenous hormones content, flowering and yield and its components of faba bean (*Vicia faba* L.). *Annals of Agricultural Science, Moshtohor* 53(3): 373-384 (2015).
31. A. Raza, A. Razzaq, S.S. Mehmood, X. Zou, X. Zhang, Y. Lv, and J. Xu. Impact of climate change on crops adaptation and strategies to tackle its outcome: a review. *Plants* 8(2): 34 (2019).
32. M.S. Elmongy, X. Wang, H. Zhou, and Y. Xia. Humic acid and auxins induced metabolic changes and differential gene expression during adventitious root development in azalea microshoots. *HortScience* 55(6): 926-935 (2020).
33. S.M. McKim. How plants grow up. *Journal of Integrative Plant Biology* 61(3): 257-277 (2019).
34. F.G. Rahbar, A. Vaziri, M.H. Asil, S.T. Sasani, and J. Olfati. Effects of humic acid on antioxidant defense system and senescence-related gene expression in leaves of *longiflorum* × *asiatic lilies* (LA lilium hybrid). *Journal of Soil Science and Plant Nutrition* 23(3): 3500-3507 (2023).
35. H.M. Fan, T. Li, X. Sun, X.Z. Sun, and C.S. Zheng. Effects of humic acid derived from sediments on the postharvest vase life extension in cut chrysanthemum flowers. *Postharvest Biology and Technology* 101: 82-87 (2015).
36. T. Zhou, X. Qiu, L. Zhao, W. Yang, F. Wen, Q. Wu, and J. Pei. Optimal light intensity and quality increased the saffron daughter corm yield by inhibiting the degradation of reserves in mother corms during the reproductive stage. *Industrial Crops and Products* 176: 114396 (2022).
37. W.H. Mohamed. Effects of humic acid and calcium forms on dry weight and nutrient uptake of maize plant under saline condition. *Australian Journal of Basic and Applied Sciences* 6(8): 597-604 (2012).
38. M.A. Shajari, P.R. Moghaddam, R. Ghorbani, and A. Koocheki. Increasing saffron (*Crocus sativus* L.) corm size through the mycorrhizal inoculation, humic acid application and irrigation managements. *Journal of Plant Nutrition* 41(8): 1047-1064 (2018).
39. R. Sarje, A.K. Abhangrao, S. Jayakumar, R. Gupta, S. Pathania, and B.V. Sree. Effect of pre and postharvest factors on vase life of gladiolus or effect of different floral preservatives on vase life of gladiolus. *International Journal of Plant & Soil Science* 36(7): 297-303 (2024).
40. M. Hamad and M. Tantawy. Effect of different humic acids sources on the plant growth, calcium and iron utilization by sorghum. *Egyptian Journal of Soil Science* 58(3): 291-307 (2018).
41. M. Ahmad and A. Rab. Exogenous application of calcium improved the vegetative attributes and corm production in gladiolus. *Sarhad Journal of Agriculture* 35(3): 1011-1019 (2019).
42. M. Wyszkowski, N. Kordala, and M. S. Brodowska. Trace element content in soils with nitrogen fertilisation and humic acids addition. *Agriculture*

13(5): 968 (2023).
43. M. Ahmad, W. Iqbal, U. Ahmed, A. Jamal, M.F. Saeed, M.S. Elshikh, M.F. Elsadek, M.A. Ali, J. Černý, and D. Ronga. Enhancing floret persistence and bloom duration in gladiolus through foliar-applied calcium: a sustainable approach to floriculture. *The Journal of Horticultural Science and Biotechnology* 100(6): 775-788 (2025).
44. X. Wang, J. Zhang, J. Shen, L. Zhang, P. Wei, A. Liu, and H. Song. The alleviating effect on the growth, chlorophyll synthesis, and biochemical defense system in sunflowers under cadmium stress achieved through foliar application of humic acid. *BMC Plant Biology* 24(1): 792 (2024).

Proceedings of the Pakistan Academy of Sciences: B
Life and Environmental Sciences 62(4): 295-305 (2025)

ISSN (Print): 2518-4261; ISSN (Online): 2518-427X
http://doi.org/10.53560/PPASB(62-4)1113

Pakistan Academy of Sciences

Research Article

Developmental Biology and Morphometric Studies of Fall Armyworm (*Spodoptera frugiperda*) on Cotton under Laboratory Conditions

Munesh Kumar[1], Arfan Ahmed Gilal[1*], Lubna Bashir Rajput[1], Sohail Ahmed Otho[2], and Jay Kumar Sootaher[3]

[1]Department of Entomology, Faculty of Crop Protection, Sindh Agriculture University, Tandojam, Sindh, Pakistan

[2]Department of Plant Protection, Faculty of Crop Protection, Sindh Agriculture University, Tandojam, Sindh, Pakistan

[3]Barley and Wheat Research Institute, Tandojam, Wheat Research Center, Sakrand, Sindh, Pakistan

Abstract: The life cycle and morphometric characteristics of fall armyworm, *Spodoptera frugiperda* (Lepidoptera: Noctuidae), on cotton were studied under laboratory conditions at the Stored Grain Research Laboratory, Department of Entomology, Faculty of Crop Protection, Sindh Agriculture University, Tandojam. Ten individuals of each stage, i.e., egg, six larval instars, pupae, and adults (males and females) were observed to observe their development duration and record various morphometric parameters which were then presented as mean ± SE calculated using MS-Excel. The obtained results indicated that the mean egg hatching period was recorded as 2.33 ± 0.05 days. The mean developmental duration of six larval instars was recorded as 5.11 ± 0.30, 6.17 ± 0.27, 5.81 ± 0.21, 5.78 ± 0.26, 5.63 ± 0.27, and 4.53 ± 0.27 days, respectively, with total larval development completed in 32.06 ± 0.21 days. The mean pupal period was 9.63 ± 0.23 days, as the total life cycle of *S. frugiperda* was completed in 43.92 ± 0.72 days. Mean adult longevity of males was recorded as 7.90 ± 0.29 days and 9.60 ± 0.19 days for females. Mean fecundity of *S. frugiperda* was recorded as 407.50 ± 13.76 eggs per female. The lengths of the six larval instars were 1.68 ± 0.05, 3.32 ± 0.07, 6.94 ± 0.07, 12.87 ± 0.46, 19.78 ± 0.34, and 31.95 ± 0.27 mm, respectively, while their mean width was 0.30 ± 0.01, 0.60 ± 0.02, 1.43 ± 0.06, 1.91 ± 0.04, 3.26 ± 0.11, and 4.41 ± 0.07 mm, respectively. The head capsule radius of all six instars was recorded as 0.14 ± 0.01, 0.23 ± 0.01, 0.37 ± 0.01, 0.76 ± 0.01, 1.02 ± 0.02, and 1.83 ± 0.03 mm. The mean larval weight from the 3rd to 6th instars and pupa was 0.08, 0.14, 0.23, 0.42, and 0.15 g, respectively. Therefore, obtained results clearly indicated that *S. frugiperda* has the potential to survive and grow on cotton, a major cash crop in Pakistan. Therefore, it is recommended that appropriate measures should be taken to restrict its spread on key crops of Pakistan, i.e., cotton, to reduce economic losses.

Keywords: Fall Armyworm, Invasive Insect Pest Species, Morphometrics, Cotton Crop.

1. INTRODUCTION

Fall armyworm, *Spodoptera frugiperda* (J.E. Smith) (Lepidoptera: Noctuidae) has recently emerged as one of the most destructive insect pests of maize and other important crops [1, 2]. *Spodoptera frugiperda* is a polyphagous pest, damaging different crops such as maize, millet, cotton, rice, sorghum, sugarcane, and more than 80 other crops in subtropical and tropical regions [3-5]. *Spodoptera frugiperda* is capable of feeding on almost all above-ground plant components of its hosts. On immature corn, larvae eat on the surface of the leaves, leaving behind just white papery areas known as windowpanes. Older larvae devour more tissues, have stronger mandibles, and cut huge parts of plant tissues with high silica content, such as seedlings, leaves, tassels, cobs, husks, and

Received: August 2025; Revised: November 2025; Accepted: December 2025
* Corresponding Author: Arfan Ahmed Gilal <aagilal@sau.edu.pk>

developing kernels [6]. Adults of *S. frugiperda* can travel 100 kilometers in a single night, hence contribute to its spread and invasiveness. The presence of this migratory pest also spread in Africa and Australia in 2016 and 2020 in Asia. In Asia, it causes more damage and becomes a major pest of maize [3].

Temperature has a significant impact on growth as the Fall armyworm completes its life cycle in one month during the summer at a temperature of 28 °C, it takes between 60 and 90 days throughout the spring, fall, and winter months [7]. *Spodoptera frugiperda* has four life stages, i.e., egg, larva, pupa, and adult. The female lays 100-200 eggs in clusters during its whole life span on the underside or surface of the leaf, as well as on the top apex of the leaf and on other surfaces such as stems [7]. Duration of egg stage is only 2–3 days during warm conditions. Newly hatched larvae consume little amount of food but when they reach at fifth to sixth larval stage, they consume large amount of food [8]. Constant pest fecundity under favorable environmental conditions is expected to cause significant crop damage [6]. The larvae are the most harmful stage of *S. frugiperda* because early first and second instars eat on one side of the leaves, skeletonizing them, whereas final instars feed on all above-ground parts of their hosts [3]. *Spodoptera frugiperda* do the most harm between stages 3 and 6 of maize, when they reach the whorls' protective zones. Feeding in the early stages destroys the growth points, resulting in no further leaf or cob development. Normally, one or two larvae feed in a whorl as larger larvae might feed on smaller larvae to lessen competition [9].

Fall armyworms can quickly destroy a crop, causing significant economic damage to farmers. The fall armyworm is a very damaging pest of many economically essential crops throughout the world [9]. In 2018, *S. frugiperda* caused a massive loss in maize for the first time in India [10]. *Spodoptera frugiperda* can cause huge profit losses in various economically important crops as a notorious pest. Bannor *et al.* [11] observed that corn plant is favorite of *S. frugiperda* and normally causes 15-73% yield losses in maize; they concluded that the decrease in maize yield by *S. frugiperda* is about 8.3 to 20.6 million tons annually. Mostly soft leaf parts are eaten by fresh caterpillars, creating holes in leaves; this is the characteristic loss sign of *S. frugiperda* [12]. All six instars of *S. frugiperda* caterpillars are the harmful stage for their host. The initial two instars of the caterpillar generally eat from the sides of the leaves and empty them, and the final instars eat all parts of their host's plant [11]. Despite its importance, there is still a lack of knowledge on its biology and life cycle, which hampers the development of effective management strategies [13]. The life cycle of *S. frugiperda* is comprised of egg, six larval instars, pupa, and adult male and female, which make their effective management more difficult [7]. Therefore, continuous research on the various biological aspects and management options of *S. frugiperda* could be very helpful in its effective management [14].

Morphometrics analysis can reveal important information about the growth and development of insects [15]. The length and width of the head capsule of an insect can provide an estimate of its age and nutritional status, while the length and weight of the body segments can indicate the rate of growth and development [16]. *S. frugiperda*, previous studies have shown that the morphometrics of larvae can be influenced by various factors, such as temperature, humidity, and host plants [17]. As *S. frugiperda* is a highly polyphagous pests that can survive on alternate hosts in absence of its primary host (maize), therefore, this study was conducted to understand its life cycle parameters and morphometric on cotton, a cash crop of Pakistan under laboratory conditions. The obtained results could help to take appropriate measures to prevent *S. frugiperda* losses to cotton that is already vulnerable to many insect pests, and the same can result in improved cotton yield.

2. MATERIALS AND METHODS

The research work was carried out at the Stored Grain Research laboratory, located within the Department of Entomology, Faculty of Crop Protection at Sindh Agriculture University in Tandojam during 2023-24.

2.1. Rearing and Handling of *Spodoptera frugiperda*

The initial culture of *S. frugiperda* was obtained by collecting larvae from a field near Tandojam. The culture was carefully collected from the growing maize in the field, put in plastic jars covered with

a fine mesh net, and brought into the laboratory. In the lab, the larvae were shifted into plastic bowls provided with freshly cut cotton leaves as food till the pupation. After pupation, the pupae were transferred into a glass cage covered with a net for adult emergence. The laboratory was maintained at a temperature of 28 ± 2 °C and a relative humidity of 75 ± 5% throughout the process [18]. After the emergence of adults, the adults were placed in an insect cage along with fresh cotton leaves for egg laying, whose petiole was surrounded with wet cotton to retain their freshness, and a 10% honey mixed with water solution was given to the adults as food. On a daily basis, the eggs deposited on cotton leaves were separated and placed in a petri dish for hatching. This process has been used to rear the culture of *S. frugiperda* [19].

2.2. Experimental Set-up and Data Collection

The bunch of eggs was kept in a Petri dish at a laboratory-maintained temperature until they hatched. When the eggs hatched, the 1st instar larvae were counted and then placed in a Petri dish and given soft cotton leaves regularly to eat until they reached the 3rd instar. After reaching the 3rd instar, all the larvae were separated and put in plastic bowls separately to avoid cannibalism. All the life cycle parameters, i.e., hatching period, development period of larvae and pupae, along with longevity of adults (male and female) were observed. Ten individuals of respective *S. frugiperda* stages were observed to record various morphometric parameters, i.e., length, width, and head capsule radius. After adult emergence, the 10 pairs of *S. frugiperda* adults were kept in glass cages, and observed regularly to recorded data regarding pre-oviposition, oviposition, and post-oviposition period along with fecundity per female on cotton.

2.3. Egg Duration

The bunch of 370 eggs was kept in a petri dish at a controlled laboratory temperature of 28 ± 2 °C and humidity of 75 ± 5% for 2-3 days. The eggs were observed daily. After three days, the eggs were hatched, and the larvae were counted to determine the percentage of hatching. Then they were given soft cotton leaves as food for eating for their further development [18].

2.4. Larval Duration and Development

Ten fall army larvae were separately placed in plastic bowls with small holes in the bowls for aeration. They were fed fresh cotton leaves on a daily basis until they reached the pupal stage [3]. During the larval period, changes in shape and weight were recorded throughout six larval stages. The weight of 3rd to 6th larval instars was measured on an electronic weight balance; the weight of 1st and 2nd instars was not taken in this study because of their minimal weight, as the same was not possible using the available balance. The length and width of the 1st to 3rd instars were taken using a digital USB microscope. While the length and width of 4th-6th instar larvae were measured using a digital Vernier caliper. The head capsule's radius was also measured using a digital USB microscope. Additionally, ten pre-pupae were placed in separate pupal glass containers to monitor the percentage of pupation, and their progress was observed for adult emergence [20].

2.5. Pupal Duration and Development

The newly developed pupae were placed inside a glass cage and observed until adult moths emerged. The time period between pupation and adult emergence was noted. The weight of pupae was measured on an electronic weight balance, and the pupal length and width were measured and recorded.

2.6. Adult Longevity

Adult male and female moths (with a ratio of 1 male to 1 female) were placed in a glass cage. A cotton ball soaked in a 10% honey solution was given as food for eating. The number of male and female moths that died in each cage was recorded daily until the last adult in the cage had died. This data was utilized as an indicator of the adult moths' lifespan [21].

2.7. Data Analysis and Presentation

MS-Excel was used to determine the mean and standard error values of the various recorded parameters [22].

3. RESULTS

3.1. Life Cycle of *Spodoptera frugiperda* on Cotton Crop

3.1.1. Development period of various life stages of Spodoptera frugiperda on cotton crop

Table 1 shows the results regarding the development period of various life stages of *S. frugiperda* on cotton. The data on the hatching period of *S. frugiperda* eggs indicated that they have an average hatching period of 2.33 ± 0.05 days, with the lowest and highest hatching intervals recorded as 1.85 and 2.80 days, respectively. *Spodoptera frugiperda* larval development consists of six instars, each of which has a different color, shape, and size. The 1st instar larvae of *S. frugiperda* were greenish with a black head and body covered with tiny hairs, as its average development duration was recorded as 5.11 ± 0.30 days with a minimum and maximum developmental duration of 3.55 and 5.11 days, respectively. The 2nd instar larvae of *S. frugiperda* have shown morphological features like a yellow-white body and brownish-colored head with inverted Y-line on frons which is the main character for its identification. The mean development period of 2nd instar larvae was observed as 6.17 ± 0.27 days with minimum and maximum duration of 4.98 and 7.56 days, respectively. The 3rd instar *S. frugiperda* larvae was active having four black spots on its body, as it completed its development in mean duration of 5.81 ± 0.21 days as its minimum and maximum development durations were recorded as 4.55 and 6.43 days, respectively. Similarly, minimum and maximum development durations of 4th instar *S. frugiperda* larvae were recorded as 3.93 and 6.21 days, respectively, with mean development period of 5.78 ± 0.26 days. A change in color was observed in 5th instar which become greyish brown as its minimum and maximum development were completed within 4.23 and 6.54 days, respectively, whereas its mean period of development was observed as 5.63 ± 0.27 days. The final 6th instar larvae were flashy and cylindrical in shape which completed their development within mean duration of 4.53 ± 0.27 days, whereas their minimum and maximum development periods were observed as 3.12 and 5.97 days, respectively. Overall, the entire larval period of *S. frugiperda* on cotton leaves was recorded as 32.06 ± 0.21 days. The newly developed pupa of *S. frugiperda* was soft and greenish in color, later it changed to dark brown color till the emergence of the adult. The observed data showed that the minimum and maximum durations of the pupal stages varied from 8.45 to 10.55 days, respectively, with a mean duration of 9.63 ± 0.23 days. Thus, the total life cycle (egg to adult) of *S. frugiperda* was noted as 43.92 ± 0.72 days (Table 1).

3.1.2. Adult longevity (male and female) of Spodoptera frugiperda on cotton crop

The results regarding the adult longevity of *S. frugiperda* feeding on cotton are given in Table 2. It was observed in the study that female adults lived comparatively a little longer than males. The forewing of the male is shaded with gray and brown, with a triangular white patch at the apical region and a circular spot at the center of the wing. The mean observation longevity of *S. frugiperda* male

Table 1. Development period of various life stages of *Spodoptera frugiperda* on cotton.

Developmental period	Days		
	Minimum	Maximum	Average
Hatching Period	1.85	2.80	2.33 ± 0.05
1st instar Larva	3.55	5.11	5.11 ± 0.30
2nd instar Larva	4.98	7.56	6.17 ± 0.27
3rd instar Larva	4.66	6.77	5.81 ± 0.21
4th instar Larva	4.55	6.43	5.78 ± 0.26
5th instar Larva	4.23	6.54	5.63 ± 0.27
6th instar Larva	3.12	5.97	4.53 ± 0.27
Total Larval Duration (six instars)	-	-	32.06 ± 0.21
Pupal Period	8.45	10.55	9.63 ± 0.23
Total Life Cycle (egg to adult)	-	-	43.92 ± 0.72

Table 2. Adult longevity of *Spodoptera frugiperda* on cotton.

Life stage	Days		
	Minimum	Maximum	Average
Male	6.55	9.12	7.90 ± 0.29
Female	8.77	10.56	9.60 ± 0.19

adults was recorded as 7.90 ± 0.29 days, whereas its lowest and highest intervals were recorded as 6.55 and 9.12 days, respectively. The forewing of the female is uniform grayish brown to a fine mottling of gray and brown. The hind wing is silver, white with a narrow dark border in both male and female. The result showed that *S. frugiperda* female adult's minimum and maximum longevity intervals was observed as 8.77 and 10.56 days respectively, and its mean longevity was recorded as 9.60 ± 0.19 days.

3.2. Morphometric Parameters of *Spodoptera frugiperda* on Cotton Crop

3.2.1. Morphometric of various larvae instars and pupae of Spodoptera frugiperda on cotton crop

Table 3 describes the results of various morphometric parameters of *S. frugiperda* larval instars and pupa when reared on cotton. According to the results of the study, minimum and maximum lengths of 1st, 2nd, 3rd, 4th, 5th, and 6th instar larvae were recorded as 1.44 and 1.91 mm, 3.11 and 3.71 mm, 6.54 and 7.25 mm, 11.20 and 15.50 mm, 17.60 and 21.10 mm, and 30.40 and 33.10 mm, respectively. The average length of *S. frugiperda* larvae from 1st to 6th instars were recorded 1.68 ± 0.05, 3.32 ± 0.07, 6.94 ± 0.07, 12.87 ± 0.46, 19.78 ± 0.34, and 31.95 ± 0.27 mm, respectively. Moreover, the mean width of *S. frugiperda* larvae from 1st to 6th instars were also recorded as 0.30 ± 0.01, 0.60 ± 0.02, 1.43 ± 0.06, 1.91 ± 0.04, 3.26 ± 0.11, and 4.41 ± 0.07 mm, respectively. The minimum width of *S. frugiperda* larvae from 1st to 6th instars were recorded as 0.28, 0.49, 1.15, 1.7, 2.6 and 4.2 mm, respectively. The maximum width of *S. frugiperda* larvae from 1st to 6th instars were observed as 0.34, 0.70, 1.71, 2.11, 3.9 and 4.9 mm, respectively. The lowest and highest length of *S. frugiperda* pupae was recorded as 11.50 and 14.80, whereas their minimum and maximum widths were observed as 3.20 and 4.20 mm, respectively. Moreover, the average length and width of the pupae were recorded as 12.87 ± 0.31 and 3.81 ± 0.10 mm, respectively.

3.2.2. Morphometrics of eggs and various larval instars and heads of Spodoptera frugiperda on cotton crops

During the studies, the radius of *S. frugiperda* eggs and larval instars was also observed and are given in Table 4. It was observed that the minimum and maximum radius of *S. frugiperda* eggs were recorded as 0.13 and 0.15 mm, respectively, with an average radius of 0.14 ± 0.00 mm. Moreover, the minimum radius of *S. frugiperda* larvae head from 1st to 6th instars were observed as 0.10, 0.19, 0.32, 0.69, 0.93, and 1.65 mm, respectively. Moreover, the maximum radius from 1st to 6th instars was recorded as 0.18, 0.26, 0.41, 0.81, 1.13, and 1.97 mm, respectively. The mean radius of *S. frugiperda* larvae heads from 1st to 6th instars were observed as 0.14 ± 0.01, 0.23 ± 0.01, 0.37 ± 0.01, 0.76 ± 0.01, 1.02 ± 0.02, and 1.83 ± 0.03 mm, respectively.

Table 3. Morphometrics of various larval instars and pupae of *Spodoptera frugiperda* on cotton.

Life stage	Length (mm)			Width (mm)		
	Minimum	Maximum	Average	Minimum	Maximum	Average
1st instar	1.44	1.91	1.68 ± 0.05	0.28	0.34	0.30 ± 0.01
2nd instar	3.11	3.71	3.32 ± 0.07	0.49	0.70	0.60 ± 0.02
3rd instar	6.54	7.25	6.94 ± 0.07	1.15	1.71	1.43 ± 0.06
4th instar	11.20	15.50	12.87 ± 0.46	1.70	2.11	1.91 ± 0.04
5th instar	17.60	21.10	19.78 ± 0.34	2.60	3.90	3.26 ± 0.11
6th instar	30.4	33.10	31.95 ± 0.27	4.20	4.90	4.41 ± 0.07
Pupae	11.50	14.80	12.87 ± 0.31	3.20	4.20	3.81 ± 0.10

Table 4. Radius of *Spodoptera frugiperda* eggs and head of larval instars on cotton.

Life stage	Radius (mm)		
	Minimum	Maximum	Average
Eggs	0.13	0.15	0.14 ± 0.00
1st instar	0.10	0.18	0.14 ± 0.01
2nd instar	0.19	0.26	0.23 ± 0.01
3rd instar	0.32	0.41	0.37 ± 0.01
4th instar	0.69	0.81	0.76 ± 0.01
5th instar	0.93	1.13	1.02 ± 0.02
6th instar	1.65	1.97	1.83 ± 0.03

3.2.3. Weight of various larval instars and pupae of Spodoptera frugiperda on cotton crop

During the research work, the weight of *S. frugiperda* larvae instars and pupae was recorded in grams (g). Only the 3rd, 4th, 5th, and 6th instar larvae and pupae weights were recorded and given in Table 5. It was observed that the minimum weight of *S. frugiperda* larvae in the 3rd to 6th instars was recorded as 0.06 g, 0.11 g, 0.19 g, and 0.36 g, respectively. The maximum weight of *S. frugiperda* larvae from 3rd to 6th instars were observed as 0.10 g, 0.17 g, 0.30 g, and 0.50 g, respectively. Moreover, the average weight of *S. frugiperda* larvae from 3rd to 6th instars were also observed as 0.08 ± 0.00 g, 0.14 ± 0.01 g, 0.23 ± 0.01 g, and 0.42 ± 0.01 g, respectively. The weight of *S. frugiperda* pupa was also recorded as its minimum and maximum weight was recorded as 0.09 and 0.19 g, respectively, whereas its average weight was observed as 0.13 ± 0.01 g.

Table 5. Weight of various larvae instars and pupae of *Spodoptera frugiperda* on cotton crop**.**

Life stage	Weight (g)		
	Minimum	Maximum	Average
3rd instar	0.06	0.10	0.08 ± 0.00
4th instar	0.11	0.17	0.14 ± 0.01
5th instar	0.19	0.30	0.23 ± 0.01
6th instar	0.36	0.50	0.42 ± 0.01
Pupae	0.09	0.19	0.13 ± 0.01

3.2.4. Various ovipositional parameters of Spodoptera frugiperda on cotton crop

During the study, pre-oviposition, oviposition, post-oviposition period, and the average number of eggs were also recorded and given in Table 6. It was observed that *S. frugiperda* females, on average, started their oviposition on 3.33 ± 0.21 days, with a maximum and minimum interval of 4 and 3 days, respectively. The mean oviposition period of *S. frugiperda* females was recorded with a minimum and maximum interval of 3 and 4 days, with an average of 3.33 ± 0.21 days. After completion of egg laying, the *S. frugiperda* female lived an average of 2.33 ± 0.21 days, with a minimum and maximum interval of 2 and 3 days, respectively. The egg-laying capacity of females varied from 360 to 449 eggs, with an average of 407.50 ± 13.76 eggs per female recorded during the study.

4. DISCUSSION

Fall Armyworm is one of the most important invasive polyphagous pests due to its transcontinental migration, highly destructive nature, and adaptability to a wide host range of about 353 plant species [23]. In this study, the life cycle and morphometric parameters of *S. frugiperda* were examined on cotton to understand the behavior of the pest, which enables it to feed on so many plants of economic importance, and the same will be helpful to design an effective control strategy. It was observed in our studies that cotton greatly affected the developmental period of *S. frugiperda* as compared to its preferred host maize, as it took a longer time to complete the development of various life stages.

During the present study, it was observed that the mean developmental time of six instars of *S. frugiperda* was recorded much higher than those observed by Sharma *et al.* [20], who observed much lower developmental duration of all six

Table 6. Various ovipositional parameters of *Spodoptera frugiperda* on cotton.

Life stage	Days		
	Minimum	Maximum	Average
Pre-oviposition period	3 days	4 days	3.33 ± 0.21 days
Oviposition period	3 days	4 days	3.33 ± 0.21 days
Post-oviposition period	2 days	3 days	2.33 ± 0.21 days
Eggs per female	360 eggs	449 eggs	407.50 ± 13.76 eggs

instars of *S. frugiperda* when reared on maize as the developmental time from 1st to 6th larvae instars were noted as 2.98 ± 0.37, 2.90 ± 0.39, 1.98 ± 0.021, 2.19 ± 044, 2.63 ± 0.076, and 3.63 ± 0.048 days, respectively, whereas, the total larval developmental of *S. frugiperda* on maize was recorded as 16.31 ± 0.205 days.

Keerthi *et al.* [24] studied the larval developmental duration of *S. frugiperda* on sorghum from the 1st to 6th larval instars, which were recorded as 2.26 ± 0.11, 2.00 ± 0.08, 1.95 ± 0.20, 2.05 ± 0.05, 2.28 ± 0.20, and 4.79 ± 0.73 days, respectively. While the larval development of *S. frugiperda* on maize from 1-6 larval instars was recorded as 2.40 ± 0.36, 2.11 ± 0.36, 2.00 ± 0.05, 2.00 ± 0.00, 2.21 ± 0.29, and 5.08 ± 0.74 days, respectively. The larval developmental period on artificial diet was recorded as 2.54 ± 0.22, 2.31 ± 0.35, 2.25 ± 0.33, 2.38 ± 0.40, 2.56 ± 0.10, and 5.88 ± 0.58 days, respectively. Moreover, the overall larval development was recorded as 13.88 ± 0.76, 14.04 ± 0.25, 16.07 ± 1.66 days on sorghum, maize, and artificial diet, respectively. In addition, Praveen and Mallapur [25] also studied various hosts; the entire larval developmental duration of *S. frugiperda* was recorded as 28.40 ± 0.51, 18.51 ± 1.19, 19.80 ± 1.31, 29.40 ± 0.51, and 21.00 ± 1.05 days on cotton, sorghum, maize, cabbage, and wheat, respectively. The results of Keerthi *et al.* [24] and Praveen and Mallapur [25] showed variance between our findings and their results, the genetic strain, the environment they grow in (such as temperature and laboratory techniques), the food they consume (nutrition and plant defenses), and the experiences of their mother all influence the surprisingly different larval development times of *Spodoptera frugiperda*. For instance, the high protein and low fiber content of maize promotes growth, whereas cotton or cabbage slows it down, and warmer, ideal temperatures (27 ± 2 °C) further accelerate development.

Moreover, the pupal period was also influenced by the cotton, as larvae reared on the cotton had a longer pupal period, it takes 9.63 ± 0.23 days on cotton. However, the results of Sharma *et al.* [20] are almost similar to our findings; they recorded 9.69 ± 0.145 days on maize. Bankar and Bhamare [26] found the lowest pupal duration while reared on various hosts; the pupal duration of *S. frugiperda* was recorded as 6.76 ± 0.44, 7.99 ± 0.24, 7.61 ± 0.38, and 8.49 ± 0.42 days on maize, pearl millet, sorghum, and sugarcane, respectively. In addition, Praveen and Mallapur [25] also studied various host crops, the pupal period of *S. frugiperda* on cotton, maize, and sorghum was mostly similar to our findings, it was recorded as 9.00 ± 0.00, 9.00 ± 0.00, and 8.00 ± 0.00 days, respectively. However, the results of pupal duration on wheat and cabbage were much higher compared to our findings on cotton. Pupal period of *S. frugiperda* on wheat and cabbage was recorded as 13.00 ± 0.00 and 12.00 ± 0.00 days, respectively.

The mean hatching period was observed 2.33 ± 0.05 days; when compared with the recent studies on different host crops, the number of *S. frugiperda* eggs laid on cotton was much lower. The mean egg laying capacity in the present study was recorded as 407.50 ± 13.76 eggs per female. Keerthi *et al.* [24] observed variation in the fecundity period of *S. frugiperda* reared on maize and sorghum. It was much higher and recorded as 1009.24 ± 133.31 eggs on maize, and 1086.6 ± 188.13 eggs on sorghum. However, Bankar and Bhamare [26] noted almost similar results of *S. frugiperda* fecundity on maize, which was recorded as 436.44 ± 22.44 eggs. In addition, Praveen and Mallapur [25] experimented on various host crops, as she noted 650.45 ± 88.53, 680.54 ± 91.52, 565.23 ± 27.78 eggs on sorghum, maize, and wheat, respectively. Such huge variation in the fecundity in the fecundity of *S. frugiperda* observed in above-mentioned studies may be attributed to different host plants used in the studies, experimental conditions, and the insects used in the study. Moreover, the results of Acharya *et al.* [27] were very low, with a record of 231.54 ± 28.48 eggs on potato. The reasons behind the highest and lowest fecundity on different hosts can be due to the fact that some host plants may not provide the nutritional requirements required for growth and development, thereby resulting in decreased fecundity. As we know, maize, sorghum, millet, and some other fodder crops are the favorites of *S. frugiperda*; on these hosts, their egg laying capacity was much better compared to sugarcane and potato.

Regarding morphometrics, various stages of *S. frugiperda* larvae instars and pupae were observed on the cotton crop. The morphometric analysis revealed that diet did significantly affect the radius of *S. frugiperda* eggs on cotton as the mean radius of eggs were recorded as 0.14 ± 0.00

mm. Navasero and Navasero [28] observed much higher radius and diameter of eggs on maize than our findings, as she noted 0.195 ± 0.00 and 0.39 ± 0.00 mm, respectively. However, it did influence the weight of various *S. frugiperda* larvae instars and pupae. The result showed that the mean length of *S. frugiperda* larvae from 1st to 6th instars was recorded as 1.68 ± 0.05, 3.30 ± 0.07, 6.94 ± 0.07, 12.87 ± 0.46, 19.78 ± 0.34, and 31.95 ± 0.27, mm, respectively. The measurement of width was also noted; it was observed as 0.30 ± 0.01, 0.60 ± 0.02, 1.43 ± 0.06, 1.91 ± 0.04, 3.26 ± 0.11, and 4.4 ± 0.07 mm, respectively. The present results are in line with the findings of Sharma *et al.* [20] on maize, as they observed that the mean length of *S. frugiperda* larvae from 1st to 6th instars was recorded as 1.5 ± 0.013, 3.56 ± 0.017, 7.12 ± 0.052, 11.60 ± 0.181, 18.5 ± 0.212, 34.39 ± 0.351 mm, respectively. The mean width of *S. frugiperda* larvae from 1st to 6th instars was observed shortened on maize, noted 0.35 ± 0.011, 0.47 ± 0.03, 0.80 ± 0.04, 1.37 ± 0.06, 2.11 ± 0.13, and 2.70 ± 0.13 mm, respectively. In addition, Navasero and Navasero [28] observed that the mean length of *S. frugiperda* larvae from 1st to 6th instars was recorded as 1.77 ± 0.49, 2.79 ± 0.35, 7.41 ± 0.58, 14.57 ± 2.09, 21.25 ± 1.47, and 30.79 ± 3.14 mm, respectively. The mean width was observed 0.23 ± 0.30, 0.35 ± 0.05, 0.89 ± 0.28, 1.86 ± 0.18, 2.99 ± 1.47, and 3.82 ± 0.26 mm, respectively. Some variance can be observed in the 2nd, 4th, 5th, and 6th instars' length with our findings, whereas width was also observed shorter in the 2nd, 3rd, 5th, and 6th instars with our results.

Moreover, the weight of various *S. frugiperda* larvae instars was measured on cotton, during study mean weight of 3rd, 4th, 5th, and 6th instars was recorded as 0.8 ± 0.00, 0.14 ± 0.01, 0.23 ± 0.01, and 0.42 ± 0.01 g, respectively. The observations of previous studies also supported our findings as the weight of the 3rd instar larvae of *S. frugiperda* when fed on corn was recorded as 0.08 g [29]. Similarly, Firake and Behere [30] found that the larval weight of the final instar was recorded as 0.42 g. Furthermore, the mean weight of *S. frugiperda* pupae was also observed on cotton, and it was recorded as 0.13 ± 0.01 g. The results of Sari *et al.* [31] showed that the pupal weight of *S. frugiperda* was directly affected by the host plant cotton. As he noted 0.16 g on corn and 0.18 g on mustard, respectively.

The findings of this study have shown that *S. frugiperda* is capable of feeding and successfully completing its various life stages on cotton and the same highlighted the importance of the host feeding in controlling the duration of the various life stages, i.e., larvae, pupae, and adult longevity of both males and females [31]. Accordingly, such findings could provide a base for its proper management because it confirmed the significant role of host range in feeding, development, and population dynamics of *S. frugiperda* [32].

Besides its main host maize, recent studies have shown that *S. frugiperda* is also capable of feeding and developing on cotton, hence confirming its polyphagous feeding niche [33]. Despite the minimal development duration of larvae, highest survival of various life stages, and relatively higher fecundity was recorded on maize; Ahmad *et al.* [33] confirmed that cotton and sorghum can also support significant growth, survival, and reproduction of *S. frugiperda.* In another comparative study regarding biological parameters of tow armyworm species, i.e., *S. littoralis* and *S. frugiperda* on cotton, maize, coriander, and tomatoes, coriander was found to be the preferred host for both the species as it causes lowest larval mortality along with shortest development period, maximum pupal weight, highest fecundity and net reproductive rate [34]. All the observed parameters of *S. littoralis* and *S. frugiperda* were not significantly different from those recorded on maize, their main host. Moreover, cotton was also found suitable for the growth and reproductive parameters of *S. frugiperda* and *S. littoralis*, whereas tomato was found to be the most unfavorable host [34]. Additionally, exploring the specific nutritional components of the natural diet that contribute to the observed effects on the biological parameters of *S. frugiperda* could be valuable for understanding the underlying mechanisms driving these differences and can be exploited for its adequate management [35].

5. CONCLUSIONS

Life cycle and morphometrics data generated from the present study confirm that the pest can shift to other hosts in the absence of its main host, i.e., maize, to continue its survival. The average incubation period was 2.33 ± 0.05 days, larval duration from 1st to 6th instars was 32.06 ± 0.21 days, and pupal development was 9.63 ± 0.23 days,

whereas the entire life cycle was completed in 43.92 ± 0.72 days. Adult longevity was 7.90 ± 0.29 (for males) and 9.60 ± 0.19 days (for females), whereas the mean fecundity was 407.50 ± 13.76 eggs. The results of this study are useful for designing the *S. frugiperda* management strategy.

6. ACKNOWLEDGEMENT

We would like to sincerely thank the Stored Grain Research Laboratory, Department of Entomology, Faculty of Crop Protection, Sindh Agriculture University, Tando Jam, for providing the necessary facilities and resources to carry out this study.

7. ETHICAL STATEMENT

This study was conducted in accordance with the ethical guidelines of Sindh Agriculture University, Tando Jam. All procedures involving *Spodoptera frugiperda* were performed with care to minimize unnecessary harm to the insects. No endangered or protected species were involved in the research.

8. CONFLICT OF INTEREST

The authors declare no conflict of interest.

9. REFERENCES

1. A.A. Gilal, L. Bashir, M. Faheem, A. Rajput, J.A. Soomro, S. Kunbhar, A.S. Mirwani, T. Zahra, G.S. Mastoi, and J.G.M. Sahito. First record of invasive fall armyworm (*Spodoptera frugiperda* (Smith) (Lepidoptera: Noctuidae)) in corn fields of Sindh, Pakistan. *Pakistan Journal of Agricultural Research* 33(2): 247-252 (2020).
2. Z. Bhatti, A.M. Ahmed, I. Khatri, Q. Rattar, S. Rajput, M. Tofique, and H. Younas. First report of morphometric identification of *Spodoptera frugiperda* J.E Smith (Lepidoptera: Noctuidae), an invasive pest of maize in Southern Sindh, Pakistan. *Asian Journal of Agriculture and Biology* 2021(1): 1-8 (2021).
3. R. Day, P. Abrahams, M. Bateman, T. Beale, V. Clottey, M. Cock, Y. Colmenarez, N. Corniani, R. Early, J. Godwin, J. Gomez, P. Moreno, S. T. Murphy, B. Oppong-Mensah, N. Phiri, C. Pratt, S. Silvestri, and A. Witt. Fall armyworm: Impacts and implications for Africa. *Outlooks on Pest Management* 28(5): 196-201 (2017).
4. M.J.W. Cock, P.K. Beseh, A.G. Buddie, G. Cafá, and J. Crozier. Molecular methods to detect *Spodoptera frugiperda* in Ghana, and implications for monitoring the spread of invasive species in developing countries. *Scientific Report*s 7(1): 4103 (2017).
5. D.G. Montezano, A. Specht, D.R. Sosa-Gómez, V.F. Roque-Specht, J.C. Sousa-Silva, S.V. Paula-Moraes, J.A. Peterson, and T.E. Hunt. Host plants of *Spodoptera frugiperda* (Lepidoptera: Noctuidae) in the Americas. *African Entomology* 26(2): 286-300 (2018).
6. G. Goergen, P.L. Kumar, S.B. Sankung, A. Togola, and M. Tamò. First report of outbreaks of the fall armyworm *Spodoptera frugiperda* (J.E. Smith) (Lepidoptera: Noctuidae), a new alien invasive pest in West and Central Africa. *PLOS One* 11(10): e0165632 (2016).
7. D. Marri, S.A. Mensah, D.A. Kotey, J. Abraham, M.K. Billah, and M. Osae. Basic developmental characteristics of the fall armyworm, *Spodoptera frugiperda* (J.E. Smith) (Lepidoptera: Noctuidae) reared under laboratory conditions. *Psyche: A Journal of Entomology* 2023(1): 6917316 (2023).
8. M. Ramzan, H. Ilahi, M. Adnan, A. Ullah, and A. Ullah. Observation on fall armyworm, *Spodoptera frugiperda* (Lepidoptera: Noctuidae) on maize under laboratory conditions. *Egyptian Academic Journal of Biological Sciences (A. Entomology)* 14(1): 99-104 (2021).
9. S.S. Deshmukh, B.M. Prasanna, C.M. Kalleshwaraswamy, J. Jaba, and B. Choudhary. Fall armyworm (*Spodoptera frugiperda*). In: Polyphagous Pests of Crops. Omkar (Ed.). *Springer, Singapore* pp. 349-372 (2021).
10. S. Sharanabasappa, C.M. Kalleshwaraswamy, J. Poorani, M.S. Maruthi, H.B. Pavithra, and J. Diraviam. Natural enemies of *Spodoptera frugiperda* (J.E. Smith) (Lepidoptera: Noctuidae), a recent invasive pest on maize in South India. *The Florida Entomologist* 102(3): 619-623 (2019).
11. R.K. Bannor, H. Oppong-Kyeremeh, D.A. Aguah, and S.K.C. Kyire. An analysis of the effect of fall armyworm on the food security status of maize-producing households in Ghana. *International Journal of Social Economics* 49(4): 562-580 (2022).
12. O. Navik, A.N. Shylesha, J. Patil, T. Venkatesan, Y. Lalitha, and T.R. Ashika. Damage, distribution and natural enemies of invasive fall armyworm *Spodoptera frugiperda* (J.E. Smith) under rainfed maize in Karnataka, India. *Crop Protection* 143: 105536 (2021).
13. A. Abbas, F. Ullah, M. Hafeez, X. Han, M.Z.N.

Dara, H. Gul, and C.R. Zhao. Biological control of fall armyworm, *Spodoptera frugiperda*. *Agronomy* 12(11): 2704 (2022).
14. L.B. Chhetri and B. Acharya. Fall armyworm (*Spodoptera frugiperda*): A threat to food security for South Asian country: Control and management options: A review. *Farming and Management* 4(1): 38-44 (2019).
15. V.L. Roth and J.M. Mercer. Morphometrics in development and evolution. *American Zoologist* 40(5): 801-810 (2000).
16. B. Wikantyoso, S.P. Tseng, S.K. Himmi, S. Yusuf, and T. Yoshimura. Morphometric analysis of *Coptotermes* spp. soldier caste (Blattodea: Rhinotermitidae) in Indonesia and evidence of *Coptotermes gestroi* extreme head-capsule shapes. *Insects* 12(5): 477 (2021).
17. N. Cañas-Hoyos, E.J. Marquez, and C.I. Saldamando-Benjumea. Heritability of wing size and shape of the rice and corn strains of *Spodoptera frugiperda* (JE Smith) (Lepidoptera: Noctuidae). *Neotropical Entomology* 45(4): 411-419 (2016).
18. H. Du Plessis, M.L. Schlemmer, and J. Van den Berg. The effect of temperature on the development of *Spodoptera frugiperda* (Lepidoptera: Noctuidae). *Insects* 11(4): 228 (2020).
19. A.A. Gilal, L.B. Rajput, M.I. Kubar, G.M. Kaleri, T. Zahra, M.I. Mastoi, and Z. Rasheed. Life Table Studies of Invasive *Spodoptera frugiperda* (Lepidoptera: Noctuidae) on Maize under Laboratory Conditions. *Pakistan Journal of Agricultural Research* 35(2): 259-265 (2022).
20. S. Sharma, S. Tiwari, R.B. Thapa, S. Neupane, G.V. Reddy, S. Pokhrel, and R. Muniappan. Life cycle and morphometrics of fall armyworm (*Spodoptera frugiperda*) (Lepidoptera: Noctuidae) on maize crop. *SAARC Journal of Agriculture* 20(1): 77-86 (2022).
21. M. Kruger, J.B.J. Van Rensburg, and J. Van den Berg. Transgenic Bt maize: farmers' perceptions, refuge compliance and reports of stem borer resistance in South Africa. *Journal of Applied Entomology* 136(1-2): 38-50 (2012).
22. B. Bhat and A.S.R. Bajracharya. Biology and Life Table of Fall Armyworm *Spodoptera frugiperda* on Maize at Laboratory Conditions in Nepal. *Nepal Journal of Science and Technology* 21(2): 1-8 (2022).
23. R.N. Nagoshi and R.L. Meagher. Behavior and distribution of the two fall armyworm host strains in Florida. *Florida Entomologist* 87(4): 440-449 (2004).
24. M.C. Keerthi, H.S. Mahesha, N. Manjunatha, A. Gupta, R.P. Saini, K.T. Shivakumara, H. A. Bhargavi, G. Gupta, and N.S. Kulkarni. Biology and oviposition preference of fall armyworm, *Spodoptera frugiperda* (J.E. Smith) (Lepidoptera: Noctuidae) on fodder crops and its natural enemies from Central India. *International Journal of Pest Management* 69(3): 215-224 (2023).
25. T. Praveen and C.P. Mallapur. Studies on host range of fall armyworm, *Spodoptera frugiperda* (J.E. Smith) under laboratory conditions. *Journal of Entomology & Zoology Studies* 7(4): 1385-1387 (2019).
26. D.R. Bankar and V.K. Bhamare. Growth and development of fall armyworm *Spodoptera frugiperda* on cereals. *Indian Journal of Entomology* 85(4): 969-972 (2023).
27. R. Acharya, M.J. Malekera, S.K. Dhungana, S.R. Sharma, and K.Y. Lee. Impact of rice and potato host plants is higher on the reproduction than growth of corn strain fall armyworm, *Spodoptera frugiperda* (Lepidoptera: Noctuidae). *Insects* 13(3): 256 (2022).
28. M. Navasero and M.V. Navasero. Life cycle, morphometry and natural enemies of fall armyworm, *Spodoptera frugiperda* (J.E. Smith) (Lepidoptera: Noctuidae) on *Zea mays* L. in the Philippines. *Journal of the International Society for Southeast Asian Agricultural Sciences* 26(2): 17-29 (2020).
29. S. Ginting, T. Sunardi, C.B. Sari, and R.H. Wibowo. Evaluation of various natural diets for mass rearing of *Spodoptera frugiperda* J.E. Smith (Lepidoptera: Noctuidae). *Jurnal Hama dan Penyakit Tumbuhan Tropika* 21(1): 43-48 (2021).
30. D.M. Firake and G.T. Behere. Bioecological attributes and physiological indices of invasive fall armyworm, *Spodoptera frugiperda* (J.E. Smith) infesting ginger (*Zingiber officinale* Roscoe) plants in India. *Crop Protection* 137: 105233 (2020).
31. J.M.P. Sari, S. Herlinda, and S. Suwandi. Endophytic fungi from South Sumatra (Indonesia) in seed-treated corn seedlings affecting development of the fall armyworm, *Spodoptera frugiperda* J.E. Smith (Lepidoptera: Noctuidae). *Egyptian Journal of Biological Pest Control* 32(1): 103 (2022).
32. R. Gopalakrishnan and V.K. Kalia. Biology and biometric characteristics of *Spodoptera frugiperda* (Lepidoptera: Noctuidae) reared on different host plants with regard to diet. *Pest Management Science* 78(5): 2043-2051 (2022).
33. N. Ahmad, M. Ishtiaq, M.R. Shahid, F. Baig, and R.M. Hassan. Comparative demographic parameters

of fall armyworm (*Spodoptera frugiperda*) on five host plants. *Journal of Animal & Plant Sciences* 35(1): 250-261 (2025).

34. S.A. Shoman, N.M. Ghanim, N.H. Harraz, and W.Z. Aziz. Effect of four host plants on biological characteristics of *Spodoptera frugiperda* and *Spodoptera littoralis* (both Lepidoptera: Noctuidae). *International Journal of Tropical Insect Science* 45(4): 1909-1919 (2025).
35. C. Kasoma, H. Shimelis, and M.D. Laing. Fall armyworm invasion in Africa: implications for maize production and breeding. *Journal of Crop Improvement* 35(1): 111-146 (2021).

Proceedings of the Pakistan Academy of Sciences: B
Life and Environmental Sciences 62(4): 307-313 (2025)

ISSN (Print): 2518-4261; ISSN (Online): 2518-427X
http://doi.org/10.53560/PPASB(62-4)1119

Pakistan Academy of Sciences

Research Article

Prevalence of Malaria and its Association with ABO Blood Groups in District Battagram

Muhammad Iftikhar[1]*, Tasneem Ullah[1], Muhammad Mubarik[2], Sheryar Jamil[3], Tahir Sarfraz[1], and Majid Khan[1]

[1]Department of Zoology, Government Postgraduate College, Mandian Abbottabad, Khyber Pakhtunkhwa, Pakistan
[2]Department of Zoology, Hazara University, Mansehra, Khyber Pakhtunkhwa, Pakistan
[3]Department of Microbiology, Government Postgraduate College, Mandian Abbottabad, Khyber Pakhtunkhwa, Pakistan

Abstract: Malaria is a protozoan disease caused by the Plasmodium parasite and is moderately endemic in Pakistan. This study examined the correlation among malaria prevalence, ABO blood groups, and environmental risk factors in District Battagram. A total of 200 participants were screened for malaria by blood smear microscopy, and an agglutination test was performed to determine the blood group. The malarial prevalence was found to be 11.5%, reporting *Plasmodium vivax* 10.5% (n = 21) and *falciparum* 1% (n = 2). The highest number of malaria cases were in people with blood group B (10.35%), followed by blood group A (4.27%), and AB (0.07%), while no case was reported in participants having blood group O. Among the risk factors, sleeping outdoors and not having a past malaria history were two of the risk factors that were significantly associated with malaria positivity ($p < 0.05$). Other variables such as age, gender, closeness to stagnant water, and utilization of mosquito nets showed the prevalence but did not demonstrate a significant statistical correlation. It is suggested that blood group and malaria susceptibility can inform the targeted public health strategies for malaria prevention and control.

Keywords: Malaria, ABO Blood Group, *Plasmodium,* Epidemiology, Risk Factors.

1. INTRODUCTION

Malaria is a protozoan disease cause by *Plasmodium* and transmitted via female Anopheles mosquitos. To date, 120 species of *Plasmodium* are known so far; 5 species of the *Plasmodium* cause malaria: *P. malariae P. vivax, P. falciparum, P. ovale*, and *P. knowlesi*. *P. falciparum* causes high mortality, constituting over 99% of global malaria-related fatalities. While *P. vivax* has traditionally been considered a causative agent of mild malaria; however, evidence indicates its potential to induce severe illness [1]. Similarly*, P. malariae P. ovales*, and *P. knowlesi* are known to cause malaria in humans. In a study, 128 malaria patients were studied in Parma Italy, 8 *Plasmodium ovale curtisi* and 4 *Plasmodium ovale wallikeri* infections were discovered, but no *P. knowlesi* infections were found [2]. Malaria affects about half of the global population and is endemic in tropical and subtropical regions, which encompass, Eastern Mediterranean, South-East Asia, Western Pacific, the Americas, and, Sub-Saharan Africa [3]. 2.38 million cases per annum were reported in India from 1990 and 2000 which have been declined by 91% from 2011-2022 due to advancement in treatment and vector control strategies. The decline can be attributed to significant interventions, including the Intensified Malaria Control Project (IMCP), Enhanced Malaria Control Project (EMCP), artemisinin-based combination therapy (ACT), bivalent rapid diagnostic tests (RDT-Pf/Pv), and the participation of Accredited Social Health Activists (ASHAs). Holt's models and Autoregressive Integrated Moving Average

Received: July 2025; Revised: October 2025; Accepted: December 2025
* Corresponding Author: Muhammad Iftikhar <muhammad1222335@gmail.com>

(ARIMA) forecast zero indigenous cases in India by 2027-2028. The population density, literacy rates, health facilities, and accessibility to healthcare facilities have reported to greatly impact malaria incidence and outcome [4]. The case fatality rate of malaria in Sub-Saharan Africa constituted 94% of total deaths. Children under five years old represent the highest proportion of severe disease burden, constituting 67% of global mortality [5]. Pakistan has a high malaria incidence, with over 670,000 cases and 3159 deaths reported cases in 2013 [6].

According to the WHO report, Pakistan has ~700,000 cases of malaria in year 2019 [7]. In 2024, WHO published its yearly report on global malaria control and elimination trends [8]. Despite advancements in malaria prevention, the data indicates that routine vaccinations, there were still over 11 million more cases in 2023 compared to 2022. WHO predictions indicate that there were 263 million cases of malaria globally in 2023 (95% CI 238 million to 294 million). According to the WHO report published in 2023, by 2025, the Global Technical Strategy for Malaria 2016-2030 aims to reduce the malaria fatality rate by 75% [5].

Malaria is highly endemic in the region and a study from neighboring district "Shangla" in 2017 reported *Plasmodium* in 13.9% (n = 87) of the suspected cases. The percentage of positive cases was greater in males 65.24% while females had a positive rate of 34.76%. In the study sample, the highest prevalence of malaria was found in Group B 51.34%, followed by Group A 33.68%. In Pakistan *P. falciparum* and *P. vivax* are common [9]. In another study conducted in a neighbor district Mansehra, malaria was found in 154 cases 1999-2004, which includes 114 males and 46 females. There were 142 cases of *P. vivax* and 12 of *P. falciparum* [10].

The clinical symptoms of malaria vary significantly between children and adults. Patients with uncomplicated malaria may show modest symptoms such as fever and chills. Severe malaria, on the other hand, can cause life-threatening complications such as severe anemia, acute respiratory distress syndrome, hypoglycemia, shock, metabolic acidosis, acute renal injury, and cerebral malaria. This diversity emphasizes the importance of quick identification and treatment, particularly in youngsters, who are more likely to experience poor disease consequences. Understanding these clinical manifestations is critical for malaria management in endemic areas [11].

The antigens of human ABO blood types exhibit distinct phenotypes and glycoconjugate structures on the surface of red blood cells, influencing both physiology and disease. Researchers have been studying the association between blood type and disease since the early 1900s. It was found that antibodies and antigens are inherited traits. Some blood types lack antigens, leading to debate over the link between blood group and susceptibility to specific diseases [12]. In 1967, Athreya and Coriell [13] conducted an early review, suggesting a possible association between ABO blood groups and malaria. Later, Rowe *et al.* [14] demonstrated that *P. falciparum* rosetting, a virulence factor linked to severe malaria, occurs at lower levels in blood group O erythrocytes compared to blood groups A, B, and AB. A study proposed that blood group O provides resistance to severe *falciparum* malaria through a mechanism involving reduced rosetting. Malaria remains to be a significant global health challenge, especially in tropical and subtropical areas, causing significant morbidity and mortality. Prevalence of malaria and its association have not been studied in district Battagram. Some of the previous studies in Pakistan have tried to establish correlation between ABO blood groups and malaria susceptibility and severity. However, exact dynamics of the relationship might vary across different population. The specific problem is determining the prevalence of malaria in targeted population with different blood groups and socioeconomic parameters and understanding if certain blood groups are more susceptible or resistant to malaria infection in the study population.

The present research aimed to investigate the statistical relationship among blood group types and the incidence of malaria. Malaria is prevalent in district Battagram due to environmental factors favorable to mosquito breeding. Certain blood groups have been implicated to offer some degree of protection against severe malaria, while Blood groups A and B show greater susceptibility. A few global studies have looked into the relationship between malaria and blood groups, but there is limited data on this association in Pakistan, district Battagram in particular.

2. MATERIALS AND METHODS

2.1. Study Area

The present study was carried out in District Battagram which shares geographical boarders with Kohistan to the North, Mansehra to the East and South East, Torghar to the South, and Shangla to west. It has an elevation of approximately 1038 meters from sea level and located in 34°41'N latitude 73°1'E longitude as shown in Figure 1. The research study was conducted from September 2024 to May 2025 in the District Battagram. The rainfall varies throughout the year, from July to September, with the monsoon season contributing the precipitation, resulting in providing favorable condition for mosquito's reproduction and growth. The average annual rainfall is estimated to be around 800 to 1,000 millimeters. The rainy season provides significant moisture to the area.

2.2. Blood Typing (Agglutination Test) for ABO Blood Group

A total of 200 individuals were randomly selected in District Battagram but the sample classes were not balanced. Finger prick was performed on each participant using aseptic blood lancet. A drop of blood was placed on a clean microscopic glass slide and antisera was added to performed agglutination test followed by documenting of results [15].

2.3. Preparation of Blood Smear for Malarial Parasite (MP) Test

Blood smears were prepared from each blood sample collected from participant in targeted population. Sample collection will be performed via finger pricking, thick and thin smear were made followed by soaking the prepared slides in methanol for chemical fixation. The chemically fixed smear were stained with Giemsa stain and incubated for fifteen minutes. Finally, the sample were washed with clean water with precaution to avoid any damage to smear. The resulting slides was stored in a designated slide box for future microscopic reconfirmation in the college laboratory [16].

2.4. Microscopy

The stained blood smears were examined under a microscope at 100x objective lens. After carefully identifying any *Plasmodium* parasites, the data were recorded in excel sheets. According to Maqsood *et al.* [17] detection of malaria from the microscopic blood smears was 96.82% accurate.

2.5. Data Analysis Using SPSS Software

Data collected via questionnaires were summarized and input into Microsoft Excel 2013. A chi-square test was applied to examine the relationship between test results and associated risk factors utilizing SPSS [15].

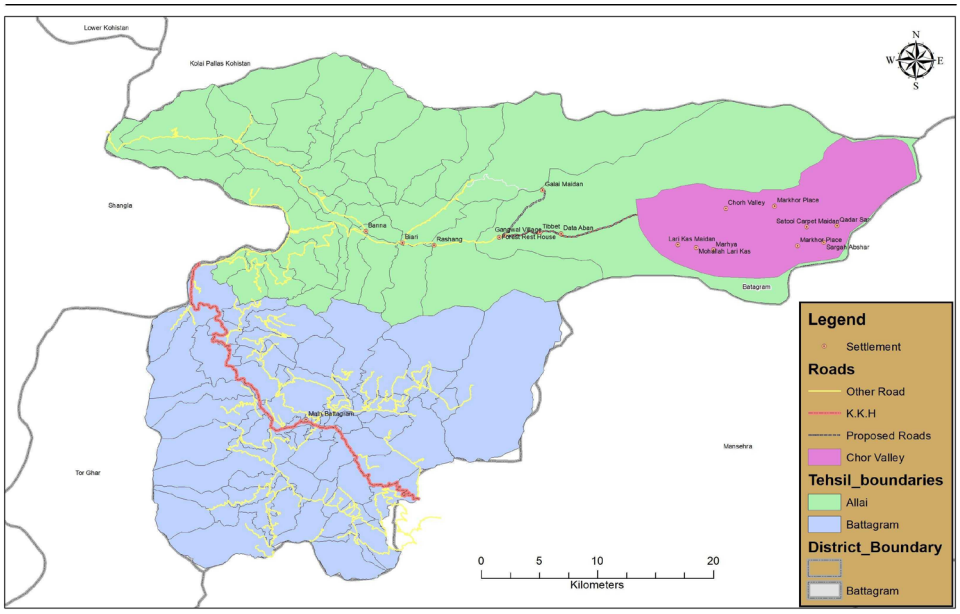

Fig.1. Geographical map of district Battagram.

3. RESULTS AND DISCUSSION

Plasmodium species are usually spread by an arthropods, most often the female Anopheles mosquito [18]. The prevalence rate of malaria in (200) blood sample was 11.5% (n = 23). Among them, 91.3% (n = 21) was *P. vivax* and 8.7% (n = 2) was *P. falciparum*. According to WHO, >1.8 million cases were being reported every year in Pakistan [19]. In 2020, the cases were reduced by 40% compared to 2015 but again soar to over 2 million in 2022 [20].

ABO Blood group is a system for compatibility and ABO antigen association with infection [21]. The result of ABO Blood group showed a percentage prevalence of 10.35% (n = 15) in blood group "B", 4.27% (n = 7) in blood group "A", 0.07% (n = 2) in blood group "AB" while no case was found positive in "O" blood group (Figure 2). The research demonstrates that individuals possessing blood group O may have a comparative protective benefit against malaria infection. This finding supports other studies showing that RBC's of blood group O are less able to clump together, which is a process that helps parasites stick and can cause serious illness. As a result, the lower ability of blood group O to form rosettes may play a vital role in reducing the susceptibility to malaria. Although blood groups A and B have the same percentage exposure to malaria in the studied population, blood group B is observed to be more prevalent. Similar results were reported by Tadesse *et al.* [15] showing higher prevalence in A (40%) and B (34.1) blood group followed by AB (14.3%) and O (5.1%), respectively. Likewise, Panda *et al.* [22] reported that the prevalence of blood group 'B' was significantly higher in patients with severe malaria relative to those with uncomplicated cases ($P < 0.0001$). Regardless of clinical severity, blood group 'B' demonstrated a significant relationship with cerebral malaria ($P < 0.0001$).

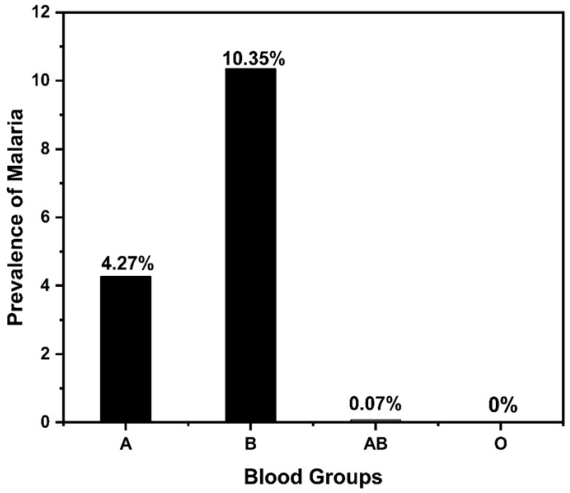

Fig. 2. Percentage prevalence of Malaria in different blood groups.

Many risk factors associated including demographic and epidemiological variables were studied. The study documented the prevalence of malarial is 25.49% in patient who slept outdoor while 6.76% was recorded in patients sleeping indoor. Parameters Like, sleeping area and past malaria history showed a significant relationship ($p < 0.05$) with the presence of malarial parasites in blood, which is mentioned in Table 1. The results indicate that both sleeping area and past malaria history are strongly linked to the infection caused by *Plasmodium*. The finding suggests that both factors may be important in how malaria spreads in the study population. This aligns with previous research that outdoor sleepers and night time activities were prevalent and could substantially increase the risk of malaria. The study documented 42% of the participants sleeping outdoors were at risk of malaria infection in southern Ghana [23]. Studies have demonstrated a 50% decrease in indoor vector density, resulting in a subsequent drop in malaria, due to the screening and windows doors [24]. Most of the positive malaria cases have been seen in homes that don't have window screens. Therefore, windows mesh is very significant for lowering the number of malaria cases in malaria endemic regions [25].

The parameters like patient age, gender, standing water, rice paddies, use of mosquito repellent coils, use of anti-malarial spray, and use of mosquito nets showed trend and act as a risk factor but are found to be non-significant ($p > 0.05$) with the presence of malarial parasites in blood. Higher prevalence was observed in patients over the age of 20 years (10.44%), and the percentage in the patients of the age group less than 20 years was (4.69%). Our study co-relates with the population-based study that identified the prevalence of malaria across several age groups in Colombia, identifying the highest risk age range as 20-30 years [26]. On the other hand, factors including gender, closeness to standing water and rice paddies, and the use of

Table 1. Demographic features, epidemiological variables, and risk factors associated with malaria.

Variables		Prevalence (%)	Significant difference (df)	Chi-square value	P-value
Patient Age	6-10	0.4	3	1.196	0.754
	11-15	1.23			
	15-20	3.06			
	>20	10.44			
Gender	Male	13.3	1	1.797	0.132
	Female	9.36			
Sleeping Area	Outdoor	25.49%	1	13.022	0.001
	Indoor	6.76%			
Standing Water	Yes	19.05	1	0.009	0.561
	No	5.68			
Rice Paddies	Yes	11.76	1	0.089	0.469
	No	11.11			
Past Malarial History	Yes	1.52	1	19.176	<0.001
	No	27			
Symptoms	Chills	3.1	3	4.753	0.191
	Episodic Fever	8.1			
	Anemia	0			
	Other	3.96			
Anti-Malarial spray	Yes	2.52	1	0.388	0.350
	No	26.69			
Mosquito Net	Yes	5.44	1	0.004	0.559
	No	19.65			
Health Facilities	Yes	19.05	1	0.022	0.539
	No	5.76			
Family member	1-5	3.1	2	1.197	0.550
	6-10	8.1			
	>10	4.48			
Climate	Dry	32.8	1	0.371	0.394
	Rainy	1.05			
Blood Group	A	4.27	3	15.151	0.002
	B	10.35			
	AB	0.07			
	O	0			

mosquito repellents, and mosquito nets did not demonstrate a significant correlation. Our study report contrasting results with the study conducted in Ethiopia [27]. The use of anti-malaria spray in homes has been identified as an effective method for decreasing the risk of malaria. The health of individuals can have a significant impact on the probability of individuals to suffer from malaria as well. Winskill *et al.* [28] conducted research study in north-east Tanzania and using anti-mosquito nets demonstrated to be highly effective in preventing malaria, reducing the risk by 25%, children aged 5 to 13 exhibited a 71% increased risk of malaria compared to those under five, because they were less likely to sleep under insecticide-treated mosquito nets compared to younger children. Similarly, another study was conducted in Charsadda and Swabi districts of Pakistan reported contrasting results which demonstrated that the effective implementation of barriers such as window screens,

housing types, and bed nets significantly decreases the incidence of malaria [29]. The study documented episodic fever in 8.1% of patients, followed by chills in 3.1% and other related symptoms in 3.96% of the patients. Laboratory findings do not report anemia in any of the participating patient.

4. CONCLUSIONS

The current study reported that patients having blood group B are more vulnerable to *Plasmodium* infection. Participants sleeping in open environments were commonly affected due to exposure to vector-related factors, and those who sleep indoors but are affected by Malaria are due to lack of protective measures, such as using mosquito nets and mosquito repellent coils. This study shows the prevalence of malaria in a number of cases but is not statistically significant in the District Battagram. The findings of this study will be helpful in raising awareness among the local population about the association between blood group, sleeping area, and the risk factors associated with malaria.

5. ACKNOWLEDGEMENTS

We are sincerely thankful to all those who supported and contributed to this research. First we extend our heartfelt thanks to our teacher, Muhammad Ejaz, for their invaluable guidance, encouragement, and feedback throughout the study. We also want to acknowledge the support of the Department of Zoology, Government Post Graduate College, Mandian Abbottabad, Pakistan for providing the necessary research facilities.

6. ETHICAL STATEMENT

The above study was conducted in accordance with the ethical standards of the institutional and national research committee. Before the data collection, ethical approval (106A) was obtained from the Department of Zoology, Government Post Graduate College, Mandian Abbottabad, Pakistan. The objectives of the research were clearly explained to each participant, and their privacy was ensured throughout the research process. Participation was voluntary, and participants had the right to withdraw at any time. No personal identifiers were used in the data analysis or reporting, and all data collected were stored securely and used solely for academic purposes only.

7. CONFLICT OF INTEREST

The authors declare no conflict of interest.

8. REFERENCES

1. C. Naing, M.A. Whittaker, V.N. Wai, and J.W. Mak. Is *Plasmodium vivax* malaria a severe malaria?: a systematic review and meta-analysis. *PLoS Neglected Tropical Diseases* 8(8): e3071 (2014).
2. A. Calderaro, G. Piccolo, C. Gorrini, S. Rossi, S. Montecchini, M.L. Dell'Anna, F.D. Conto, M.C. Medici, C. Chezzi, and M.C. Arcangeletti. Accurate identification of the six human *Plasmodium* spp. causing imported malaria, including *Plasmodium ovale wallikeri* and *Plasmodium knowlesi*. *Malaria Journal* 12: 321 (2013).
3. A. Monroe, N.A. Williams, S. Ogoma, C. Karema, and F. Okumu. Reflections on the 2021 World Malaria Report and the future of malaria control. *Malaria Journal* 21(1): 154 (2022).
4. M.P. Singh, H. Rajvanshi, P.K. Bharti, A.R. Anvikar, and A.A. Lal. Time series analysis of malaria cases to assess the impact of various interventions over the last three decades and forecasting malaria in India towards the 2030 elimination goals. *Malaria Journal* 23(1): 50 (2024).
5. W.H. Organization. World malaria report 2023. *Geneva: World Health Organization* Licence: CC BY-NC-SA 3.0 IGO (2023). https://www.who.int/teams/global-malaria-programme/reports/world-malaria-report-2023.
6. C.J.L. Murray, K.F. Ortblad, S.S. Lim, C. Guinovart, K.H. Jacobsen, R.M. Barber, T.M. Wolock, N. Graetz, E.A.D.A. Roberts, *et al*. Global, regional, and national incidence and mortality for HIV, tuberculosis, and malaria during 1990-2013: a systematic analysis for the Global Burden of Disease Study 2013. *The Lancet* 384(9947): 1005-1070 (2014).
7. W.H. Organization. Strategic Advisory Group on Malaria Eradication. Malaria eradication: benefits, future scenarios and feasibility. A report of the Strategic Advisory Group on Malaria Eradication. *Geneva: World Health Organization* Licence: CC BY-NC-SA 3.0 IGO (2020). https://www.who.int/publications/i/item/9789240003675.
8. W.H. Organization. World malaria report 2024: Addressing inequity in the global malaria response. *Geneva: World Health Organization* Licence: CC BY-NC-SA 3.0 IGO (2024). https://www.who.int/teams/global-malaria-programme/reports/world-

malaria-report-2024.

9. S. Rahman, F. Jalil, H. Khan, M.A. Jadoon, I. Ullah, M. Rehman, A.M. Khan, A. Khan, A. Hayat and Z. Iqbal. Prevalence of malaria in district shangla, Khyber Pakhtunkhwa, Pakistan. *Journal of Entomology and Zoology Studies* 5(1): 678-682 (2017).
10. Jalal-ud-Din, S.A. Khan, and S.H. Ally. Malaria in children: study of 160 cases at a private clinic in Mansehra. *Journal of Ayub Medical College Abbottabad* 18(3): 44-45 (2006).
11. S.N. Balaji, R. Deshmukh, and V. Trivedi. Severe malaria: Biology, clinical manifestation, pathogenesis and consequences. *Journal of Vector Borne Diseases* 57(1): 1-13 (2020).
12. S.B. Abegaz. Human ABO blood groups and their associations with different diseases. *BioMed Research International* 2021: 6629060 (2021).
13. B.H. Athreya and L.L. Coriell. Relation of blood groups to infection. A survey and review of data suggesting possible relationship between malaria and blood groups. *American Journal of Epidemiology* 86(2): 292-304 (1967).
14. J.A. Rowe, I.G. Handel, M.A. Thera, A.M. Deans, K.E. Lyke, A. Koné, D.A. Diallo, A. Raza, O. Kai, K. Marsh, C.V. Plowe, O.K. Doumbo, and J.M. Moulds. Blood group O protects against severe *Plasmodium falciparum* malaria through the mechanism of reduced rosetting. *Proceedings of the National Academy of Sciences USA* 104(44): 17471-17476 (2007).
15. H. Tadesse and K. Tadesse. Assessing the association of severe malaria infection and ABO blood groups in northwestern Ethiopia. *Journal of Vector Borne Diseases* 50(4): 292-296 (2013).
16. N. Tangpukdee, C. Duangdee, P. Wilairatana, and S. Krudsood. Malaria diagnosis: a brief review. *The Korean Journal of Parasitology* 47(2): 93-102 (2009).
17. A. Maqsood, M.S. Farid, M.H. Khan, and M. Grzegorzek. Deep malaria parasite detection in thin blood smear microscopic images. *Applied Sciences* 11(5): 2284 (2021).
18. S. Sato. *Plasmodium*—a brief introduction to the parasites causing human malaria and their basic biology. *Journal of Physiological Anthropology* 40: 1 (2021).
19. W.H. Organization. World malaria report 2013. *WHO Library Cataloguing-in-Publication Data* ISBN: 9 789241 56469 4 (2013). https://www.who.int/publications/i/item/9789241564694.
20. W.H. Organization. World malaria report 2022. *Geneva: World Health Organization*. Licence: CC BY-NC-SA 3.0 IGO (2022). https://www.who.int/teams/global-malaria-programme/reports/world-malaria-report-2022.
21. C.M. Cserti and W. H. Dzik. The ABO blood group system and *Plasmodium falciparum* malaria. *Blood* 110(7): 2250-2258 (2007).
22. A.K. Panda, S.K. Panda, A.N. Sahu, R. Tripathy, B. Ravindran, and B.K. Das. Association of ABO blood group with severe *falciparum* malaria in adults: case control study and meta-analysis. *Malaria Journal* 10: 309 (2011).
23. A. Monroe, O. Asamoah, Y. Lam, H. Koenker, P. Psychas, M. Lynch, E. Ricotta, S. Hornston, A. Berman, and S.A. Harvey. Outdoor-sleeping and other night-time activities in northern Ghana: implications for residual transmission and malaria prevention. *Malaria Journal* 14: 35 (2015).
24. M.J. Kirby, D. Ameh, C. Bottomley, C. Green, M. Jawara, P.J. Milligan, P.C. Snell, D.J. Conway, and S.W. Lindsay. Effect of two different house screening interventions on exposure to malaria vectors and on anaemia in children in The Gambia: a randomised controlled trial. *The Lancet* 374(9694): 998-1009 (2009).
25. J. Bradley , A.M. Rehman, C. Schwabe, D. Vargas, F. Monti, C. Ela, M. Riloha and I. Kleinschmid. Reduced prevalence of malaria infection in children living in houses with window screening or closed eaves on Bioko Island, Equatorial Guinea. *PLOS One* 8(11): e80626 (2013).
26. M.J. Olivera, J.C.P. Rodriguez, P.E.C. Narváez, and W.L. Quevedo. Epidemiology of *Plasmodium vivax* malaria infection in Colombia. *The Microbe* 5: 100209 (2024).
27. D.G. Ayele, T.T. Zewotir, and H.G. Mwambi. Prevalence and risk factors of malaria in Ethiopia. *Malaria Journal* 11: 195 (2012).
28. P. Winskill, M. Rowland, G. Mtove, R.C. Malima, and M.J. Kirby. Malaria risk factors in north-east Tanzania. *Malaria Journal* 10: 98 (2011).
29. Q. Jamal, S.B. Rasheed, N. Naz, and S. Iltaf. An Exploratory Case study of the effect of Ecology on Malaria Risk Factors in Northern Pakistan: Malaria Risk Factors in Northern Pakistan. *The Sciencetech* 6(1): 61-72 (2025).

Proceedings of the Pakistan Academy of Sciences: B
Life and Environmental Sciences 62(4): 315-334 (2025)

ISSN (Print): 2518-4261; ISSN (Online): 2518-427X
http://doi.org/10.53560/PPASB(62-4)1122

Pakistan Academy of Sciences

Research Article

Treatment of Malathion by using Plant-Bacteria Consortia in Constructed Wetlands

Vijiha Nasir[1], Rija Khalid[1*], Asma Jamil[1], and Sajida Rasheed[2]

[1]Department of Earth and Environmental Sciences, Bahria School of Engineering and Applied Sciences (BSEAS), Bahria University, H-11 Campus, Islamabad, Pakistan

[2]Department of Biotechnology, University of Kotli Azad Jammu and Kashmir, Kotli, Pakistan

Abstract: Malathion, a widely used organophosphate pesticide, poses serious environmental and health risks due to its persistence and toxicity. This study investigates the bioremediation potential of bacterial consortia and plant-bacterial systems in constructed wetland settings for the degradation of malathion-contaminated soil at varying concentrations (50, 100, and 200 mg/L). The four consortia (C1-C4) were constructed from three purified soil isolates and mixed in equal proportions and two plant species (*Canna indica* and *Mentha arvensis*) were tested individually and in combination over an eight-week period. All isolates were characterized by Gram staining and basic biochemical tests and identified as Gram-positive, catalase-negative *Bacillus* spp.; species-level molecular identification was not performed. Colorimetric analysis revealed that all bacterial treatments (bacteria + soil) achieved high removal efficiencies, showing degradation rates between 99.2% and 99.78% at 50mg/L and 100mg/L, reaching up to 99.99% at 200 mg/L in seventh week. Plant-based treatments also exhibited robust degradation, achieving up to 99.8% efficiency by the first week and reaching 100% in the third week at higher concentrations. Efficiency was generally higher at greater malathion concentrations, suggesting possible enzyme induction or microbial adaptation. Soil parameter analysis confirmed active microbial and plant-based remediation, with shifts in pH, organic matter, nitrate, sodium, and potassium supporting degradation processes. While bacterial consortia acted more rapidly, plant systems contributed significantly to sustained removal. Two-way ANOVA confirmed significant effects of time and pesticide dose on degradation efficiency across all treatments. Overall, all treatments achieved > 99% malathion degradation, with bacterial and plant-bacterial consortia showing promise as effective, low-cost, and environmentally friendly strategies for remediating pesticide-contaminated soils.

Keywords: Biodegradation, Organophosphate Pesticide, Colorimetric Analysis, Constructed Wetlands, Plant Microbes, Rhizosphere Interaction, Environmental Sustainability.

1. INTRODUCTION

According to Al-Saeed *et al.*[1] one of the most used pesticides, malathion (MLT) poses multiple hazards to humans and animals. The wide use of malathion, an organophosphate insecticide, as both a tool of agriculture and a chemical weapon in urban areas poses a great environmental challenge due to this insecticide's persistence and associated health risks. Many research works have been carried out to meet the need to address malathion contamination, and through it, much attention is paid to bioremediation strategies in constructed wetlands. A major investigation was carried out by Uniyal *et al.* [2] investigating the biodegradation of malathion in constructed wetlands by indigenous bacterial plant associations. As one of the dominant organophosphate insecticides embedded in agricultural and urban settings, it requires the rigorous analysis of effective remediation methods**.** The U.S. Environmental Protection Agency (U.S. EPA) [3] highlighted the effectiveness of malathion as a pest control agent. Malathion is one of the most widely used organophosphate insecticides both in agriculture and public health, especially in Mosquito control operations for crop protection and vector born disease management. Although, U.S. Geological Survey (USGS) [4] reported an alarming

Received: July 2025; Revised: November 2025; Accepted: December 2025
* Corresponding Author: Rija Khalid <rijakhalid@greenthinktanks.com>

information: malathion and its metabolites occurs in over 80% of the tested streams in more than 30 states during year of 1992-2001, highlighting an uninviting presence within aquatic environment. This widespread identification, despite close label compliance, demonstrates the environmental mobility and persistence of malathion.

Malathion is bioactivated to malaoxon, an oxon derivative which is more toxic than the parent compound, and a stronger inhibitor of acetylcholinesterase; hence, its toxicity is greater. A study of toxicity on zebrafish by Cui *et al.* [5] showed that malaoxon is about 32 times more toxic than malathion, indicating the increased danger associated with its formation. Hydrolysis of malathion yields malathion monocarboxylic acid (MCA) and malathion dicarboxylic acid (DCA). These are metabolites that are less toxic and participate in the mammalian detoxification process. Urinary analyses in human studies showed more malathion monocarboxylic acid than dicarboxylic acid, suggesting efficient excretion of these metabolites. More DCA and dimethylthiophosphate (DMTP) were found in zebrafish, indicating that the carboxylesterase pathway of hydrolysis is the major metabolic pathway [5]. The human body efficiently eliminates malathion, primarily through urinary excretion of its metabolites. Malathion monocarboxylic acids have been found to be the predominant urinary metabolites post ingestion because the body is able to detoxify and eliminate the compound within 12-24 hours. Environmental factors such as temperature and pH alter degradation pathways (ester hydrolysis and elimination) according to computational studies by Lamb *et al.* [6]. According to Vaishali *et al.* [7] Moreover, microorganisms, such as *Pseudomonas stutzeri* bacteria, also play a role in malathion's environmental breakdown through microbial degradation resulting in monocarboxylic and dicarboxylic acid derivatives.

The detoxification of malathion is thus carried out by diverse methods which include chemical treatment, photodecomposition, volatilization and incineration. Unfortunately, they are inefficient, costly, and environmentally unfriendly, so their application for complete removal of contaminants from solutions at low concentration is not viable. Bioremediation methodologies, mainly microbial and Phyto degradation have been adopted in recent years for pesticide removal. Bacterial genera such as *Bacillus* [8], *Pseudomonas* [7], *Flavobacterium* [9], *Sphingomonas* [10], and *Agrobacterium* [11] have shown efficacy towards malathion biodegradation.

Malathion exposure poses critical considerations in genotoxic and carcinogenic hazards. Acetylcholinesterase inhibition activity and its subsequent interference with the transmission of nerve impulse, accumulation of acetylcholine at synaptic junctions, and ultimately induction of its associated adverse health effects such as headache, dizziness, nausea, vomiting, bradycardia, and miosis have been associated with toxicity. According to Olakkaran *et al.* [12] Malathion toxicity in humans has been reported as oxidative stress. In vitro studies in human cell cultures and animal cells exposed to malathion demonstrated DNA damage and chromosomal alterations. In vivo experimental studies by Bastos *et al.* [13] have shown sufficient evidence regarding the potential of pesticides both in inducing genetic damage and inducing neoplasms in mammals. Epidemiological studies have shown statistically significant positive associations for thyroid, breast, and ovarian cancer in menopausal women. Malathion has been commonly used in the world in arbovirus control programs. In 2015, the International Agency for Research on Cancer (IARC) classified it as a probable carcinogen to humans [13].

Petsas and Vagi [14] conducted a study in which indigenous soil bacteria, like *Pseudomonas* sp., were used to degrade malathion. This indicates how these bacteria could provide a viable bioremediation contribution to wetland systems. Specific bacterial strains with the ability to degrade malathion provide a basis for developing plant-bacterial consortium for higher removal. The aim was to isolate and characterize malathion degrading bacteria from agricultural soil. They had identified *Pseudomonas* sp. through their experiments as a potential candidate for the degradation of malathion.

Further studies confirming the potential of plant-bacterial associations to enhance malathion degradation, are drawn from foundational work [2]. Additionally, the study by Cedillo-Herrera *et al.* [15] also further supports the role of wetland plants as hosts for malathion degrading bacteria as pointed out by Uniyal *et al.* [2]. In their work with microbial

consortium enriched from activated sludge, they show that microbial communities in wetlands can be used to promote increased malathion removal.

In the study conducted by Dar and Kaushik [16] bioremediation potential of pure bacterial strains and their consortia isolated form agricultural soil for degradation of the organophosphate pesticide malathion was evaluated. Individual strains degraded 50.16 - 68.47% malathion in 15 days, but complete degradation was observed in a mixed bacterial consortium of *Micrococcus aloeverae*, *Bacillus cereus* and *Bacillus paramycoides*. The degradation rates of partial consortia showed lower values (70.95 - 88.61%). Several intermediate metabolites, namely malaoxon, malathion monocarboxylic acid, diethyl fumarate, and trimethyl thiophosphate accumulated and disappeared successively during bioremediation process.

Study by Geed *et al.* [17] used the response surface methodology (RSM) to optimize the biodegradation parameters for malathion. They investigated malathion removal efficiency vs. pH and hydraulic retention time (HRT) in a batch and continuous flow system. However, their findings illustrated that under optimal conditions, the biodegradation process was greatly improved and were thus offered as a means for improving treatment systems where environments are contaminated with malathion. Isolation of bacterial strains capable of mineralizing malathion from agricultural soil revealed complete mineralization of malathion with butanedioic acid as the major metabolite. According to Jimenez-Torres *et al.* [18] the presence of non-oxidative degradation pathway is further supported by the absence of harmful intermediate metabolites. The use of such bacterial strains in wetlands may promote the removal of malathion and may open the possibility of using plant-bacterial consortia in bioremediation.

Although pesticide use in Pakistan is known to be heaviest on cotton—accounting for more than half of national consumption—other major crops such as rice, vegetables, fruits, sugarcane, and various horticultural crops are also treated with insecticides, including Malathion. However, no recent nationwide database provides crop-wise Malathion application patterns, and available information is limited to scattered residue studies and supplier recommendations reporting its presence in rice, pulses, vegetables, and mango. This lack of localized, site-specific data indicates a large disparity in knowledge and emphasizes the need to study Malathion degradation under Pakistan-specific conditions. The convincing results of the previous work suggested that plant-bacterial consortia hold great bioremediation potential for organophosphate pesticides in wetland settings. Wetlands harbor dynamic microbial communities and plant-microbe interactions, increasing the degradation pathways. Accordingly, the present study aims to enhance the performance of Malathion degradation utilizing wetland plants and plant-bacterial consortia in conjunction with monitoring efficiencies concurrently. Continued development of optimized bioremediation strategies and effective degraders can establish constructed wetlands as a sustainable solution for mitigating Malathion contamination in local ecosystems.

2. METHODOLOGY

2.1. Study Area and Sample Collection

This study evaluates the effects of plant-bacterial consortia for the removal of malathion from contaminated soil and water under controlled laboratory conditions. Soil samples were collected from agricultural land in Islamabad, Pakistan. Samples were taken at a depth of 0 - 15 cm using a sterile soil auger. Soil was collected, stored airtight and transported to the laboratory and then stored at 4 °C to prevent microbial degradation before analysis. To prepare a uniform soil matrix, large debris, plant matter and rocks were first removed with 2 mm sieve. After mixing the soil to make it homogeneous, physicochemical analyses and bioremediation experiments are conducted.

In this research, the bioremediation potential of plant associated bacterial consortia to remove malathion was explored, a method of colorimetric quantification was employed. In this approach, we combined the advantages of plant-bacterial interactions and analytical capability to meet the challenge of sustainable pesticide remediation. Early reports exposed bioremediation as a greener solution to pesticide pollution. Knowing plant associated bacteria and their ability to degrade different types of pollutants, we base our work on this knowledge. The overall aim was to test the reserve of plant bacterial consortia to disintegrate

malathion by using a colorimetric method [19]. The symbiotic relations between plants and bacteria were hypothesized to enhance Malathion removal rate and colorimetric approach was suggested for remediation monitoring.

2.1.1. Selection of plant-bacterial consortia

For development of a cost-effective bioremediation strategy for malathion degradation, the plant species which host pesticide degrading bacteria in their rhizosphere were identified carefully. This was primarily selected from a review of existing literature and past studies which indicate that certain plants associated with microbial communities could degrade organophosphate pesticides, like malathion [16].

After shortlisting the potential plant species, bacterial strains capable of proven pesticide degradation were isolated from its rhizosphere [20]. To accomplish this task soil from the root zone of these plants was collected, cultured, and screened to find many of the bacterial populations of these plants that can degrade malathion. The bacterial isolates were analyzed by microbiological and molecular techniques used to confirm their identity and degradation efficacy. The most effective strains for further experimentation were identified through analysis of key enzymatic pathways that degrade malathion.

Four bacterial consortia (C1 - C4) were prepared from the isolates obtained from malathion-contaminated soil. All isolates were characterized using Gram staining, oxidase and catalase tests, and were identified as Gram-positive, catalase-negative *Bacillus* spp. Although species-level molecular identification was not performed, isolates were grouped based on their biochemical profiles and malathion-degrading ability. The consortia were formulated by mixing the isolates in equal proportions: C1 (Isolate 1 + Isolate 2), C2 (Isolate 1 + Isolate 3), C3 (Isolate 2 + Isolate 3), and C4 (Isolate 1 + Isolate 2 + Isolate 3). These consortia were used for all subsequent biodegradation experiments.

2.1.2. Experimental design

To evaluate the efficiency of biodegradation of plant bacteria consortia, experimental design setup involved setting up controlled environments with different malathion concentrations [16]. The plant species associated with known degrading bacteria were selected for isolating some pesticide degrading bacteria from their rhizosphere and they were introduced into the plant rhizosphere in the experimental setups. The rate of malathion degradation over time was determined through colorimetric assays. This research opted for the colorimetric method as it is simple and low-cost, as well as effective in checking how malathion degrades in constructed wetlands. The color change that takes place during a chemical reaction with certain reagents helps quickly and accurately determine the concentration of malathion. As colorimetry does not depend on any of these expensive analysis tools but is easily performed, it is a convenient method for treating and comparing the samples from different laboratory experiments. Moreover, the data collected was obtained from credible sources and compatible with statistical analysis of assessing the effectiveness of bioremediation options. The colorimetric technique adopted a procedure similar to that suggested in the previous study by Sharma *et al*. [21], based on the variation of color produced by malathion degradation, analyzed using spectrophotometry. Differences in degradation between treatments were tested with ANOVA, and bacterial population dynamics and colorimetric data were related to determine the influence of plant-bacterial consortia on malathion removal efficiency.

2.2. Experimental Procedure

The soil samples were collected from malathion sprayed soil in the screening and isolation of malathion degrading bacteria [20]. Soil samples are spread on nutrient agar media using the spread plate method and the streak plate method is used to select and purify morphologically distinguishable colonies.

2.2.1. Isolation of bacteria

Soil samples where malathion was already introduced were used to isolate the bacteria for bioremediation [22]. Soil samples from malathion-treated sites were air-dried, sieved (2 mm) and 1 g of each sample was suspended in 9 ml sterile saline, followed by serial ten-fold dilutions up to 10^{-6}. Aliquots (100 µL) from appropriate dilutions

were spread on nutrient agar plates and incubated at 37 °C for 24 - 48 h. Distinct colonies were picked based on morphology, purified by repeated streaking, and maintained on nutrient agar slants. Representative isolates were stored as glycerol stocks at 4 °C for further characterization and used to prepare consortia.

2.2.2. Identification of bacteria

1.3 g of Nutrient broth was added to 100 milliliters of distilled water to enrich Bacterial culture. The solution was then sterilized by autoclaving at 121 °C for 15 mins [23]. Then, 10 ml of the nutrient broth was poured into a test tube, and a bacterial culture was added with a micropipette after autoclaving. To allow bacterial growth, the test tube was incubated at 37 °C for 48 hours. A total of three distinct bacterial isolates were purified from malathion-treated soil and used for consortium development.

2.2.2.1. Bacterial enrichment:

Nutrient broth was prepared by dissolving 13 g of the nutrient powder in one liter of distilled water. For a 100 ml solution, the amount was calculated as (13/1000) × 100 = 1.3 grams. This correctly weighed quantity was dissolved in 100 ml distilled water to obtain the culture medium for growth of bacteria. The nutrient broth was sterilized at 121 °C for 15 min by autoclaving [23]. Water boils at 100 °C and when the temperature rises to 121 °C, steam is formed which provides wet sterilization in autoclave. The autoclave was not immediately opened after the completion of 15 min sterilization run. The sample was cooled to a temperature of less than 72 °C and then opened [24].

The laminar flow hood was disinfected with spirit after being autoclaved for the sterility of working areas. The blower was turned on for clean airflow generation. Then, 10 ml of the sterilized nutrient broth was transferred into a test tube. Using a micropipette, 5 ml of the nutrient broth was taken, and the bacterial culture was added to the medium (Figure 1). The test tube was then incubated under controlled conditions at 37 °C for 48 hours to allow bacterial growth, facilitating enrichment of the bacterial culture. The bacterial characterization was done through gram staining according to standard protocols [25].

2.2.3. Constructed wetland

A constructed wetland [26] was established using pots filled with coarse and fine gravel, coarse gravel (20-30 mm diameter), fine gravel (2-10 mm diameter), sand, and soil from a specific site as shown in Figure 2. The local plants *Canna indica* and *Mentha arvensis* were selected. A total of 12 constructed wetland arrangements were maintained under different conditions: control, with isolated bacterial strains, soil alone, with plant and soil alone, and with a bacterial-plant consortium. The constructed wetland units were maintained in batch mode, and malathion-spiked soil/water remained in each system until the next sampling interval. Thus, the effective retention time was 14 days between consecutive samplings, consistent with common practice in small-scale wetland studies [16, 17]. All treatments were conducted in triplicate for each malathion concentration. Each replicate acted as an independent unit, and mean values were used for analysis to ensure statistical reliability and reduce experimental variation.

2.2.4. Soil parameters analysis

The soil of the constructed wetland used for malathion treatment was also examined for various properties such as saturation, pH, texture, organic matter, nitrogen content, P and K. The soil was 51% saturated and had a basic pH of 8.12. Its texture was considered as clay loam having 0.059% organic matter, 16 ppm N, and 131 ppm K. The pH value of the soil samples was analyzed by a pH meter for alkaline or acidic character. The organic matter proportion was determined using the same approach as above. All values of NO_3^- in soil samples were determined by UV spectrophotometer [27]. Moreover, concentrations of potassium and

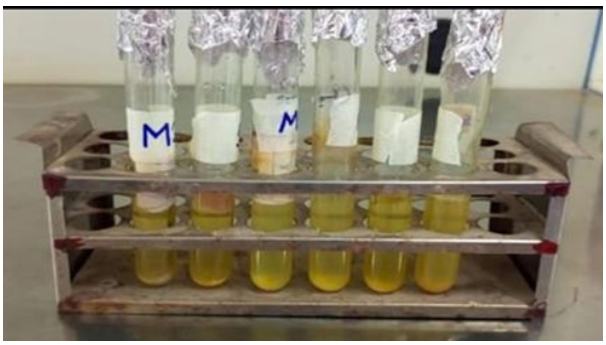

Fig. 1. Enrichment cultures in selective media for bacterial growth under controlled conditions.

Fig. 2. Lab based constructed wetland setup.

sodium in soil samples were determined by flame photometer. The test may be performed on any water sample and the results are detected in terms of flame color. Standards were originally run with sample in photometer. The blue changed to yellow in the flame colors, indicating that sodium and potassium are present. Measurements are easy to read on the meter. The parameters represented the conditions of an experiment to study the potential for bioremediation by a bacterial consortia in constructed wastelands. Beginning at a pH of 10 signified an extremely alkaline condition. This was applicable because certain bacterial populations dominate the acidic conditions which in turn are major contributors to biodegradation. The test was designed to study the way these modified bacteria led to remediation within wastelands. The presence of 1 g of organic matter acted as a carbon source for the bacteria.

This material was used as substrate for growth of and energy source for microorganisms; in fact, it allowed the biodegradation of pollutants in the constructed wasteland. One gram of total nitrate was added for its nitrogen, a second nutrient necessary for bacteria to proliferate and be active. Both potassium and sodium contents were 5 g. These components were necessary for various processes with bacterial cells. Potassium functioned for the activation of enzymes while sodium maintained cell turgor and osmotic pressure. They promoted bacterial growth and activity for bioremediation. By controlling initial conditions for the experiment, a suitable environment is established which allows growth and working of certain bacterial communities. These consortia are capable of degrading a variety of pollutants and providing remediation in the constructed wetlands. All soil characteristics (pH, organic matter, nitrate, potassium and sodium) were determined with triplicate samples for each treatment and sampling week. Three subsamples from each wetland unit were extracted and analyzed separately to maintain spontaneous soil parameter variation.

The removal efficiency (%) of malathion was calculated using the following formula:

$$\text{Removal efficiency} = \frac{\textit{initial concentration} - \textit{final concentration}}{\textit{initial concentration}} \times 100$$

This approach allowed for precise tracking of malathion degradation across different treatments over time.

3. RESULTS AND DICUSSION

3.1. Bacterial Characterization and Malathion Removal

Bacterial consortia isolated from the constructed wetlands have shown potential for malathion degradation. Biochemical characterization revealed that the four bacterial consortia used in this study consisted of different combinations of Gram-positive, catalase-negative *Bacillus* isolates. Since all isolates belonged to *Bacillus* spp., the performance differences observed among consortia likely reflect variations in enzyme activity and synergistic interactions rather than taxonomic differences. This isolated group of bacteria was identified as Gram-positive and catalase-negative, like the *Bacillus* spp. which are well-known to break down malathion. It is known that bacilli can degrade organophosphates by using carboxylesterases and related pathways [16]. Using Bacillus alone or in mixed cultures, it has been found to completely degrade a lot of malathion in soil. For instance, in a previous study, when both *Bacillus* and *Micrococcus* species were present, they mineralized 500 mg/kg malathion much faster

than single cultures, finishing the process within 15 to 20 days. Because our isolates were oxidase and catalase negative, they may use a unique mechanism to break down pesticides. They are consistent with recent findings suggesting Gram-positive Bacilli are good for removing organophosphates [16].

3.1.1. Biochemical characterization

Additionally, oxidase and catalase tests were conducted to further understand the metabolisms of the consortium. Results from the oxidase test were negative indicating that these bacteria do not have an enzyme (cytochrome c oxidase) normally used in aerobic respiration [28]. Furthermore, catalase test was negative, which means catalase enzyme, which breaks down hydrogen peroxide was absent [29]. These results provide useful indications of the metabolic profile of the consortium and degradation pathways. Gram staining was performed to differentiate bacterial cell wall structures. The Gram-negative staining pattern was characterized by a thin peptidoglycan layer and outer membrane [30], as Gram positive bacteria resist the crystal violet staining leaving the bacteria purple, while Gram negative bacteria do not retain the crystal violet staining and so appear pink [31]. The catalase test is performed to separate bacteria based on the formation of an enzyme called 'catalase', which helps in decomposing the hydrogen peroxide to form water and oxygen [32]. The lack of catalase activity in the isolates is consistent with the properties of certain *Bacillus* species.

3.2. Analysis

3.2.1. Bioremediation of Malathion through plant in soil

Sample collection and parameter checking was done after introducing pesticide. Each sample was collected with a gap of 2 weeks. The total time of bioremediation and sampling was eight weeks. Wetland plants contribute to malathion removal in several ways. First, plant roots can take up small amounts of pesticide from soil water, translocating it into root/shoot tissue where it may be sequestered or transformed. However, for non-volatile organophosphates like malathion, *direct* uptake tends to be limited compared to microbial breakdown [33]. The more important effect is indirect: the plant roots engineer the habitat for microbes. As noted, emergent macrophyte roots leak oxygen into the rhizosphere and exude sugars, amino acids and other carbon sources [34].

3.2.1.1. Treatment of Malathion through Canna indica and Mentha arvensis in soil sample taken from wetland media in first week of treatment process:

Figure 3 showcased remarkable bioremediation potential, reducing malathion concentrations with stunning efficiency across all initial levels. With a mere 3.2 mg/L remaining at the lowest starting concentration (50 mg/L), it achieved a near-perfect 99.34% degradation. This efficiency further increased to 99.68% and 99.9% for initial concentrations of 100 mg/L and 200 mg/L, respectively as shown in Figure 4. These findings indicate a strong metabolic potential of the bacterial consortium, when challenged with various malathion contamination levels. Efficiency was found to increase seismically with initial concentrations, suggesting possible induction or adaptation of the enzyme in the bacteria. This adaptability is crucial for real-world bioremediation where contaminant levels can vary significantly. *Canna indica and Mentha arvensis* therefore, emerges as a strong contender for effective malathion removal in constructed wastelands. Microbial communities in the rhizosphere engage in cooperative and competitive interactions, root exudates (sugars, amino acids, organic acids) boost microbial biomass and catabolic activity; microbes cometabolize malathion using enzymes induced by root-derived carbon or the pesticide itself [35].

3.2.1.2. Treatment of Malathion through Canna indica and Mentha arvensis in soil sample taken from wetland media in third week of treatment process:

Both *canna indica* and *mentha arvensis* exhibited consistent and high biodegradation efficiency across all malathion concentrations. As illustrated in Figure 5, initial concentrations of malathion at 50 mg/L, 100 mg/L, and 200 mg/L were reduced to 17 mg/L, 4 mg/L, and 2.3 mg/L respectively after treatment. This demonstrates the effective phytoremediation potential of the plant-soil system in degrading or removing malathion. Furthermore, Figure 6 highlights the removal efficiency across different concentrations. Efficiency increases with the dose from around 99.4% at 50 mg/L to

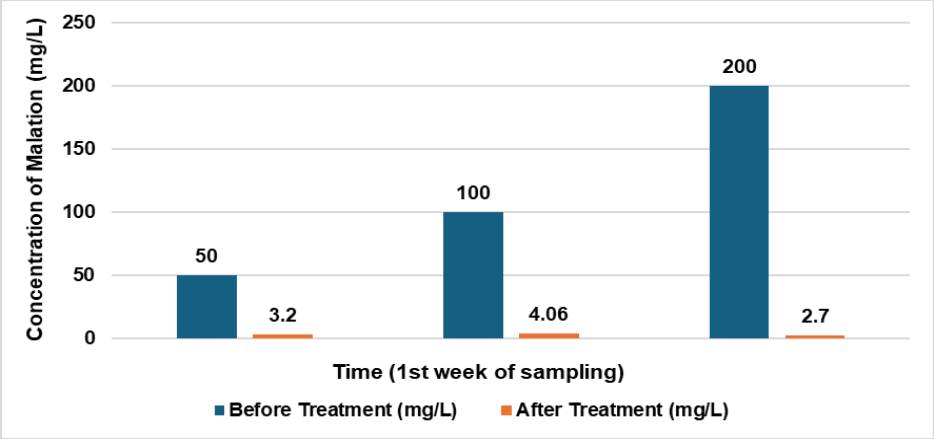

Fig. 3. Concentration of malathion before and after treatment with time (1st Sample (Plant + Soil)).

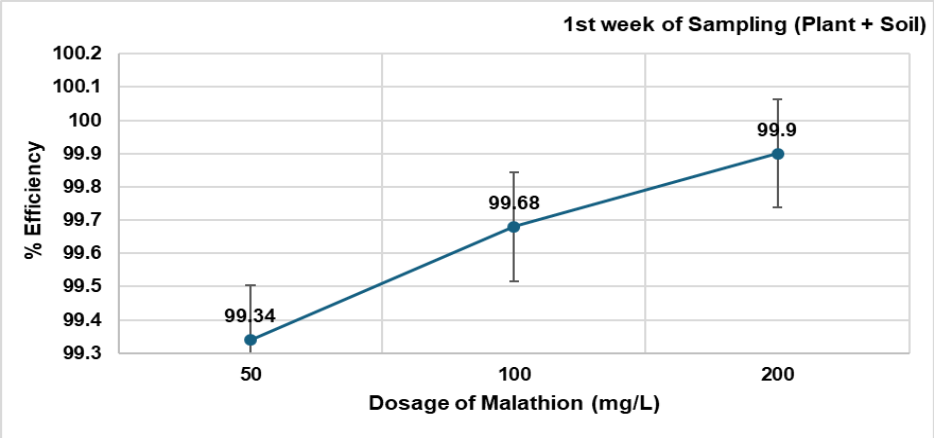

Fig. 4. Plant efficiency for treatment of different concentrations of malathion in wetland.

about 99.8% at 200 mg/L. These findings indicate that the treatment is marginally more effective at higher initial concentrations, which implies that the plant-soil system has a high ability to accept more pesticide. Despite greatly elevated resistance, it retained its functionality and is therefore a potential tool for bioremediation projects in which predictable outcomes are important. The composition and metabolism of this engineered consortium may potentially be further explored to understand its stable performance.

3.2.1.3. Treatment of Malathion through Canna indica and Mentha arvensis in soil sample taken from wetland media in fifth week of treatment process:

The treatment of malathion-contaminated soil using *Canna indica* and *Mentha arvensis* in a wetland media showed highly effective results by the fifth week of the treatment process. As illustrated in Figure 7, the efficiency of malathion removal increased with the dosage applied, reaching approximately 99.31% at 50 mg/L, 99.68% at 100 mg/L, and nearly 99.9% at 200 mg/L. This demonstrates a strong positive correlation between malathion concentration and phytoremediation efficiency, indicating the robustness of the treatment system even at higher contamination levels. Correspondingly, Figure 8 shows a significant reduction in malathion concentration in the third treatment i.e. plant + soil. Initial concentrations of 50 mg/L, 100 mg/L, and 200 mg/L were reduced to 9 mg/L, 3 mg/L, and 5.5 mg/L, respectively, after five weeks. The residual malathion concentration was lowest in the sample with 100 mg/L initial malathion concentration, indicating better performance at this level. In general, these results have revealed that the mixture of *Canna indica* and *Mentha arvensis* has an excellent efficiency for phytoremediation of malathion in soil at wetland, making it an eco-friendly tool for the control of pesticide contamination.

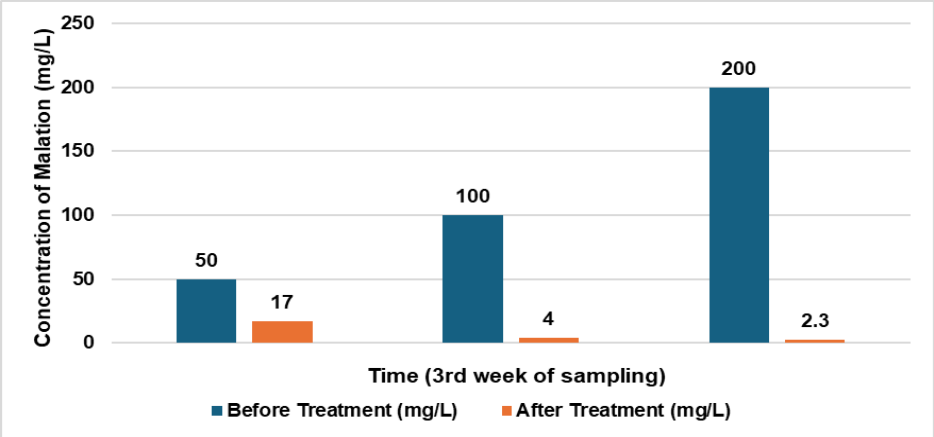

Fig. 5. Concentration of malathion before and after treatment with time (2nd Sample (Plant + Soil)).

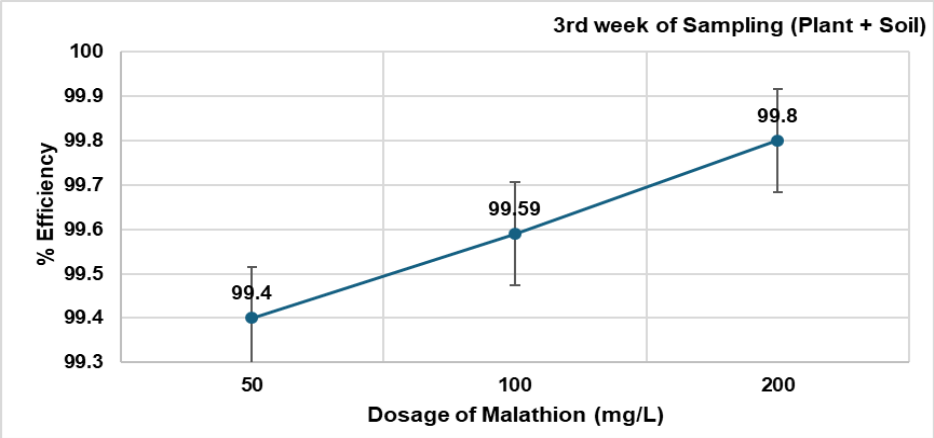

Fig. 6. Plant efficiency for treatment of different concentrations of malathion in wetland.

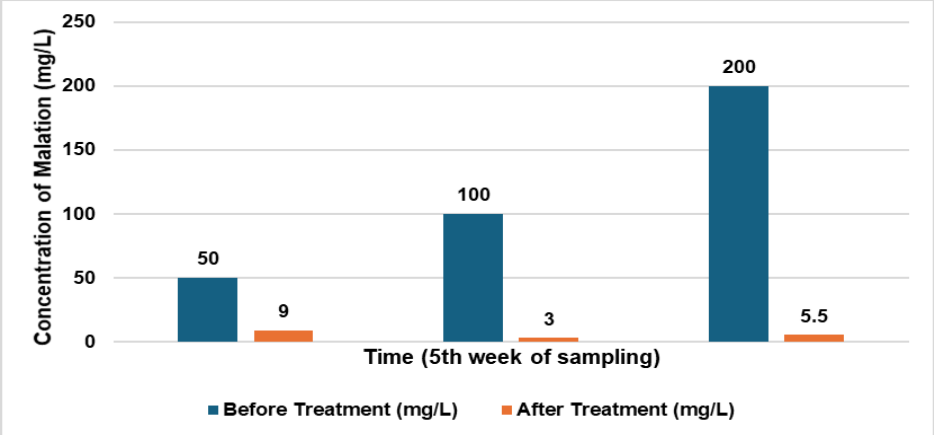

Fig. 7. Concentration of malathion before and after treatment with time (3rd Sample (Plant + Soil)).

3.2.1.4. Treatment of Malathion through Canna indica and Mentha arvensis in soil sample taken from wetland media in seventh week of treatment process:

In the seventh week of treatment, the removal of malathion from soil using *Canna indica* and *Mentha arvensis* continued to show exceptional results. Figure 9 shows that the malathion concentrations decreased significantly from 50, 100, and 200 mg/L to 2.4, 12, and 10 mg/L, respectively. The most significant reduction was observed at the 50 mg/L dosage, showing a drop to just 2.4 mg/L, indicating the high efficacy of the phytoremediation system at lower concentrations. Figure 10 presents the corresponding efficiency of malathion removal. The data shows that the system achieved an efficiency of around 99.8% at 50 mg/L,

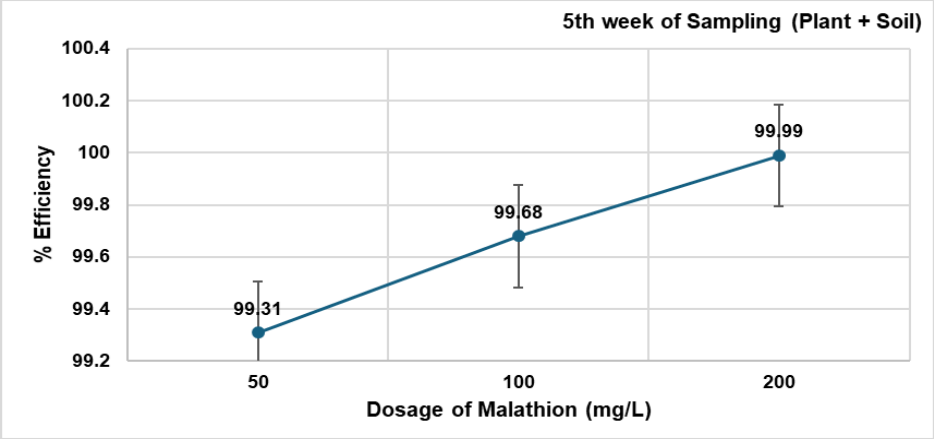

Fig. 8. Plant efficiency for treatment of different concentrations of malathion in wetland.

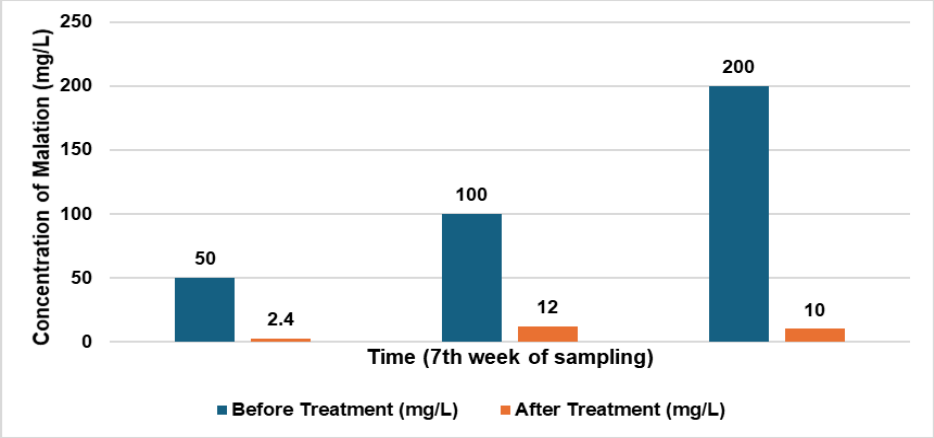

Fig. 9. Concentration of malathion before and after treatment with time (4th Sample (Plant + Soil)).

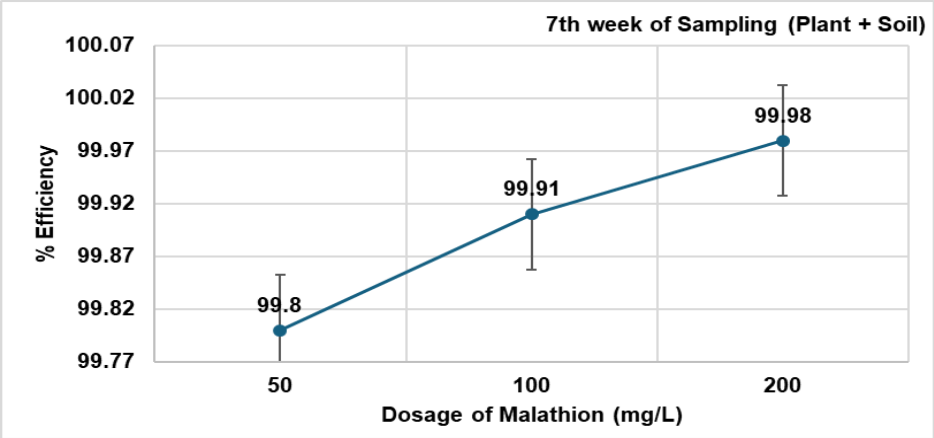

Fig. 10. Plant efficiency for treatment of different concentrations of malathion in wetland.

slightly above 99.91% at 100 mg/L, and maintained a similarly high level close to 99.98% at 200 mg/L. The near-complete removal of malathion across all concentrations by the seventh week confirms the potential of *Canna indica* and *Mentha arvensis* as reliable phytoremediators for treating pesticide-contaminated wetland soils over time. In practice, planted wetlands consistently outperform unplanted controls for pesticide removal. For example, Tang et al. [36] reported that *Canna indica* wetlands removed more pesticide mass than unplanted system.

Table 1 shows how increasing malathion concentrations (50, 100, and 200 mg/L) influenced soil properties under plant treatments P1-P4. Soil pH remained slightly alkaline across all setups, ranging from 7.30 to 7.76, with only minor shifts

as concentrations increased. Organic matter varied widely depending on the treatment, from as low as 8-10% in P1 to as high as 40 - 60% in P3. Total nitrate generally increased in several setups, such as in P3 where it rose from 251.66 mg/L at 50 mg/L to 500.83 mg/L at 200 mg/L, and in P4 where it remained high (340 - 503.33 mg/L) across treatments. Potassium values ranged between 3.1 and 10.7 mEq/kg, while sodium fluctuated between 22 and 54 g/mol, without a clear concentration-dependent pattern. Overall, these values indicate that plant treatments show moderate but variable nutrient responses to malathion exposure.

The significant results from these experiments prove that phytoremediation has great potential. Many species growing in wetlands, including *Canna indica* and *Mentha arvensis*, help clean up pollutants by using their vast root systems and rhizobacteria [26]. According to other studies, organophosphate removal is successful when carried out by wetland plants and the bacteria living in wetlands. When *Canna indica*, *Mentha arvensis* and pesticide-degrading bacteria were added to a constructed wetland, chlorpyrifos was fully broken without leaving any toxic substances. As with malathion, we find that plants can quickly absorb or transform it and speed up their decomposition, resulting in > 99% removal within just a few weeks [26]. Our results show that plant-assisted systems achieved > 99% removal but took slightly longer than bacteria alone. Plants reached near-complete removal by Weeks 3-5, likely because their roots improved aeration and supported microbial activity, helping maintain continuous malathion degradation [37].

3.2.2. Bioremediation of Malathion through bacteria in soil

Sample collection and parameter checking was done after introducing pesticide. Each sample was collected with a gap of 2 weeks. Total time of bioremediation and sampling was eight weeks. Many bacteria use organophosphorus-

Table 1. Soil properties under plant treatments (P1–P4) at different malathion concentration.

Samples	Parameter	50 mg/L	100 mg/L	200 mg/L
1st week (P1)	pH	7.38	7.43	7.30
	Organic matter (%)	10	8	8
	Total nitrate (mg/L)	196.6	245.8	237.5
	Potassium (mEq/kg)	3.1	3.1	3.1
	Sodium (g/mol)	54	28	22
3rd week (P2)	pH	7.30	7.36	7.70
	Organic matter (%)	20	20	20
	Total nitrate (mg/L)	170	295.83	319.16
	Potassium (mEq/kg)	10.7	6.7	5.7
	Sodium (g/mol)	42	40	38
5th week (P3)	pH	7.54	7.64	7.66
	Organic matter (%)	60	20	40
	Total nitrate (mg/L)	251.66	330	500.83
	Potassium (mEq/kg)	7.7	5.1	7.4
	Sodium (g/mol)	38	30	34
7th week (P4)	pH	7.55	7.67	7.76
	Organic matter (%)	10	20	20
	Total nitrate (mg/L)	503.33	340	405.83
	Potassium (mEq/kg)	7.4	6.2	7.9
	Sodium (g/mol)	30	34	32

degrading enzymes (organophosphorus hydrolases/phosphotriesterases/carboxylesterases) to cleave the P-O or ester bonds in malathion, producing monocarboxylic/dicarboxylic acids and ultimately mineralization products [38].

3.2.2.1. First soil sample extracted from wetland media at first week to determine treatment of malathion through bacteria:

In the first week of treatment, the bacterial remediation of malathion-contaminated soil extracted from wetland media showed encouraging results. As illustrated in Figure 11, initial malathion concentrations of 50 mg/L, 100 mg/L, and 200 mg/L were reduced to 6.1 mg/L, 5.5 mg/L, and 4.2 mg/L, respectively, after treatment. These reductions demonstrate that the bacterial activity began to effectively degrade malathion even within a short time frame. The efficiency of removal, shown in Figure 12, was approximately 99.40% at 50 mg/L, increasing to around 99.65% at 100 mg/L and 99.70% at 200 mg/L. The trend indicates that the bacterial system performs well across varying contamination levels, with slightly higher efficiency observed at greater concentrations. Malathion is degraded by carboxylesterases to its monoacid and diacid derivatives; this is the main metabolic mechanism for the degradation of malathion by microorganisms [39]. Overall, these findings confirm the potential of bacteria as a rapid and efficient means for the biodegradation of malathion in soil, especially useful for early-stage treatment in wetland-based remediation systems.

3.2.2.2. Second soil sample extracted from wetland media at 3rd week to determine treatment of malathion through bacteria:

In the third week of treatment, the second soil sample extracted from wetland media and treated with bacteria continued to show significant

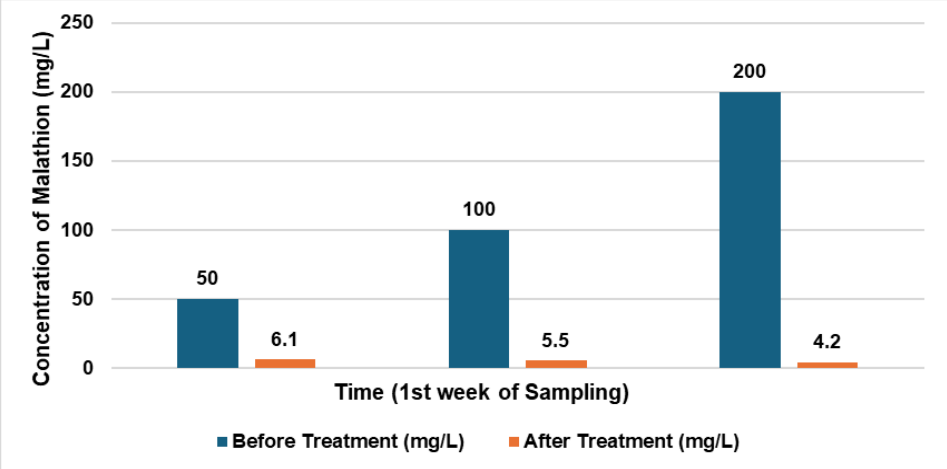

Fig. 11. Concentration of malathion before and after treatment with time (1st Sample (Bacteria + Soil)).

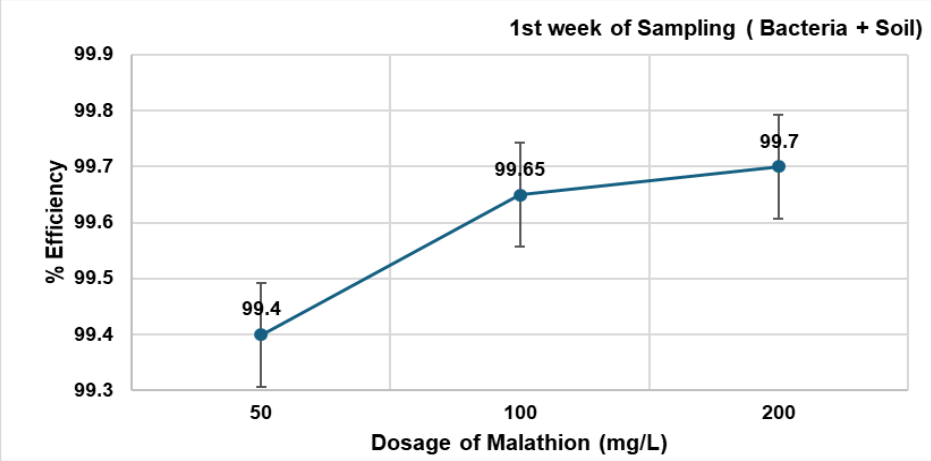

Fig. 12. Efficiency of bacteria for treatment of different concentrations of malathion in wetland.

degradation of malathion. As seen in Figure 13, malathion concentrations of 50 mg/L, 100 mg/L, and 200 mg/L were reduced to 10 mg/L, 9 mg/L, and 4.2 mg/L, respectively, after treatment. These data suggest that the bacterial activity was also retained over time, especially with larger dosages. The corresponding removal rates are illustrated in Figure 14 and they exhibited an increasing trend: about 99.15% for 50 mg/L, 99.56% for 100 mg/L, and finally rose to nearly 99.78% at the concentration of 200 mg/L.. The degradation power of malathion depends predominantly on the microorganism enzymatic activity. Enzymes are the biocatalysts which can enhance the rate of certain biochemical reaction by decreasing the activation energy [40]. This pattern demonstrates both the persistent and dose-responsive biodegradative capacity of the bacteria, which further supports its viability for use as a dependable candidate organism for treatment of malathion in wetland-based soil systems.

3.2.2.3. Third soil sample extracted from wetland media at 5th week to determine treatment of malathion through bacteria:

In the fifth week of sampling, bacteria and wetland media soil were screened for the ability to degrade malathion at different concentrations. The results presented in Figures 15 show a significant reduction in malathion levels after bacterial treatment. At 50 mg/L initial concentration, the removal of malathion was found to be 64% and decreased its concentration down to 18 mg/L. When the initial concentration was 100 mg/L, it decreased to 9.4 mg/L (removal efficiency reached 90.6%); while at the highest concentration of 200 mg/L, malathion remained at only 3.3 mg/L with removal efficiency of about 98.35% as shown in Figure16. The efficiency graph also shows that the rate of malathion removal was positively correlated with its initial concentration and reached 99.4%, 99.6%,

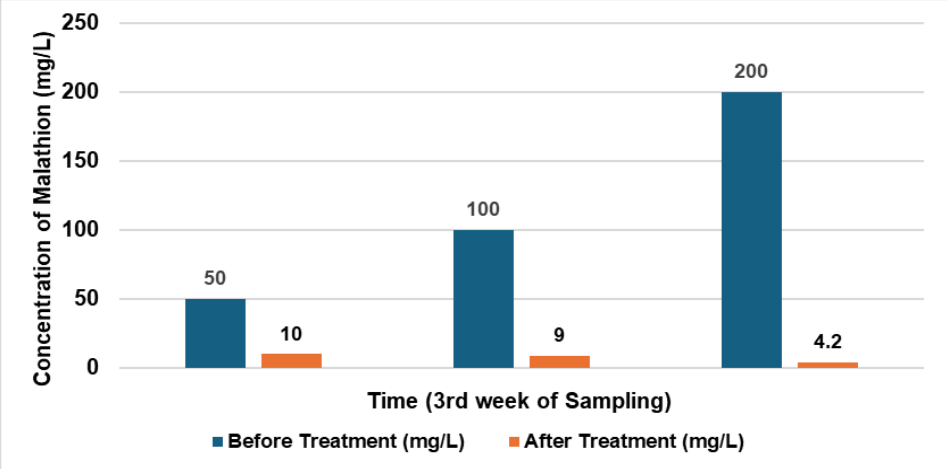

Fig. 13. Concentration of malathion before and after treatment with time (2nd Sample (Bacteria + Soil)).

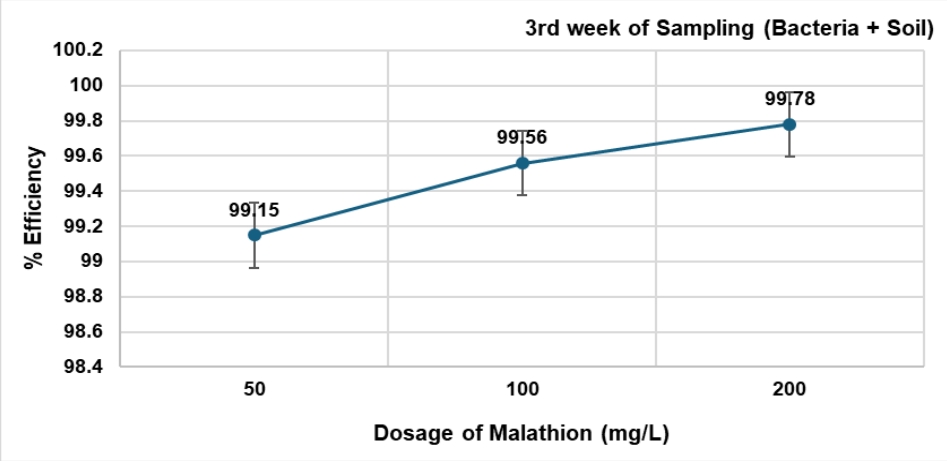

Fig. 14. Efficiency of bacteria for treatment of different concentrations of malathion in wetland.

and 99.9% for doses of 50, 100, and 200 mg/L, respectively. These results demonstrate that the bacterial activity in the wetland media is extremely effective for malathion degradation, especially at higher concentrations and has potential for use in bioremediation.

3.2.2.4. Fourth soil sample extracted from wetland media at seventh week to determine treatment of malathion through bacteria:

As can be seen from Figure 17 the malathion concentrations after treatment significantly reduced for all concentration tested. The concentration decreased from 50 mg/L to 4.6; at dosage of 100 mg/L reduced to 5.8, and dosage of 200 mg/L fell to 5.6 mg /L. This visibly suggests that a significant amount of malathion was degraded by bacteria existing in soil/wetland media and proved it that are effective against high dosages too. In addition, degradation efficiencies of about 99.80% at 50 mg/L, 99.94% at 100 mg/L and 99.97% at 200 mg/L as shown in Figure 18 indicates the high performance of bacterial system to detoxify malathion in environment. The low increase in efficiency with higher doses indicates a possible adaptation of the bacterial population or better performance under heavy pollution.

Table 2 illustrates the stronger chemical shifts observed under bacterial treatments B1 - B4. Soil pH stayed between 7.12 to 7.80, showing slight decreases at higher malathion concentrations in some setups. Organic matter ranged from 10% to 40%, depending on the treatment. A pronounced response was observed in nitrogen and nitrate levels: for example, in B1 total nitrogen increased sharply from 657.5 mg/L at 50 mg/L to 1303.3 mg/L at 100 mg/L, while B2 recorded nitrate values as high as 1747.5 mg/L at 100 mg/L. Sodium concentrations ranged from 26 to 76 mEq/kg, and higher values were found in B2 with 200 mg/L,

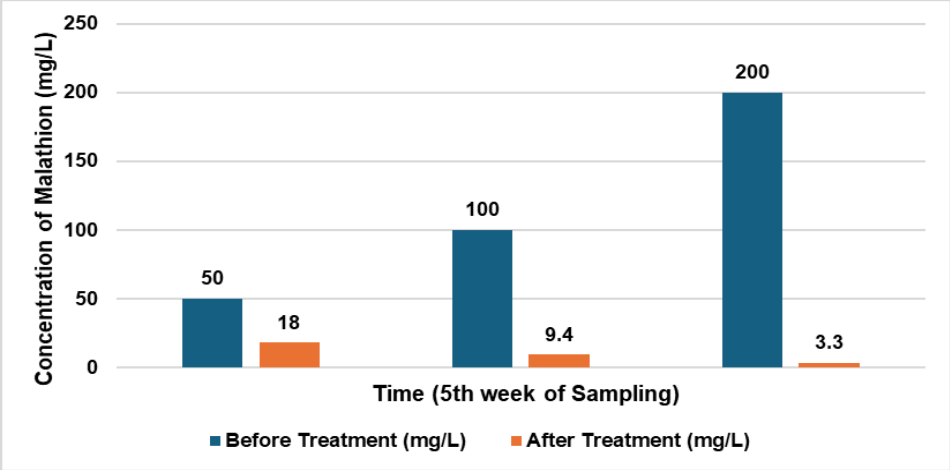

Fig. 15. Concentration of malathion before and after treatment with time (3rd Sample (Bacteria + Soil)).

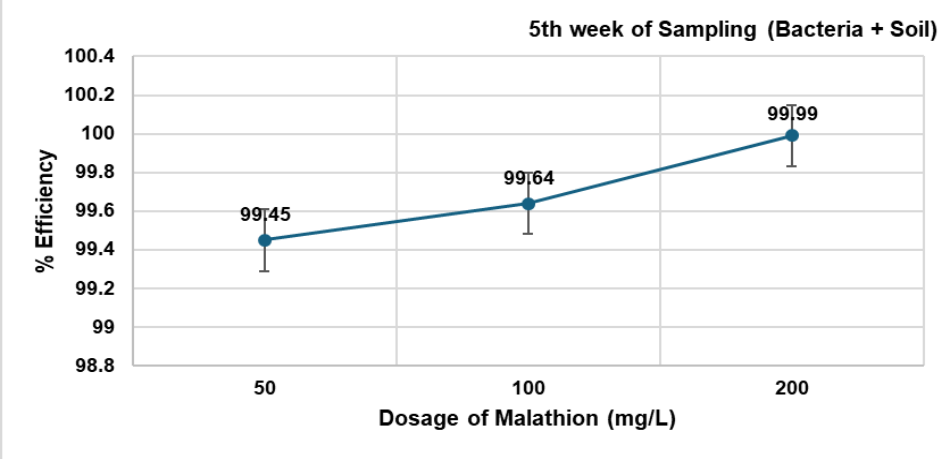

Fig. 16. Efficiency of bacteria for treatment of different concentrations of malathion in wetland.

whereas potassium varied between 4.9 and 20 g/mol, the same type of treatment led to intense changes on this element. These numbers indicate that bacterial activity induces stronger nutrient modifications than plant treatments when applied in combination with malathion.

Prior research showed that *Bacillus*-based groups could completely remove a high level of malathion, while single strains were much less effective [16]. In addition, *Pseudidiomarina* strains present in deep-sea waters degraded malathion at 500 mg/L to below detection levels in just 36 h [16]. The consortium's high performance and the trend we noticed with more pollutants indicate that enzymes are being made or microbes are becoming more tolerant of the contaminant. The same phenomenon has been spotted in other biodegradation systems, where these systems exhibit greater catabolic activity when there is a high contaminant concentration.

All systems showed almost complete malathion decomposition after eight weeks. Initially, bacterial consortia were the most effective, followed by plant systems that increased both uptake and stability. It proves that using these interactions in wetlands is a great, inexpensive way to address and clean up pesticide-polluted waters and soils

3.2.3. Two-Way ANOVA results for Malathion removal efficiency

In the plant-based treatment system, a two-factor ANOVA with replication (Table 3) was conducted to evaluate the effects of sampling week and treatment dose on the measured response variable. The analysis revealed a statistically significant main effect of week ($F = 228.44$, $p < 0.001$), indicating that the response values changed consistently across Week 1, Week 3, Week 5, and Week 7. There was also a highly significant main effect of dose level ($F = 932.59$, $p < 0.001$), demonstrating that

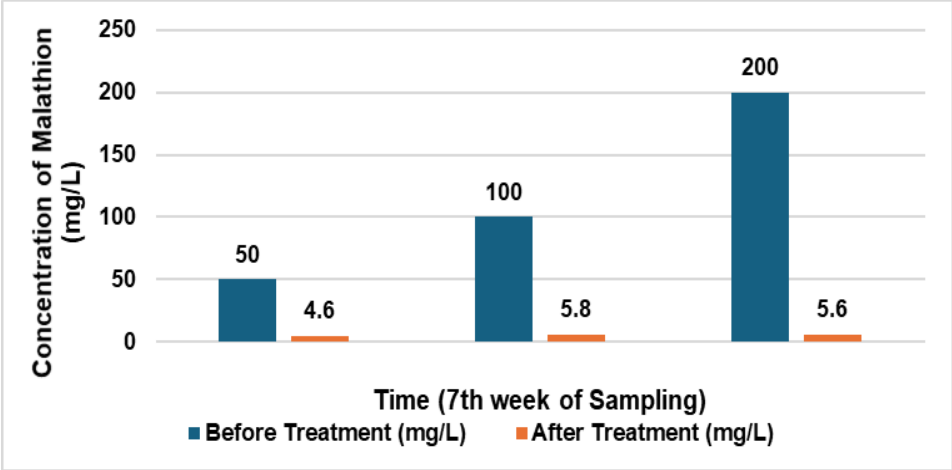

Fig. 17. Concentration of malathion before and after treatment with time (4th Sample (Bacteria + Soil)).

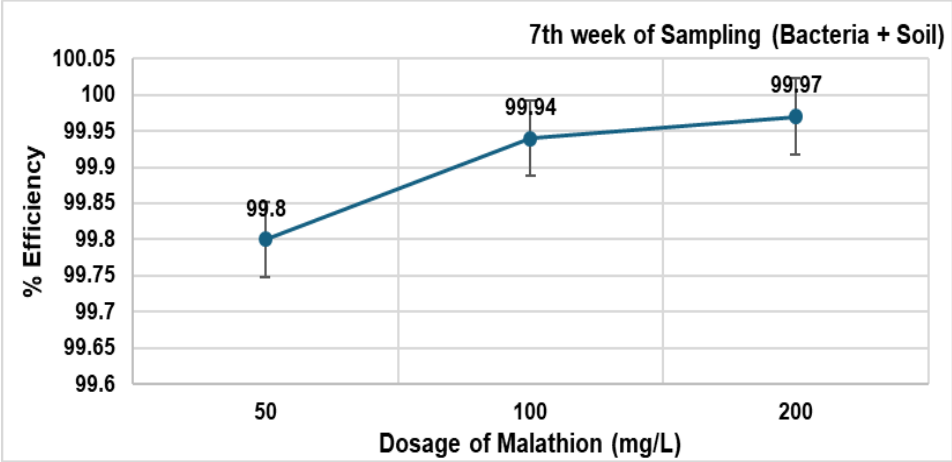

Fig. 18. Efficiency of bacteria for treatment of different concentrations of Malathion in wetland.

Table 2. Soil properties under bacterial treatments (B1 - B4) at different malathion concentrations.

Samples	Parameter	50 mg/L	100 mg/L	200 mg/L
1st week (B1)	pH	7.80	7.58	7.36
	Organic matter (%)	40	10	10
	Total nitrate (mg/L)	657.5	1303.3	577.5
	Sodium (mEq/kg)	54	59	46
	Potassium (g/mol)	14.1	12.5	12.1
3rd week (B2)	pH	7.48	7.36	7.30
	Organic matter (%)	30	10	20
	Total nitrate (mg/L)	417.5	1747.5	1245.8
	Sodium (mEq/kg)	28	38	76
	Potassium (g/mol)	4.9	7.4	20.0
5th week (B3)	pH	7.53	7.36	7.40
	Organic matter (%)	20	10	10
	Total nitrate (mg/L)	427.1	1847.6	1045.7
	Sodium (mEq/kg)	26	30	45
	Potassium (g/mol)	14.1	13.6	12.1
7th week (B4)	pH	7.20	7.12	7.40
	Organic matter (%)	10	10	20
	Total nitrate (mg/L)	412.5	1303.3	577.5
	Sodium (mEq/kg)	27	36	40
	Potassium (g/mol)	14.1	13.5	12.1

increasing the dose from 50 to 100 and 150 resulted in progressively higher mean values. There was also a significant week dose interaction ($F = 52.18$, $p < 0.001$) showing that the dose effect decreased or increased depending on week of sampling. This interaction suggests that the disparity in dose levels was not constant over time and response profile to treatment also varied as a function of time. Certainly, both factors had independent (and combined) effects in determining the resulting behavior, and very low within-group variation indicated strong statistical power.

For the bacteria-based treatment system, a 2-factor ANOVA with replication (Table 4) was performed to determine the influence of treatment level (50, 100, 150) and time points (weeks: 1, 3, 5, and 7) on response values. The analysis revealed a strong main effect of time ($F = 111.05$, $p = 3.31 \times 10^{-14}$) and treatment level ($F = 204.61$, $p = 8.36 \times 10^{-16}$), thereby demonstrating that both factors were independently associated with positive outcomes, with higher treatment levels producing higher averages. A significant interaction effect was also found ($F = 16.33$, $p = 2.05 \times 10^{-7}$), showing that

Table 3. Two-factor ANOVA results for the removal of malathion using plant-based wetland treatment across different dose levels and sampling weeks.

Source of Variation	SS	df	MS	F	P-value	F crit
Sample	0.4702	3	0.156733	228.4372	8.93E-18	3.008787
Columns	1.279717	2	0.639858	932.587	1.77E-23	3.402826
Interaction	0.214817	6	0.035803	52.18219	1.35E-12	2.508189
Within	0.016467	24	0.000686			
Total	1.9812	35				

Table 4. Two-factor ANOVA results for the removal of malathion using bacteria-based wetland treatment across different treatment levels and sampling weeks.

Source of Variation	SS	df	MS	F	P-value	F crit
Sample	0.832875	3	0.277625	111.05	3.31E-14	3.008787
Columns	1.02305	2	0.511525	204.61	8.36E-16	3.402826
Interaction	0.24495	6	0.040825	16.33	2.05E-07	2.508189
Within	0.06	24	0.0025			
Total	2.160875	35				

the impact of treatment varied across weeks. The very small within-group variance reflects strong consistency in the repeated measurements. Overall, the results confirm that both treatment level and time significantly affected the response variable.

3.2.4. Comparative performance and synergy

All the treatments effectively removed > 99% malathion, but they worked differently. Initially, bacteria-only wetlands caused a quicker drop: in just days, they brought pollutant removal close to its maximum, but plants needed weeks to clear as much. In addition, plants helped continue the loss of soil quality and structure as time passed. A wetland created with a plant–bacterial consortium would probably benefit from both methods. Scientists in constructed wetland science believe this complementary effect is strongly linked, as all removal of contaminants often results from combined efforts of substrates, plants and microbes [41]. Mechanistically, plants and microbes complement each other. Established macrophytes continuously oxygenate the rhizosphere and leak nutrients (e.g., low-molecular-weight carbon) that "awaken" soil bacteria [34]. Rapidly, malathion is attacked by microbes and plants prevent anything from the effluent coming back into contact with the soil. Our findings agree with what others have observed, that plant–microbe systems deal with pesticides effectively without leaving any harmful residues [26, 27]. Higher efficiency at higher concentrations likely reflects microbial adaptation: high malathion loads induce stronger biodegradation. For example, our consortia's near-100% removal at 200 mg/L (within 7 weeks) suggests that bacterial enzymes were fully engaged. In contrast, at 50 mg/L the process was slightly slower, perhaps because enzyme expression was lower. This inverse concentration-dependency is supported by other reports: degrading bacteria often shows greater catabolic activity under elevated pollutant stress. In summary, the observed trends can be explained by the underlying biochemistry of malathion breakdown and the synergistic ecology of the wetland rhizosphere.

4. CONCLUSIONS

The present study demonstrates that both bacterial consortia (*Bacillus* spp. isolates) and plant-based systems (*Canna indica and Mentha arvensis*), alone and in combination, achieved very high malathion removal from spiked soil: all treatments reached > 99% removal by Week 7 across tested concentrations (50, 100, 200 mg/L). Bacteria-only treatments produced the most rapid initial decline (significant main effects of time and dose: $F = 111.05$ and $F = 204.61$, respectively; $p < 1 \times 10^{-13}$), while planted systems provided sustained removal and habitat support for microbial activity (plant ANOVA: $F = 228.44$ and $F = 932.59$ for week and dose, respectively; $p < 1 \times 10^{-16}$). The higher apparent removal at larger initial doses is consistent with induction or up-regulation of catabolic activity under greater pollutant stress, although enzyme activity and metabolite profiles were not measured here and thus this remains a testable hypothesis. Mechanistically, the results are consistent with microbial hydrolysis (e.g., carboxylesterase activity) and rhizosphere-stimulated microbial degradation: bacterial consortia gave rapid biodegradation while plant roots likely enhanced oxygenation and exudation that sustained breakdown over weeks. However, this study is limited to lab-scale, colorimetric quantification and morphological/biochemical bacterial identification (no species-level molecular ID or metabolite analysis). Future work should (i) confirm degrader identity by sequencing, (ii) measure enzyme activities and

malathion metabolites to validate pathways, and (iii) evaluate pilot-scale constructed wetlands under field conditions. Overall, plant-bacterial consortia show strong potential as a low-cost, environmentally friendly option for remediation of malathion-contaminated soils, but field validation and mechanistic confirmation are required before deployment.

5. ACKNOWLEDGEMENT

The authors acknowledge the assistance and support of the laboratory staff of Bahria University, Islamabad.

6. CONFLICT OF INTEREST

The authors declare no conflict of interest

7. REFERENCES

1. F.A. Al-Saeed, S.S. Abd-Elghfar, and M.E. Ali. Efficiency of thyme and oregano essential oils in counteracting the hazardous effects of malathion in rats. *Animals* 14(17): 2497 (2024).
2. S. Uniyal, R.K. Sharma, and V. Kondakal. New insights into the biodegradation of chlorpyrifos by a novel bacterial consortium: process optimization using general factorial experimental design. *Ecotoxicology and Environmental Safety* 209: 111799 (2021).
3. U.S.E.P. Agency. Reregistration Eligibility Decision (RED) for Malathion. *U.S. EPA, Washington, DC* (2006). https://archive.epa.gov/pesticides/reregistration/web/pdf/malathion-red-revised.pdf
4. U.S.G. Survey. Pesticides in the Nation's Streams and Ground Water, 1992–2001: The Quality of Our Nation's Waters. *U. S. G. Survey, Washington, DC, USA* (2006). https://pubs.usgs.gov/circ/2005/1291/pdf/circ1291.pdf
5. J. Cui, Y. Wei, J. Jiang, S. Xiao, X. Liu, Z. Zhou, D. Liu, and P. Wang. Bioaccumulation, metabolism and toxicological effects of chiral insecticide malathion and its metabolites in zebrafish (*Danio rerio*). *Chemosphere* 318: 137898 (2023).
6. R.W. Lamb, H. McAlexander, C.M. Woodley and M.K. Shukla. Towards a comprehensive understanding of malathion degradation: theoretical investigation of degradation pathways and related kinetics under alkaline conditions. *Environmental Science: Processes & Impacts* 23(8): 1231-1241 (2021).
7. S. Vaishali, A. Surendran, and A. Thatheyus. Biodegradation of malathion using *Pseudomonas stutzeri* (MTCC 2643). *Journal of Public Health International* 2(4): 8-19 (2020).
8. M.A. Dar and G. Kaushik. Optimizing the malathion degrading potential of a newly isolated *Bacillus* sp. AGM5 based on Taguchi design of experiment and elucidation of degradation pathway. *Biodegradation* 33(5): 419-439 (2022).
9. D.G. Karpouzas and B.K. Singh. Microbial degradation of organophosphorus xenobiotics: metabolic pathways and molecular basis. *Advances in Microbial Physiology* 51: 119-225 (2006).
10. S.R. Geed, M.K. Kureel, A.K. Shukla, R.S Singh, and B.N Rai. Biodegradation of malathion and evaluation of kinetic parameters using three bacterial species. *Resource-Efficient Technologies* 2: S3-S11 (2016).
11. B. Singh, J. Kaur, and K. Singh. Microbial degradation of an organophosphate pesticide, malathion. *Critical Reviews in Microbiology* 40(2): 146-154 (2014).
12. S. Olakkaran, A.K. Purayil, A. Antony, S. Mallikarjunaiah, and G.H. Puttaswamygowda. Oxidative stress-mediated genotoxicity of malathion in human lymphocytes. *Mutation Research/Genetic Toxicology and Environmental Mutagenesis* 849: 503138 (2020).
13. P.L. Bastos, A.F.T.d.L. Bastos, A.d.M. Gurgel, and I.G.D. Gurgel. Carcinogenicidade e mutagenicidade do malathion e seus dois análogos: uma revisão sistemática. *Ciência & Saúde Coletiva* 25(8): 3273-3298 (2020).
14. A.S. Petsas and M.C. Vagi. Trends in the bioremediation of pharmaceuticals and other organic contaminants using native or genetically modified microbial strains: a review. *Current Pharmaceutical Biotechnology* 20(10): 787-824 (2019).
15. C.I. Cedillo-Herrera, A. Roé-Sosa, A.M. Pat-Espadas, K. Ramírez, J. Rochín-Medina, and L.E. Amabilis-Sosa. Efficient malathion removal in constructed wetlands coupled to UV/H_2O_2 pretreatment. *Applied Sciences* 10(15): 5306 (2020).
16. M.A. Dar and G. Kaushik. Biodegradation of malathion in amended soil by indigenous novel bacterial consortia and analysis of degradation pathway. *Soil Systems* 7(4): 81 (2023).
17. S.R. Geed, M.K. Kureel, B.S. Giri, R.S. Singh, and B.N. Rai. Performance evaluation of Malathion biodegradation in batch and continuous packed bed bioreactor (PBBR). *Bioresource Technology* 227: 56-65 (2017).
18. C. Jimenez-Torres, I. Ortiz, P. San-Martin, and R.I.

Hernandez-Herrera. Biodegradation of malathion, α-and β-endosulfan by bacterial strains isolated from agricultural soil in Veracruz, Mexico. *Journal of Environmental Science and Health, Part B* 51(12): 853-859 (2016).

19. D. Li, S. Wang, L. Wang, H. Zhang, and J. Hu. A simple colorimetric probe based on anti-aggregation of AuNPs for rapid and sensitive detection of malathion in environmental samples. *Analytical and Bioanalytical Chemistry* 411(12): 2645-2652 (2019).
20. A. Mehta, K.K. Bhardwaj, M. Shaiza, and R. Gupta. Isolation, characterization and identification of pesticide degrading bacteria from contaminated soil for bioremediation. *Biologia Futura* 72(3): 317-323 (2021).
21. D.K. Sharma, N. Thakur, A. Sharma, and P. Raj. New Spectrophotometric Method for the Analysis of Commercial Malathion Formulation and Its Residues on Some Crop Produces and Environmental Samples. *Journal of Advanced Scientific Research* 11(02): 131-136 (2020).
22. W.M. Ibrahim, M.A. Karam, R.M. El-Shahat, and A.A. Adway. Biodegradation and utilization of organophosphorus pesticide malathion by cyanobacteria. *BioMed Research International* 2014(1): 392682 (2014).
23. U.S.F.a.D. Administration. BAM Media M114: Nutrient Broth. *U.S. Food and Drug Administration, Silver Spring, MD* (2017). https://www.fda.gov/food/laboratory-methods-food/bam-media-m114-nutrient-broth
24. J. Reynolds. Media Preparation. *LibreTexts/Biology LibreTexts* (2021). https://bio.libretexts.org/Learning_Objects/Laboratory_Experiments/Microbiology_Labs/Microbiology_Labs_I/01%3A_Media_Preparation
25. J.G. Holt, N.R. Krieg, P.H.A. Sneath, J.T. Staley, and S.T. Williams (Eds.). Bergey's manual of Determinative Bacteriology (9th Edition). *Lippincott Williams & Wilkins, Baltimore, USA* (1994).
26. T. Aziz, S. Rasheed, A.H. Shah, H. Nasir, A. Fariq, A. Jamil, and S. Jannat. Bioremediation Potential of Plant-Bacterial Consortia for Chlorpyrifos Removal Using Constructed Wetland. *Frontiers in Environmental Science* 10: 880807 (2022).
27. R.S Chandan, N.R Soundaryashree, M.Umesh, A. Neogi, A.S. Aparna, E. Jacob, D. Scaria, and N.P. Gana. Analytical Method Development and Validation of Malathion by UV Spectroscopy. *Journal of Pharmaceutical Negative Results* 13(08): 2631 (2022).
28. R. Hartline. 1.19: Cytochrome c Oxidase. (2022). https://bio.libretexts.org/Bookshelves/Microbiology/Microbiology_Laboratory_Manual_(Hartline)/01:_Labs/1.19:_Cytochrome_c_Oxidase
29. M.T. Madigan, J.M. Martinko, K.S. Bender, D.H. Buckley, D.A. Stahl, and T. Brock (Eds.). Brock Biology of Microorganisms. 14th Edition. *Benjamin Cummings* (2014).
30. K. Rogers. Gram-negative bacterium. *Britannica Editors* (2025). https://www.britannica.com/science/Gram-negative-bacterium
31. G. Karki. Difference Between Gram-Positive and Gram-Negative Bacteria. (2018). https://www.onlinebiologynotes.com/difference-between-gram-positive-and-gram-negative-bacteria/
32. H. Khatoon, A. Anokhe, and V. Kalia. Catalase test: A biochemical protocol for bacterial identification. *AgriCos e-Newsletter* 3(1): 53-55 (2022).
33. Z. Tang, J. Wood, D. Smith, A. Thapa and N. Aryal. A review on constructed treatment wetlands for removal of pollutants in the agricultural runoff. *Sustainability* 13(24): 13578 (2021).
34. O.C. Overton, L.H. Olson, S.D. Majumder, H. Shwiyyat, M.E. Foltz and R.W. Nairn. Wetland removal mechanisms for emerging contaminants. *Land* 12(2): 472 (2023).
35. O.O. Babalola, O.C. Emmanuel, B.S. Adeleke, K.A. Odelade, B.C. Nwachukwu, O.E. Ayiti, T.T. Adegboyega and N.O. Igiehon. Rhizosphere microbiome cooperations: strategies for sustainable crop production. *Current Microbiology* 78(4): 1069-1085 (2021).
36. X.Y. Tang, Y. Yang, M.B. McBride, R. Tao, Y.N. Dai, and X.M. Zhang. Removal of chlorpyrifos in recirculating vertical flow constructed wetlands with five wetland plant species. *Chemosphere* 216: 195-202 (2019).
37. G. Yidong, W. Bo, G. Yongxia, L. Wen, Z. Xiaoli, and Y. Jianghua. Occurrence and fate of antibiotics in the aqueous environment and their removal by constructed wetlands in China: a review. *Pedosphere* 27(1): 42-51 (2017).
38. B.K. Singh and A. Walker. Microbial degradation of organophosphorus compounds. *FEMS Microbiology Reviews* 30(3): 428-471 (2006).
39. L. Ma, X. Dai, G. Ai, X. Zheng, Y. Zhang, C. Pan, M. Hu, C. Jiang, L. Wang, and Z. Dong. Isolation and identification of efficient malathion-degrading bacteria from deep-sea hydrothermal sediment. *Microorganisms* 10(9): 1797 (2022).
40. B. Sharma, A.K. Dangi, and P. Shukla. Contemporary enzyme based technologies for bioremediation: a

review. *Journal of Environmental Management* 210: 10-22 (2018).

41. J. Wang, G. Zhang, D. Wang, Y. Zhao, L. Wu, Y. Zheng, and Q. Liu. Low-Carbon Hybrid Constructed Wetland System for Rural Domestic Sewage: Substrate–Plant–Microbe Synergy and Annual Performance. *Water* 17(10): 1421 (2025).

Proceedings of the Pakistan Academy of Sciences: B
Life and Environmental Sciences 62(4): 335-349 (2025)

ISSN (Print): 2518-4261; ISSN (Online): 2518-427X
http://doi.org/10.53560/PPASB(62-4)1116

Pakistan Academy of Sciences

Research Article

Computational Design of a Multi-Epitope Vaccine Against Nipah Virus: Bridging Immunoinformatics and Immune Protection

Seerat Fatima†, Fatima Jawed†, and Shumaila Zulfiqar*

Department of Biotechnology, Kinnaird College for Women, Lahore, Pakistan

Abstract: Nipah virus (NiV) is a highly lethal zoonotic paramyxovirus with no licensed vaccines or targeted antiviral therapies, posing a serious global health threat. Recurrent outbreaks in South and Southeast Asia highlight the critical need for efficacious and broadly protective vaccine strategies. In this research, an immunoinformatics-based approach was utilized to construct a multi-epitope vaccine (MEV) targeting the highly conserved NiV fusion protein (NCBI ID: AAY43915.1). The protein exhibited high antigenicity, non-allergenic potential, and favorable physicochemical properties. Cytotoxic T-lymphocyte (CTL), Helper T-lymphocyte (HTL), and B-cell epitopes were predicted and rigorously screened for immunogenicity, non-toxicity, and sequence conservancy, resulting in the selection of epitopes with over 90% identity across Bangladeshi and Malaysian NiV strains. Population coverage analysis confirmed the broad applicability of Human Leukocyte Antigen (HLA), particularly in endemic regions. The finalized MEV construct, incorporating appropriate linkers and a 50S ribosomal protein adjuvant, showed structural stability following modelling, refinement, and validation. Molecular docking revealed strong binding affinity with TLR3 and TLR4, Computational immune simulations predicted robust adaptive immune responses, and codon optimization, along with in silico cloning, confirmed favorable expression in *E. coli*. Although these findings are supported by computational analyses and should be validated experimentally, the proposed MEV demonstrates strong cross-protective and immunogenic potential, offering an encouraging platform for the design of a pan-strain NiV vaccine.

Keywords: Nipah Virus, Multi-epitope Vaccine (MEV), Fusion Protein, Molecular Docking, Immunogenicity, Vaccine.

1. INTRODUCTION

The Indian subcontinent is a hotspot for zoonotic infections due to dense human-animal interactions, inadequate disease monitoring, and limited public health infrastructure [1]. Among these threats, Nipah virus (NiV) is known to be a highly fatal zoonotic paramyxovirus capable of both animal-to-human, and human-to-human transmission, with mortality rates reaching up to 100% in some outbreaks [2, 3]. Despite multiple outbreaks in Bangladesh, India, and Malaysia, there isn't a licensed human vaccination against NiV at the moment, posing a persistent threat to regional and global health [4, 5].

Nipah virus (NiV) is a membrane-bound negative-sense RNA virus of the genus Henipavirus within the Paramyxoviridae family. Its genome encodes the six structural proteins, of which the fusion protein (F) is essential for viral uptake by regulating membrane coalescence between the virus and host cells. Given its essential function and relatively conserved nature, the F protein is an attractive target for vaccine development aimed at providing broad-spectrum protection across NiV strains.

Traditional vaccine approaches for NiV, including live-attenuated, viral vector-based, and protein subunit vaccines, are still in clinical or preclinical phases [6]. These strategies face challenges such as biosafety level 4 (BSL-4) restrictions, high production costs, and prolonged development timelines [7, 8]. In contrast, a multi-epitope vaccine (MEV) design using immunoinformatics offers a safer, faster, and more cost-effective alternative for targeting highly pathogenic viruses like NiV [9, 10]. Several in silico studies have previously proposed multi-epitope vaccine (MEV) constructs against NiV,

Received: June 2025; Revised: November 2025; Accepted: December 2025
* Corresponding Author: Shumaila Zulfiqar <shumaila.zulfiqar@kinnaird.edu.pk>
†These authors contributed equally and share first authorship

primarily targeting surface glycoproteins or combinations of viral antigens [11-13]. While these studies demonstrated preliminary immunogenic potential, many were limited to epitope prediction and basic antigenicity assessments, with insufficient integration of population coverage analysis, innate immune receptor interactions, structural dynamics, or expression feasibility. Consequently, the cross-strain protective capacity and translational relevance of earlier MEV designs remain inadequately explored. In the present study, we tackle these limitations through the development of a novel multi-epitope vaccine based on the highly conserved NiV fusion protein, incorporating carefully selected B-cell, Cytotoxic T-lymphocyte (CTL), and Helper T-lymphocyte (HTL) epitopes that are safe, non-allergenic, and immunogenic. Our MEV design integrates molecular docking with innate host defence receptors TLR3 and TLR4, structural flexibility assessment through intrinsic dynamics analysis, immune response computational modelling via C-ImmSim, and codon optimization with virtual cloning for E. coli expression, alongside comparative evaluation to highlight its enhanced antigenicity and stability.

This study marks a major advancement in computational vaccinology by combining the design of a potent MEV candidate against NiV with comprehensive validation of its structural and immunological performance using multi-tiered bioinformatics strategies. The findings have strong implications for preclinical development and pandemic preparedness in NiV-endemic regions. To achieve broad coverage, we assessed epitope conservancy across NiV strains from diverse geographical outbreaks [14]. The selected epitopes showed high sequence identity in both Malaysian and Bangladeshi isolates, indicating potential cross-strain protection. Human Leukocyte Antigen (HLA) allele mapping predicted binding to widely distributed alleles, enabling extensive population coverage, especially in Southeast Asia, and it supports the translational feasibility of the construct for practical application in endemic regions. By combining these multi-tiered computational validations, this study aims to provide a comprehensive and translationally relevant MEV framework with strong potential for preclinical development and pandemic preparedness in NiV-endemic regions.

2. MATERIALS AND METHODS

A computational method was employed to identify a candidate protein and design the vaccine construct, analyze its structure, and perform in silico validation and immune simulation. Detailed methodology is outlined in Figure 1.

2.1. Retrieval and Examination of NiV Fusion Protein Sequence

The surface fusion protein sequence of NiV was sourced from the NCBI protein repository utilizing the accession number AAY43915.1. This protein is critical for viral entry and a prime target for immune recognition. The antigenic properties were evaluated utilizing the VaxiJen v2.0 computational platform (https://www.ddg-pharmfac.net/vaxijen/VaxiJen/VaxiJen.html) with a threshold of 0.4 for viral proteins. Sequences that scored more than 0.4 on antigenicity were chosen. Using AllerTOP v2.0 (http://www.ddg-pharmfac.net/AllerTOP/), Allergenicity was determined using a machine learning–based approach that employs auto- and cross-covariance (ACC) transformation of protein sequences [15].

2.2. Epitope Prediction

2.2.1. Linear B lymphocyte (LBL) epitope prediction

Linear B-cell epitopes (LBL) were predicted using BepiPred 2.0, available through the IEDB Analysis (https://www.iedb.org/). Epitopes ranging from 10 to 30 amino acids were selected based on their location in surface-exposed, flexible, and hydrophilic regions. Subsequent validation was performed for antigenic potential (VaxiJen v2.0) and allergenic profile (AllerTOP v2.0). Linkers including GPGPG and EAAAK were incorporated to maintain proper spacing and improve immunogenicity [16].

2.2.2. Cytotoxic T-Lymphocyte (CTL) epitope prediction

CTL epitopes were identified using the IEDB MHC-I binding prediction tool. Epitopes with IC_{50} values $\leq$ 500 nM and percentile ranks $\leq$ 1% were selected to ensure strong binding affinity to prevalent HLA class I alleles. These epitopes were validated for antigenicity and allergenicity,

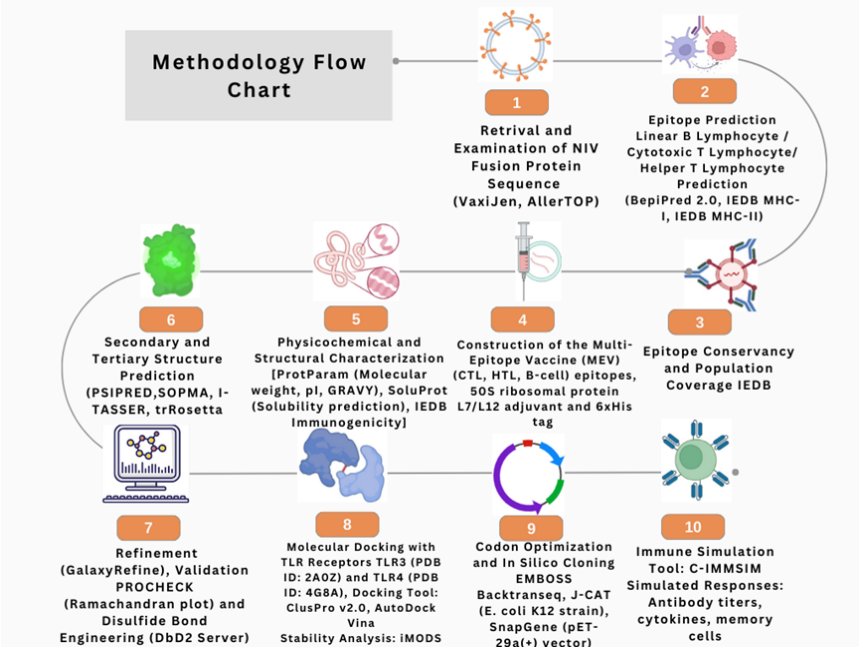

Fig. 1. Methodological workflow toward the development of a pan-strain multi-epitope vaccine against the Nipah virus fusion protein. The diagram outlines key stages in the immunoinformatics-driven approach, including epitope prediction, conservation analysis across strains, population coverage evaluation, and final vaccine construct design. This multi-step process ensures the creation of a broadly protective and immunologically relevant vaccine candidate.

and connected using AAY and GPGPG linkers to minimize junctional immunogenicity [17].

2.2.3. Helper T-Lymphocyte (HTL) epitope prediction

The IEDB MHC-II binding tool was employed to predict HTL epitopes (https://tools.iedb.org/main/tcell), and their ability to induce cytokine responses was evaluated using IL4Pred and IL10Pred servers. Epitopes exhibiting IL-4 and IL-10 induction scores exceeding 2.0 and 0.3, correspondingly, were given precedence. Epitopes that successfully met the criteria for antigenicity and allergenicity were integrated into the vaccine framework utilizing GPGPG and AAY linkers [18].

2.3. Epitope Conservancy, Cross-Strain Analysis, and Population Coverage

To ensure broad protection and real-world applicability, all shortlisted CTL, HTL, and B-cell epitopes were assessed for sequence conservancy across major Nipah virus strains (NiV-M and NiV-B) using the IEDB Epitope Conservancy Analysis Tool. Epitopes with $\geq 90\%$ sequence identity across these strains were retained for vaccine construction, thereby enhancing cross-strain efficacy and robustness. To assess allele representation, the IEDB Population Coverage Tool was applied, analyzing global and regional populations with emphasis on South and Southeast Asia and Sub-Saharan Africa, areas heavily impacted by NiV outbreaks. The final vaccine construct demonstrated a global HLA coverage of 89.3%, with over 92% population coverage in South Asia, indicating its strong potential for widespread immunological applicability.

2.4. Design of the Multi-Epitope Vaccine

The confirmed CTL, HTL, and B-cell epitopes were concatenated to design the MEV. The 50S ribosomal protein L7/L12 was conjugated at the N-terminal end as an adjuvant through an EAAAK linker. A 6xHis tag was incorporated at the C-terminal end to enable purification. Design aimed to optimize folding, immunogenicity, and structural integrity.

2.5. Physicochemical and Structural Characterization

The physicochemical properties, including molecular weight, theoretical isoelectric point (pI), aliphatic index, grand average of hydropathy (GRAVY) value, and instability index, were

assessed utilizing the ProtParam tool (https://web.expasy.org/protparam/) [19]. Solubility was predicted via SoluProt (https://bio.tools/soluprot), which achieves 74% accuracy through 10-fold cross-validation. Antigenicity, allergenicity, and immunogenicity were reconfirmed using VaxiJen, AllerTOP, and IEDB immunogenicity tools.

2.6. Prediction of Secondary Structure of the Constructed NiV Vaccine

The prediction of secondary structure elements (α-helices, β-strands, and coils) was carried out using PSIPRED (https://bioinf.cs.ucl.ac.uk/psipred/) and SOPMA (https://npsa-prabi.ibcp.fr/cgi-bin/npsa_automat.pl?page=/NPSA/npsa_sopma.html). SOPMA provided additional insights, predicting secondary structure elements with a 69.5% confidence score, using optimized parameters (e.g., window size and number of conformational states) [20].

2.7. Tertiary Structure Modeling, Refinement, and Validation

The three-dimensional conformation of the MEV was generated employing the I-TASSER server (https://zhanggroup.org/I-TASSER/), which utilizes iterative threading methodologies to achieve high-precision modeling. Furthermore, the tertiary structure of the vaccine construct was modeled using trRosetta (https://yanglab.qd.sdu.edu.cn/trRosetta/?utm) [21]. Subsequent refinement of the model was executed with GalaxyRefine (https://galaxy.seoklab.org/cgi-bin/submit.cgi?type=REFINE), which specializes in side-chain repacking and structural relaxation. Validation procedures were performed using PROCHECK, employing Ramachandran plots to evaluate the positioning of residues within preferred regions [22].

2.8. Disulfide Bond Engineering

Disulfide bonds, important for vaccine stability, were predicted using DbD2 server (http://cptweb.cpt.wayne.edu/DbD2/) [23] and verified by I-TASSER structural analysis. Residue pairs with favorable $\chi 3$ angles and energy thresholds were selected to enhance protein rigidity.

2.9. In silico Docking with TLR Receptors

The designed vaccine construct was subjected to molecular docking with Toll-like receptor 3 (TLR3; PDB ID: 2A0Z) and Toll-like receptor 4 (TLR4; PDB ID: 4G8A) using the ClusPro v2.0 server. (https://cluspro.bu.edu/login.php). Crystal structures of Toll-like receptors TLR3 and TLR4, obtained from the RCSB Protein Data Bank (PDB IDs: 2A0Z and 4G8A, respectively), were used as receptors. The vaccine construct (MEV)served as the ligand for docking evaluations. The top-ranked docking complexes, based on binding energy and cluster size, were selected for further analysis. The docked poses were visualized using PyMOL. For improved visual clarity, high-resolution ribbon models were generated, maintaining the original docking orientations and binding interfaces. Further stability assessments of docked complexes were conducted via the iMODS server (https://imods.iqf.csic.es/), which performs normal mode analysis (NMA) for evaluating complex dynamics and deformability [24].

2.10. Codon Optimization and In silico Cloning

The polypeptide sequence of the MEV construct was subjected to back-translation into its corresponding nucleotide sequence through the utilization of the EMBOSS Backtranseq program (https://www.ebi.ac.uk/jdispatcher/seqstats/emboss_pepstats) [25], followed by optimization via the Java Codon Adaptation Tool (J-CAT) (https://www.prodoric.de/JCat) [10], to enhance expression within Escherichia coli (strain K-12). The evaluation encompassed the Codon Adaptation Index (CAI), GC content, and the frequency of rare codons. Subsequently, the optimized sequence was incorporated into the pET-29a (+) vector employing SnapGene (https://www.snapgene.com/) for the purpose of simulated cloning [26].

2.11. Immune Simulation

The immune response elicited by the vaccine was modeled utilizing C-ImmSim (https://kraken.iac.rm.cnr.it/C-IMMSIM/), an agent-based simulation tool that accurately represents primary, secondary, and tertiary immune responses [26]. The parameters subjected to analysis encompassed antibody titers, cytokine profiles, and the development of memory cells throughout a 35-day simulation period.

3. RESULTS

3.1. Sequence and Structural Analysis

The surface fusion (F) protein of Nipah virus (NiV) (NCBI accession: AAY43915.1) was retrieved for downstream immunoinformatics analysis. Antigenicity analysis using VaxiJen v2.0 yielded a score of 0.4870, confirming its immunogenic potential. AllerTOP v2.0 classified the protein as non-allergenic. ProtParam analysis showed a molecular weight of 41.11 kDa and an isoelectric point (pI) of 6.54, suggesting good stability and solubility.

3.2. Prediction of B Cell and T Cell Epitope

Using BepiPred 2.0, 30 linear B-cell epitopes were predicted. Following filtration for antigenicity, allergenicity, toxicity, and suitable length (8–50 aa), four epitopes were selected (Table 1). NetMHCPan 4.1 predicted 200 CTL candidates, from which 8 were shortlisted based on strong MHC-I binding affinity (IC50 $\leq$ 500 nM) with high antigenicity, and safety criteria (Table 2). IEDB MHC-II binding predictions yielded 1000 HTL candidates. Ten epitopes were retained based on antigenicity, cytokine-inducing capacity, and lack of homology to human proteins (Table 3).

3.3. Developing a Vaccine Construct

Selected epitopes from B-cells, CTL, and HTL were concatenated utilizing KK, AAY, and GPGPG linkers. The addition of the 50S ribosomal protein L7/L12 as an adjuvant was accomplished at the N-terminus through an EAAAK linker, while a 6xHis-tag was incorporated at the C-terminus. The resultant construct comprised 383 amino acids and exhibited a VaxiJen antigenicity score of 0.6705 (Figure 2).

3.4. Physiochemical Properties of the Vaccine Construct

ProtParam revealed an instability index of 33.53 (stable), aliphatic index of 109.87, and GRAVY score of 0.155. Solubility prediction scores from ProteinSol (0.524) and SoluProt v2.0 confirmed good solubility (Table 4).

Table 1. Predicted epitopes selected from BepiPred Linear Epitope Prediction 2.0.

Protein segment (amino acid)	Peptide	Antigenicity	Antigenic score	Allergenicity	Toxicity
Fusion (25–33)	VGILHYEKL	A[a]	1.4183	NA[b]	NT[c]
Fusion (215–226)	GPNLQDPVSNSM	A	0.1771	NA	NT
Fusion (325–332)	NIEIGFCL	A	1.9336	NA	NT
Fusion (523–543)	NTYSRLEDRRVRPTSSGDLYY	A	0.7837	NA	NT

a: Antigenicity, b: Not Applicable, c: Non-Toxic.

Table 2. Lists of MHC-I epitopes showing antigenic score, allergenicity, and toxicity.

Protein segment (amino acid)	Peptide	Antigenicity	Antigenic score	Allergenicity	Toxicity
Fusion (126-135)	AQITAGVALY	A[a]	0.6530	NA[b]	NT[c]
Fusion (27-36)	ILHYEKLSKI	A	0.4121	NA	NT
Fusion (310-318)	SIVPNFILV	A	0.5759	NA	NT
Fusion (47-55)	KIKSNPLTK	A	0.7250	NA	NT
Fusion (512-521)	FISFIIVEKK	A	1.7539	NA	NT
Fusion (195-203)	TELSLDLAL	A	1.1768	NA	NT
Fusion (124-133)	TAAQITAGVA	A	0.7852	NA	NT
Fusion (125-134)	AAQITAGVAL	A	0.7441	NA	NT

a: Antigenicity, b: Not Applicable, c: Non-Toxic.

Table 3. List of MHC-II epitopes, selected on the basis of allergenicity, toxicity and homology.

Protein	Peptide	Antigenicity	Antigenic score	Allergenicity	Toxicity	Homology
Fusion (315-323)	FILVRNTLI	A[a]	0.5200	NA[b]	NT[c]	NH[d]
Fusion (179-187)	INTNLVPTI	A	0.7834	NA	NT	NH
Fusion (309-317)	ISIVPNFIL	A	0.7808	NA	NT	NH
Fusion (46-54)	YKIKSNPLT	A	0.9685	NA	NT	NH
Fusion (515-523)	FIIVEKKRN	A	2.5120	NA	NT	NH
Fusion (516-524)	IIVEKKRNT	A	1.8403	NA	NT	NH
Fusion (122-130)	IATAAQITA	A	0.7382	NA	NT	NH
Fusion (120-128)	IGIATAAQI	A	1.0247	NA	NT	NH
Fusion (518-526)	VEKKRNTYS	A	1.0619	NA	NT	NH
Fusion (410-418)	LMIDNTTCP	A	0.5036	NA	NT	NH

a: Antigenicity, b: Not Applicable, c: Non-Toxic, d: No Homology

Table 4. Physiochemical properties of the developed vaccine.

Vaccine construction characteristics	
Vaccine length	383 Amino Acid
Molecular Weight	41.18 KDa
Antigenicity	0.6705
Allergic Potential	Non allergenic
Toxicity	Nontoxic
Theoretical pI	6.73 Isoelectric point
Instability Index	33.53
Total Atom Number	5929 Atoms
Aliphatic Index (AI)	109.87
Extinction coefficient	13,410 M^{-1} cm^{-1} (at 280 nm, in water)
GRAVY score	0.155
Solubility	0.524

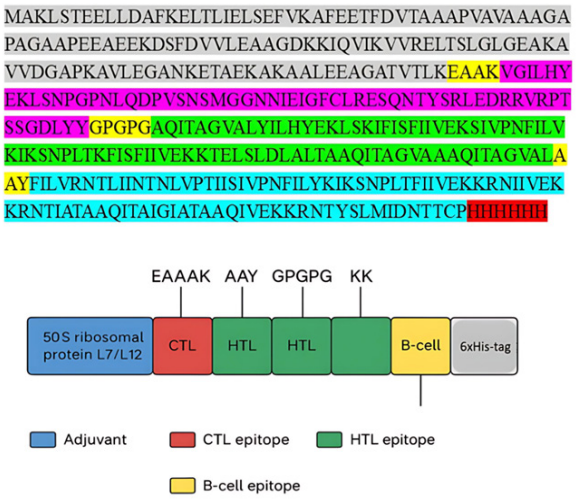

Fig. 2. Schematic representation of the multi-epitope vaccine construct. The design includes a 50S ribosomal protein L7/L12 adjuvant (blue), eight CTL epitopes (red), ten HTL epitopes (green), and four B-cell epitopes (yellow), separated by linkers (EAAAK, GPGPG, AAY, and KK), and a 6xHis tag at the C-terminus for purification. This layout enhances structural stability and immune visibility.

3.5. Structural Modeling and Validation

3.5.1. Secondary structure

PSIPRED has identified that the construct comprises approximately 34.48% alpha-helices, 19.24% extended strands, 6.58% beta-sheets, and 35.70% coils, as illustrated in Figure 3. Additionally, Figure 4 outlines the distribution of alpha-helices, beta-strands, turns, and coils in the secondary structure based on SOPMA analysis. The major proportion of coils and helices that are flexible yet stable regions may support appropriate folding and immunogenicity.

3.5.2. Tertiary structure

The 3D model generated via trRosetta (TM-score of 0.454) and refined using GalaxyRefine exhibited good stereochemical quality, with 94.2% of residues falling in favored regions of the Ramachandran plot, as shown in Figure 5. The clustering in these favored regions corresponds to typical α-helix and β-sheet conformations, with only a few outliers such as Asn143.

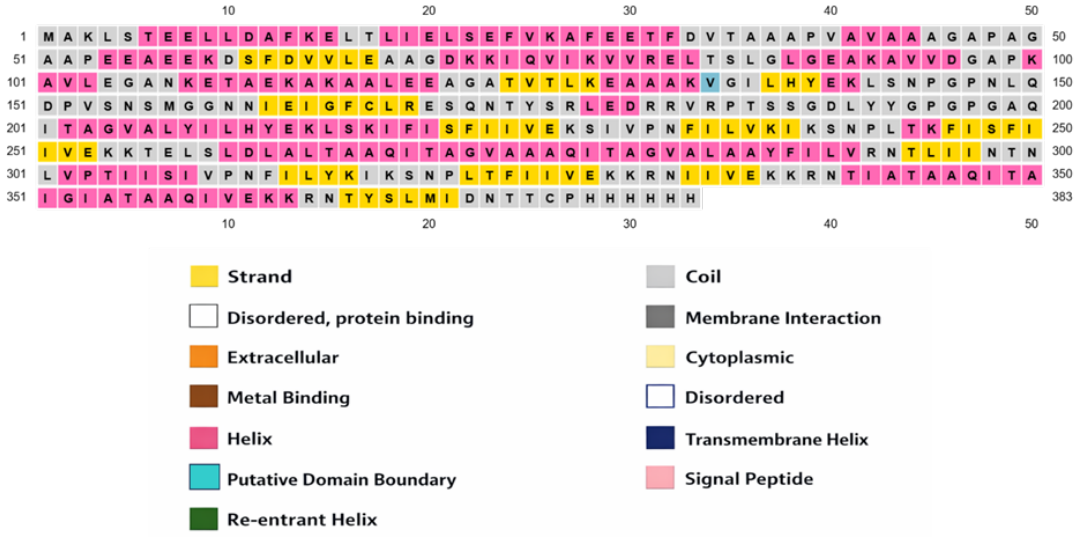

Fig. 3. The predicted secondary structure of NiV vaccine displayed using the PSIPRED server, showing distribution of α-helices, β-strands, and coils.

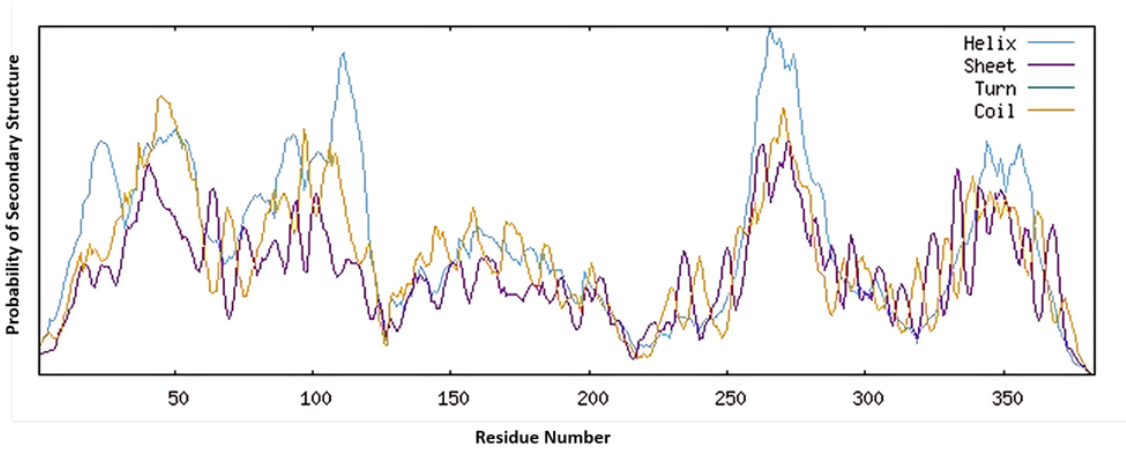

Fig. 4. SOPMA-based prediction of the NiV vaccine secondary structure. The top graph indicates the distribution percentages of different secondary structural components.

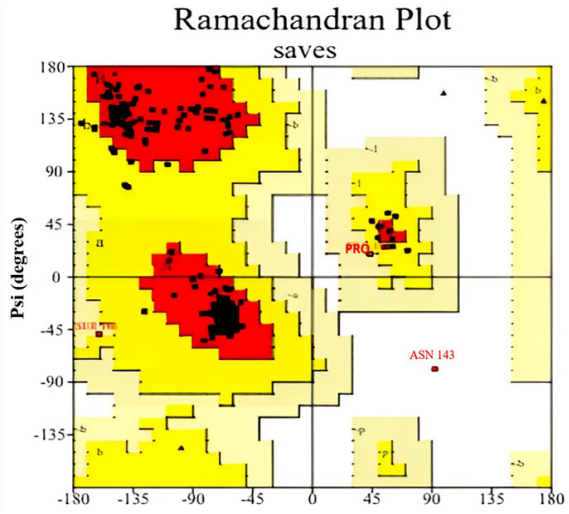

Fig. 5. Ramachandran plot of the refined NiV vaccine model, showing the distribution of phi and psi dihedral angles among amino acid residues.

3.5.3. Disulfide engineering

Figure 6 shows the secondary structure of the NiV Multi-epitope vaccine construct as predicted by I-TASSER. The model highlights the predicted disulfide bonds in grey, loops/coils in green, α-helices in blue, and β-strands in yellow. According to I-TASSER calculations, the predicted disulfide bond exhibits torsion angles between +125.95° and -65.97° and bond energies between 1.45 and 10.37 kcal/mol.

3.6. Molecular Docking and Complex Stability

ClusPro revealed strong binding between MEV and TLR3 (-885.4 kcal/mol) and TLR4 (-1366.3 kcal/mol). AutoDock Vina confirmed TLR4 binding

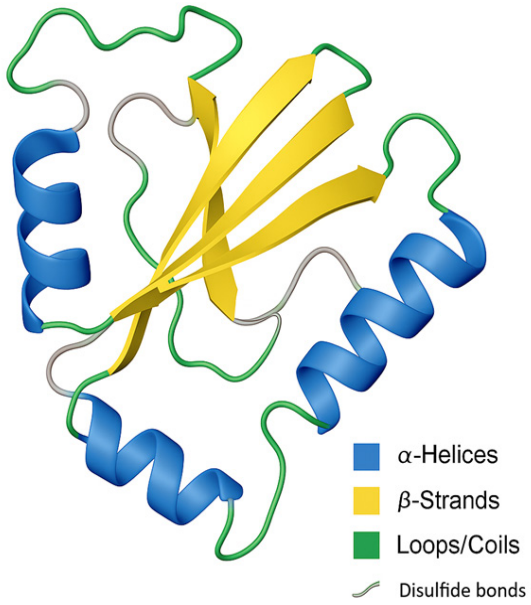

Fig. 6. 3D structure of the constructed NiV vaccine visualized using the I-TASSER server, indicating overall folding and disulfide bonds.

affinity at −8.0 kcal/mol. Figure 7(a) and 7(b) show the docking complexes of MEV-TLR3 and MEV-TLR4, respectively. Figure 7(a) demonstrates a stable and Precise binding between the engineered multi-epitope Nipah virus immunogen construct and the leucine-rich repeat (LRR) domain of Toll-like Receptor 3 (TLR3). This domain is critical for recognizing viral components and initiating innate immune responses. Molecular docking analysis demonstrated that the vaccine construct aligns effectively within the extracellular binding groove of TLR3, engaging in several non-covalent interactions, including hydrogen bonds, electrostatic forces, and van der Waals linkages –that contribute to the structural stability of the complex. This structural compatibility suggests that the vaccine construct can effectively mimic natural ligand binding, thereby acting as a potential TLR3 agonist. Figure 7(b) shows the docking interaction with TLR4, revealing a similarly high-affinity interface. The MEV binds to the ectodomain of TLR4, the region involved in initiating MyD88-dependent signalling pathways. Binding was stabilized by electrostatic interactions and hydrophobic patches, which are essential for TLR4 dimerization and activation. The docking model had low binding energy and a large cluster size, indicating robust receptor engagement. By engaging TLR3 and TLR4, the construct may trigger signalling cascades that activate antigen-presenting cells and promote cytokine production, ultimately enhancing both innate and adaptive immune responses. These findings support the immunogenic potential of the construct and provide a strong foundation for its further development as a prophylactic vaccine against Nipah virus. Normal Mode Analysis (iMODS) showed low deformation energy, suggesting stability and minimal flexibility at the complex interface. Figures 8(a) and 8(b) show the deformability of the docked complexes MEV-TLR3 and MEV-TLR4, respectively.

3.7. Immune Simulation

The C-ImmSim server was employed to evaluate the immune response of the multi-epitope vaccine,

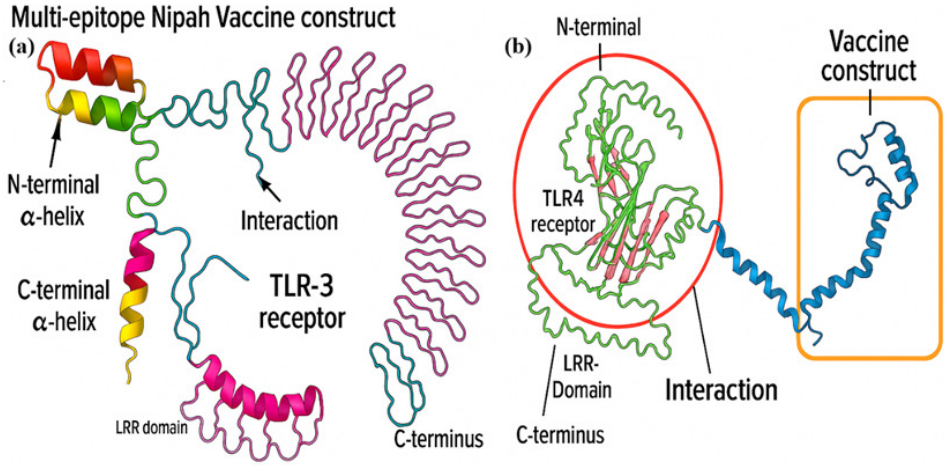

Fig. 7. Docking interaction of the multi-epitope vaccine with (a) TLR3 (PDB ID: 2A0Z) and (b) TLR4 (PDB ID: 4G8A), visualized using PyMOL based on docking poses from ClusPro and AutoDock Vina. Ribbon models highlight the binding interface.

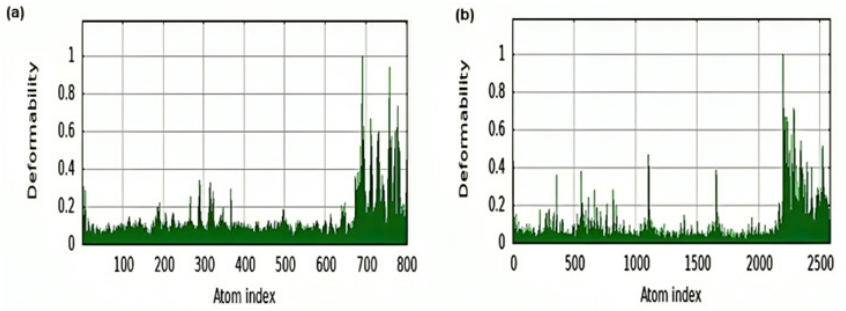

Fig. 8. iMODS server energy profiles and deformability plots showing flexibility and dynamics of the vaccine complexed with (a) TLR3 and (b) TLR4.

indicating strong and sustained protective immunity. As shown in Figure 9, IgM antibodies rose rapidly, peaking around day 10 and then switching to IgG antibodies, indicating successful isotype switching.

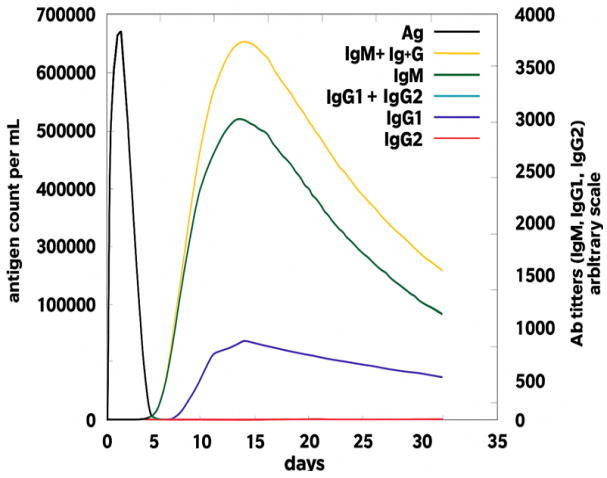

Fig. 9. Antigen levels and antibody titers over 35 days, showing transition from IgM to IgG and establishment of immunological memory.

Figure 10 demonstrates the activation of the adaptive immune system, particularly TH1 cells, which promote antiviral defence by stimulating macrophages, natural killer cells, and cytokine production. Figure 11 illustrates the dynamics of CTLs, showing an initial increase in active and replicating cells followed by the formation of memory cells, confirming long-term immune memory. Increased B-cell activity, along with HTL and CTL responses, reflected the coordinated activation of both humoral and cellular immunity. Figure 12 depicts the cytokine response with early peaks in IFN-γ and IL-2 after vaccination. Together, these results indicate effective immune stimulation and durable memory formation.

3.8. Codon Optimization and Cloning

The codon-optimized MEV gene (1146 bp) exhibited a CAI value of 0.553 and a GC content of 49.21%. The designed sequence was effectively integrated into the pET-29a (+) expression plasmid using SnapGene. Figure 13 shows the cloned plasmid

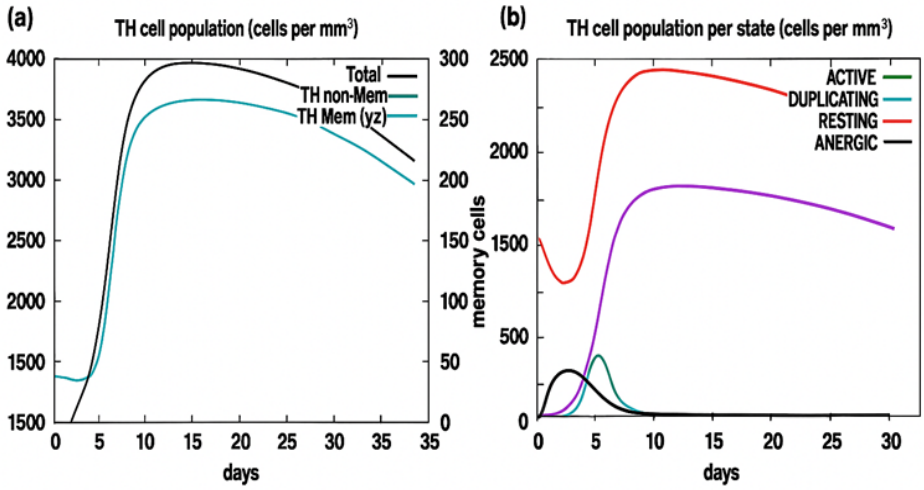

Fig. 10. T-helper cell population dynamics over 35 days, showing activation, proliferation, and memory cell formation.

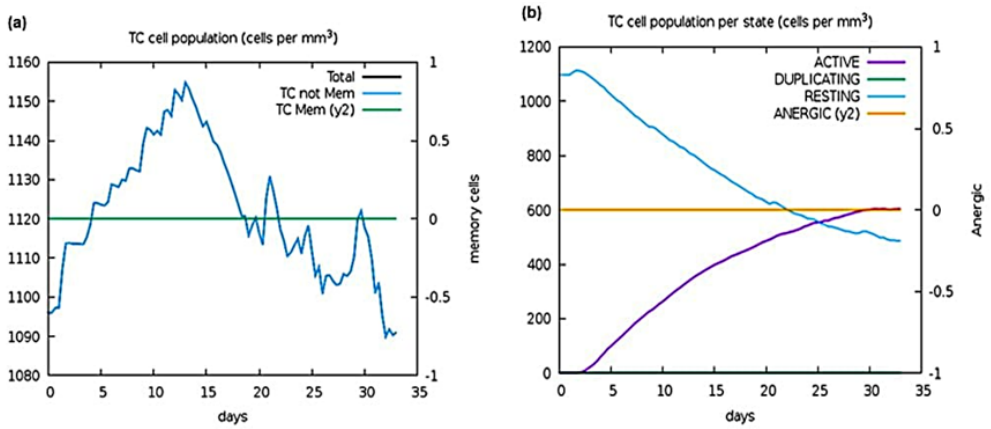

Fig. 11. Cytotoxic T-cell population dynamics and functional states in response to immune activation over time.

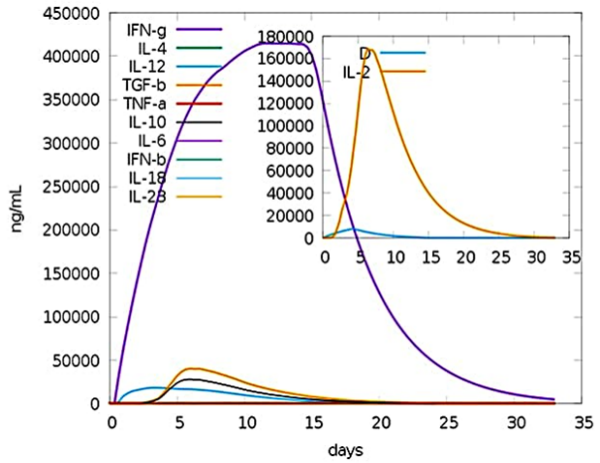

Fig. 12. Cytokine profile over 35 days, highlighting IFN-γ and IL-2 expression levels during immune response.

map. Although the initial codon adaptation index (CAI) value was moderate (0.553), we ensured balanced GC content (49.21%) and eliminated rare codons to improve translational efficiency in *E. coli*. Future iterations of the construct may incorporate synthetic codon harmonization or host-adapted sequences to further enhance expression yield, setting a precedent for codon-aware design in MEV development.

4. DISCUSSION

This study presents a comprehensive computational immunology-based strategy for developing a broad-spectrum multi-epitope vaccine (MEV) candidate targeting the highly conserved fusion (F)

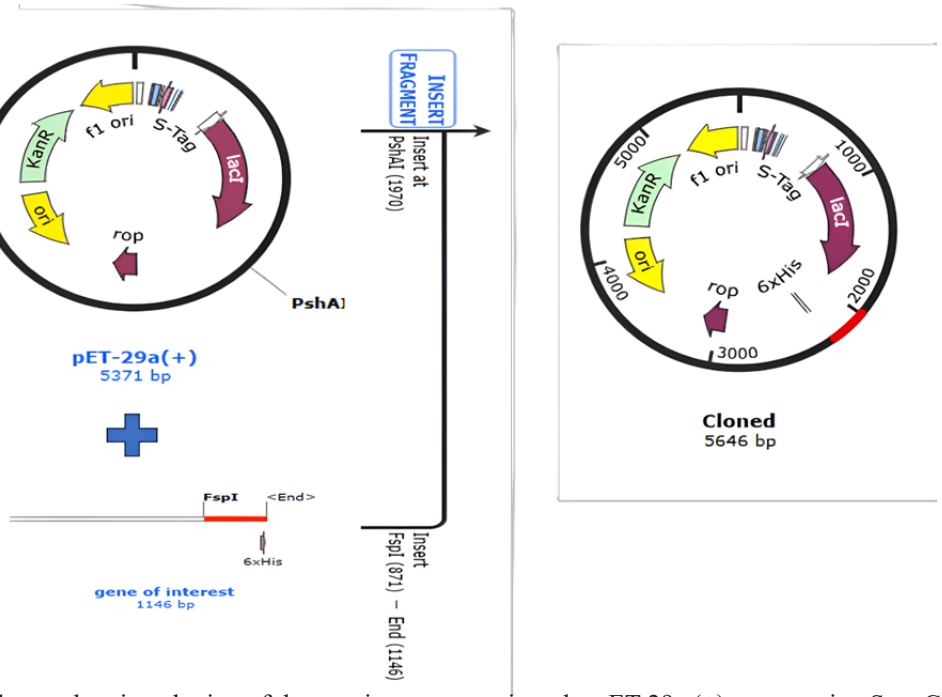

Fig. 13. Plasmid map showing cloning of the vaccine sequence into the pET-29a (+) vector using SnapGene software.

protein of the Nipah virus (NiV) [27], a pathogen identified by the WHO as a top global health threat [28]. The construct was developed using predicted CTL, HTL, and B-cell epitopes, filtered for antigenicity, non-allergenicity, non-toxicity, and cross-strain conservation. The selected epitopes showed ≥ 90% sequence identity in both Malaysian and Bangladeshi NiV isolates, supporting its broad-spectrum potential. Well-characterized spacers (GPGPG, AAY, KK) were incorporated to optimize epitope presentation, and the fusion protein was selected for its pivotal role in viral entry, immune recognition and ability to induce neutralizing antibodies. Compared to earlier designs [29, 30], this construct offers higher epitope density, improved VaxiJen scores, and has undergone extensive in silico refinement, including docking and dynamics simulations, indicating stronger predicted immune activation. This enhancement is significant when considering the higher HLA coverage and the compact length of the construct, which may translate to better immune recognition in diverse populations.

Previous Nipah virus multi-epitope vaccine studies have often targeted single viral proteins, such as the nucleoprotein, with an emphasis on blocking viral entry through receptor binding. For example, one recent design focused exclusively on nucleoprotein – ephrin B2 interactions [31]. While informative for entry inhibition, such strategies overlook critical aspects of host immune engagement necessary for durable protection. In contrast, our approach centers on the fusion protein and integrates comprehensive immune-receptor interaction analyses, particularly with TLR3 and TLR4, to enhance innate and adaptive activation. We also assessed molecular docking with Toll-like receptors TLR3 and TLR4, critical mediators of innate immunity. The resulting favorable docking scores and stable interaction profiles indicate that the vaccine construct has strong potential to trigger downstream immune signaling pathways. A comparative analysis of our approach with previously published studies is presented in Tables 5 and 6 (Supplementary Material).

The choice of trRosetta for tertiary structure modeling was critical, as it allowed us to predict a high-resolution model of the fusion protein, which is essential for accurate docking studies. Structural optimization with GalaxyRefine further ensured that the final model was physically stable and conducive to immunogenic interactions [32]. Stereochemical validation yielded a high-quality model, with 94.2% of residues in favored Ramachandran regions. Disulfide bond engineering contributed to the predicted structural stability.

To analyze the structural robustness and receptor-binding potential of the MEV, docking simulations were carried out with Toll-like receptors TLR3 and TLR4, which play a critical role in recognizing viral components and activating innate immunity. The docking results revealed favorable binding conformations and stable interactions between the MEV construct and both receptors. In the MEV–TLR3 complex, the vaccine construct was anchored within the receptor's LRR domain through multiple hydrogen bonds and hydrophobic contacts, indicating a strong affinity that could trigger antiviral signaling pathways. Similarly, the MEV–TLR4 complex showed compact binding and high surface complementarity, suggesting the potential for receptor activation and maturation of dendritic cells.

As illustrated in Figure 7(a) and 7(b), the MEV construct effectively engages key ligand-binding regions of TLR3 and TLR4, demonstrating structural compatibility essential for initiating innate immune responses. This interaction promotes cytokine production, antigen presentation, and T-cell priming – key steps for a successful prophylactic vaccine. Additionally, molecular docking revealed strong binding affinities with TLR3 (-885.4 kcal/mol) and TLR4 (-1366.3 kcal/mol), further supporting robust innate immune activation [33]. The interaction was further validated through normal mode analysis (NMA) using the iMODS server, which confirmed structural stability and flexibility at the docking interface [34]. Immune simulation results revealed early IgM peaks followed by strong secondary IgG responses, persistent memory cell populations, and increased levels of IL-2 and IFN-γ – indicative of a potent Th1-driven immune response. Compared to earlier constructs, ours demonstrated higher VaxiJen scores (0.6705 vs. 0.52 stated by Mohammed *et al.* [30]*),* a compact length (383 vs. 427 amino acids), and broader HLA allele coverage (> 92% in South Asia) reported by Majee *et al.* [29]. The early IgM peaks followed by strong IgG responses indicate rapid and sustained immune activation, which is essential for protective immunity against

NiV. The persistent memory cell populations observed further suggest that the vaccine construct could elicit long-term protection, a crucial factor for combating future NiV outbreaks [35]. Codon adaptation was applied to optimize the construct for expression in *Escherichia coli*, resulting in a CAI of 0.553 and a GC content of 49.21%. Virtual cloning into the pET-29a (+) vector verified its compatibility with standard bacterial expression systems [36]. Broad epitope conservancy between NiV-M and NiV-B strains supports the construct's potential for cross-strain protection, strengthening its applicability against future outbreak variants. Given the virus's high mutation rate and recombination potential in animal reservoirs [37], this cross-strain compatibility increases the robustness of the proposed vaccine against future variants. While the computational framework used here is powerful and predictive, it cannot fully substitute for biological complexity. Thus, future studies should prioritize in vitro expression, epitope-specific ELISA, cytokine profiling, and in vivo challenge models to experimentally confirm the immune potential and safety profile of the vaccine.

Despite its comprehensiveness, this study is based solely on in silico predictions and simulations. Although widely validated, these computational tools may not capture the full spectrum of host immune responses. No in vitro or in vivo data are available at this stage, and the vaccine's performance in biological systems remains to be determined. Future wet-lab validation will be critical to confirm the construct's safety, stability, immunogenicity, and protective efficacy. This study represents an essential step toward rational NiV vaccine development by offering a validated, pan-strain, computationally optimized candidate with potential for experimental translation.

Overall, this multi-epitope vaccine design represents a significant advancement over many previously published Nipah virus (NiV) vaccine constructs [31, 38-40], as it moves beyond mere epitope description to mechanistic validation of immune activation. Recent NiV immunoinformatics studies have similarly emphasized integration of conserved T and B-cell epitopes and receptor engagement, yet few have combined this with comprehensive innate receptor analysis and broad HLA coverage in the context of fusion protein targeting [9, 41]. Furthermore, our construct also demonstrates favorable interactions with important receptors like TLR3 and TLR4 important in predicting innate and adaptive activation that may enhance antigen presentation and Th1 responses. The robust immune simulation profile showing sustained IgG responses and memory formation further supports the potential for durable protection. Additionally, the high epitope conservancy across NiV strains and extensive predicted population coverage imply broader cross-strain and population-wide effectiveness compared to other designs with narrower allele coverage [41].

Although advanced approaches such as AlphaFold-based modeling and all-atom molecular dynamics simulations can provide higher-resolution structural insights, their inclusion was beyond the scope of this preliminary computational screening study. Instead, validated tools suitable for multi-epitope chimeric vaccine constructs were employed. Future work will incorporate MD simulations, AlphaFold-based refinement, and expanded immune simulations to further validate structural stability and immune dynamics. Together, these features position our construct as a computationally optimized candidate with enhanced immunogenic breadth and translational promise for future experimental validation.

5. CONCLUSIONS

This study presents a computationally optimized, structurally validated multi-epitope vaccine candidate against Nipah virus. By integrating pan-strain conserved epitopes, population-specific HLA coverage, and a robust immunoinformatics workflow, the proposed vaccine construct exhibits strong translational potential. Its successful docking with immune receptors, favorable immune simulation profile, and expression compatibility in E. coli further strengthen its candidacy for experimental validation. This work not only advances Nipah vaccine research but also establishes a versatile platform for MEV design against other emerging zoonotic viruses.

6. ETHICAL STATEMENT

This study did not involve any human participants, animals, or clinical data, and therefore did not require ethical approval.

7. ACKNOWLEDGEMENTS

The authors declare that they received no financial support or external assistance for this study.

8. CONFLICT OF INTEREST

The authors declare no conflict of interest.

9. REFERENCES

1. V. Sharma, S. Kaushik, R. Kumar, J.P. Yadav, and S. Kaushik. Emerging trends of Nipah virus: *Reviews in Medical Virology* 29(1): e2010 (2019). https://doi.org/10.1002/rmv.2010
2. S. Gazal, N. Sharma, M. Tikoo, D. Shikha, G.A. Badroo, M. Rashid, and S.J. Lee. Nipah and Hendra viruses: deadly zoonotic paramyxoviruses with the potential to cause the next pandemic. *Pathogens* 11(12): 1419 (2022). https://doi.org/10.3390/pathogens11121419
3. N. Sharif, N. Sharif, A. Khan, and S.K. Dey. Tackling the outbreak of nipah virus in Bangladesh amidst COVID-19: A potential threat to public health and actionable measures. *Health Science Reports* 7(4): e2010 (2024). https://doi.org/10.1002/hsr2.2010
4. S. Kim, H. Kang, L. Skrip, S. Sahastrabuddhe, A. Islam, S.M. Jung, J.F. Vesga, A. Endo, W.J. Edmunds, and K. Abbas. Progress and challenges in Nipah vaccine development and licensure for epidemic preparedness and response. *Expert Review of Vaccines* (2025). https://doi.org/10.1080/14760584.2025.2476523
5. F. Waheed, A.S. Khan, and U. Nisa. Nipah virus; an overview and potential for outbreak in Pakistan. *Journal of the Pakistan Medical Association* 74(12): 2214-2215 (2024). https://doi.org/10.47391/jpma.20661
6. T.P. Monath, R. Nichols, F. Feldmann, A. Griffin, E. Haddock, J. Callison, K. Meade-White, A. Okumura, J. Lovaglio, and P.W. Hanley. Immunological correlates of protection afforded by PHV02 live, attenuated recombinant vesicular stomatitis virus vector vaccine against Nipah virus disease. *Frontiers in Immunology* 14: 1216225 (2023). https://doi.org/10.3389/fimmu.2023.1216225
7. B. Tigabu, L. Rasmussen, E.L. White, N. Tower, M. Saeed, A. Bukreyev, B. Rockx, J.W. LeDuc, and J.W. Noah. A BSL-4 high-throughput screen identifies sulfonamide inhibitors of Nipah virus. *Assay and Drug Development Technologies* 12(3): 155-161 (2014). https://doi.org/10.1089/adt.2013.567
8. F.H. Tan, A. Sukri, N. Idris, K.C. Ong, J.P. Schee, C.T. Tan, S.H. Tan, K.T. Wong, L.P. Wong, and K.K. Tee. A systematic review on Nipah virus: global molecular epidemiology and medical countermeasures development. *Virus Evolution* 10(1): veae048 (2024). https://doi.org/10.1093/ve/veae048
9. B. Kaur, A. Karnwal, A. Bansal, and T. Malik. An immunoinformatic-based In silico identification on the creation of a multiepitope-based vaccination against the Nipah virus. *BioMed Research International* 2024(1): 4066641 (2024). https://doi.org/10.1155/2024/4066641
10. M.T.U. Qamar, A. Rehman, K. Tusleem, U.A. Ashfaq, M. Qasim, X. Zhu, I. Fatima, F. Shahid, and L.L. Chen. Designing of a next generation multiepitope based vaccine (MEV) against SARS-COV-2: Immunoinformatics and in silico approaches. *PLOS One* 15(12): e0244176 (2020). https://doi.org/10.1371/journal.pone.0244176
11. P.K. Yadav and M. Mishra. Computational epitope prediction and docking studies of glycoprotein-G in Nipah virus. *International Journal of Bioinformatics and Biological Science* 1(1): 55-61 (2013).
12. M. Shahab, M.W. Iqbal, A. Ahmad, F.M. Alshabrmi, D.Q. Wei, A. Khan, and G. Zheng. Immunoinformatics-driven in silico vaccine design for Nipah virus (NPV): integrating machine learning and computational epitope prediction. *Computers in Biology and Medicine* 170: 108056 (2024). https://doi.org/10.1016/j.compbiomed.2024.108056
13. R. Saha and B.V. Prasad. In silico approach for designing of a multi-epitope based vaccine against novel Coronavirus (SARS-COV-2). *BioRxiv* 2020.03. 31.017459 (2020). https://doi.org/10.1101/2020.03.31.017459
14. K.T. Wong, W.J. Shieh, S. Kumar, K. Norain, W. Abdullah, J. Guarner, C.S. Goldsmith, K.B. Chua, S.K. Lam, and C.T. Tan. Nipah virus infection: pathology and pathogenesis of an emerging paramyxoviral zoonosis. *The American Journal of Pathology* 161(6): 2153-2167 (2002). https://doi.org/10.1016/S0002-9440(10)64493-8
15. A. Sette, B. Livingston, D. McKinney, E. Appella, J. Fikes, J. Sidney, M. Newman, and R. Chesnut. The development of multi-epitope vaccines: epitope identification, vaccine design and clinical evaluation. *Biologicals* 29(3-4): 271-276 (2001). https://doi.org/10.1006/biol.2001.0297
16. K. Srivastava, and V. Srivastava. Prediction of conformational and linear B-cell epitopes on envelop

protein of zika virus using immunoinformatics approach. *International Journal of Peptide Research and Therapeutics* 29(1): 17 (2023). https://doi.org/10.1007/s10989-022-10486-y

17. G. Anandhan, Y.B. Narkhede, M. Mohan, and P. Paramasivam. Immunoinformatics aided approach for predicting potent cytotoxic T cell epitopes of respiratory syncytial virus. *Journal of Biomolecular Structure and Dynamics* 41(21): 12093-12105 (2023). https://doi.org/10.1080/07391102.2023.2191136
18. Medha, P. Bhatt, Priyanka, M. Sharma, and S. Sharma. Prediction and identification of T cell epitopes of COVID-19 with balanced cytokine response for the development of peptide based vaccines. *In Silico Pharmacology* 9(1): 40 (2021). https://doi.org/10.1007/s40203-021-00098-7
19. S. Kumar, O. Nath, S. Govil, and A. Pathak. Computational 3D structure prediction, evaluation and analysis of pyruvate dehydrogenase an effective target for filarial infection by *Brugia pahangi* using homology modeling approach. *International Journal of Pharmaceutical Sciences and Drug Research* 6(2): 120-123 (2014). http://www.ijpsdr.com/pdf/vol6-issue2/7.pdf
20. S. Ahmad, F.M. Demneh, B. Rehman, T.N. Almanaa, N. Akhtar, H. Pazoki-Toroudi, A. Shojaeian, M. Ghatrehsamani, and S. Sanami. In silico design of a novel multi-epitope vaccine against HCV infection through immunoinformatics approaches. *International Journal of Biological Macromolecules* 267: 131517 (2024). https://doi.org/10.1016/j.ijbiomac.2024.131517
21. Z. Du, H. Su, W. Wang, L. Ye, H. Wei, Z. Peng, I. Anishchenko, D. Baker, and J. Yang. The trRosetta server for fast and accurate protein structure prediction. *Nature Protocols* 16(12): 5634-5651 (2021). https://doi.org/10.1038/s41596-021-00628-9
22. S.R. Mahapatra, J. Dey, T. Kaur, R. Sarangi, A.A. Bajoria, G.S. Kushwaha, N. Misra, and M. Suar. Immunoinformatics and molecular docking studies reveal a novel multi-epitope peptide vaccine against pneumonia infection. *Vaccine* 39(42): 6221-6237 (2021). https://doi.org/10.1016/j.vaccine.2021.09.025
23. D.B. Craig and A.A. Dombkowski. Disulfide by Design 2.0: a web-based tool for disulfide engineering in proteins. *BMC Bioinformatics* 14: 346(2013). https://doi.org/10.1186/1471-2105-14-346
24. S. Zaib, N. Rana, N. Hussain, H. Alrbyawi, A.A. Dera, I. Khan, M. Khalid, A. Khan, and A. Al-Harrasi. Designing multi-epitope monkeypox virus-specific vaccine using immunoinformatics approach. *Journal of Infection and Public Health* 16(1): 107-116 (2023). https://doi.org/10.1016/j.jiph.2022.11.033
25. S. Raju, D. Sahoo, and V.K. Bhari. In silico design of multi-epitope vaccine against Nipah virus using immunoinformatics approach. *Journal of Pure & Applied Microbiology* 15(1): 212-231(2021). https://doi.org/10.22207/JPAM.15.1.16
26. M.A. Soltan, M.A. Eldeen, N. Elbassiouny, I. Mohamed, D.A. El-Damasy, E. Fayad, O.A.A. Ali, N. Raafat, R.A. Eid, and A.A. Al-Karmalawy. Proteome-based approach defines candidates for designing a multitope vaccine against the Nipah virus. *International Journal of Molecular Sciences* 22(17): 9330 (2021). https://doi.org/10.3390/ijms22179330
27. M. Lu, Y. Yao, H. Liu, X. Zhang, X. Li, Y. Liu, Y. Peng, T. Chen, Y. Sun, and G. Gao. Vaccines based on the fusion protein consensus sequence protect Syrian hamsters from Nipah virus infection. *JCI Insight* 8(23): e175461 (2023). https://doi.org/10.1172/jci.insight.175461
28. D. Klingelhöfer, M. Braun, C.A. Naser, D. Brüggmann, and D.A. Groneberg. Emerging Nipah virus with pandemic potential and high mortality rates: is the scientific community learning from former pandemics? *Reviews in Medical Virology* 35(2): e70028 (2025). https://doi.org/10.1002/rmv.70028
29. P. Majee, N. Jain, and A. Kumar. Designing of a multi-epitope vaccine candidate against Nipah virus by in silico approach: a putative prophylactic solution for the deadly virus. *Journal of Biomolecular Structure and Dynamics* 39(4): 1461-80 (2021). https://doi.org/10.1080/07391102.2020.1734088
30. A.A. Mohammed, S.W. Shantier, M.I. Mustafa, H.K. Osman, H.E. Elmansi, I.A.A. Osman, R.A. Mohammed, F.A. Abdelrhman, M.E. Elnnewery, and E.M. Yousif. Epitope-based peptide vaccine against glycoprotein G of Nipah henipavirus using immunoinformatics approaches. *Journal of Immunology Research* 2020(1): 2567957 (2020). https://doi.org/10.1155/2020/2567957
31. M.A. Shabbir, A. Amin, A. Hasnain, A. Shakeel, and A. Gul. Immunoinformatics-driven design of a multi-epitope vaccine against nipah virus: a promising approach for global health protection. *Journal of Genetic Engineering and Biotechnology* 23(2): 100482 (2025). https://doi.org/10.1016/j.

jgeb.2025.100482

32. R. Santhoshkumar and A. Yusuf. In silico structural modeling and analysis of physicochemical properties of curcumin synthase (CURS1, CURS2, and CURS3) proteins of Curcuma longa. *Journal of Genetic Engineering and Biotechnology* 18(1): 24 (2020). https://doi.org/10.1186/s43141-020-00041-x
33. M.H.U. Masum, A.A. Mahdeen, L. Barua, R. Parvin, H.P. Heema, and J. Ferdous. Developing a chimeric multiepitope vaccine against Nipah virus (NiV) through immunoinformatics, molecular docking and dynamic simulation approaches. *Microbial Pathogenesis* 197: 107098 (2024). https://doi.org/10.1016/j.micpath.2024.107098
34. A. Alibakhshi, A.A. Bahrami, E. Mohammadi, S. Ahangarzadeh, and M. Mobasheri. In silico design of a new multi-epitope vaccine candidate against SARS-CoV-2. *Acta Virologica* 67: 12481 (2024). https://doi.org/10.3389/av.2023.12481
35. N. Rapin, O. Lund, M. Bernaschi, and F. Castiglione. Computational immunology meets bioinformatics: the use of prediction tools for molecular binding in the simulation of the immune system. *PLOS One* 5(4): e9862 (2010). https://doi.org/10.1371/journal.pone.0009862
36. R. Khandia, S. Singhal, U. Kumar, A. Ansari, R. Tiwari, K. Dhama, J. Das, A. Munjal, and R.K. Singh. Analysis of Nipah virus codon usage and adaptation to hosts. *Frontiers in Microbiology* 10: 886 (2019). https://doi.org/10.3389/fmicb.2019.00886
37. K. Li, S. Yan, N. Wang, W. He, H. Guan, C. He, Z. Wang, M. Lu, W. He, and R. Ye. Emergence and adaptive evolution of Nipah virus. *Transboundary and Emerging Diseases* 67(1): 121-32 (2020). https://doi.org/10.1111/tbed.13330
38. A. Kumar, G. Misra, S. Mohandas, and P.D. Yadav. Multi-epitope vaccine design using in silico analysis of glycoprotein and nucleocapsid of Nipah virus. *PLOS One* 19(5): e0300507 (2024). https://doi.org/10.1371/journal.pone.0300507
39. E.C. Banico, E.M.J.S. Sira, L.E. Fajardo, A.N.G. Dulay, N.M.O. Odchimar, A.M. Simbulan, and F.L. Orosco. Advancing one health vaccination: in silico design and evaluation of a multi-epitope subunit vaccine against Nipah virus for cross-species immunization using immunoinformatics and molecular modeling. *PLOS One* 19(9): e0310703 (2024). https://doi.org/10.1371/journal.pone.0310703
40. A. Albutti. An integrated multi-pronged reverse vaccinology and biophysical approaches for identification of potential vaccine candidates against Nipah virus. *Saudi Pharmaceutical Journal* 31(12): 101826 (2023). https://doi.org/10.1016/j.jsps.2023.101826
41. S. Sharma, P.D. Yadav, and S. Cherian. Comprehensive immunoinformatics and bioinformatics strategies for designing a multi-epitope-based vaccine targeting structural proteins of Nipah virus. *Frontiers in Immunology* 16: 1535322 (2025). https://doi.org/10.3389/fimmu.2025.1535322

Proceedings of the Pakistan Academy of Sciences: B Life and Environmental Sciences 62(4): S1 (2025)

ISSN (Print): 2518-4261; ISSN (Online): 2518-427X

Pakistan Academy of Sciences

Supplementary Data

Computational Design of a Multi-Epitope Vaccine Against Nipah Virus: Bridging Immunoinformatics and Immune Protection

Seerat Fatima†, Fatima Jawed†, and Shumaila Zulfiqar*

Department of Biotechnology, Kinnaird College for Women, Lahore, Pakistan

Table SI. Comparative Analysis of Multi-Epitope Vaccine Constructs for Nipah Virus.

Study	Target Protein(s)	No. of CTL Epitopes	No. of HTL Epitopes	TLR Docking	Immune Simulation	Codon Optimization	Strain Coverage	Expression System
Majee *et al.* (2021) [29]	Glycoprotein G	6	8	TLR3 only	Yes	No	NiV-M	Not addressed
Mohammed *et al*. (2020) [30]	Glycoprotein G	5	7	Not done	No	No	NiV-M	Not addressed
This study	Fusion protein (NiV-B/M conserved)	8	10	TLR3 & TLR4 (ClusPro + Vina)	Yes (C-ImmSim)	Yes (J-CAT, SnapGene)	NiV-B + NiV-M	Optimized for *E. coli*

Table S2. Comparison of Immunoinformatics-Based Vaccine Design Studies Against Nipah Virus.

Parameter	Our Study	Kumar *et al.* [38]	Banico *et al.* [39]	Albutti [40]	Shabbir *et al.* [31]
Target Protein(s)	Fusion (F) protein	Glycoprotein (G) and nucleocapsid (N) proteins	All NiV proteins: (structural & non-structural)	V protein	Nucleoprotein (N)
Number of HTL, CTL and B cell epitopes	8, 10 and 4	Not explicitly stated	10,8 and 10	9,1 and 3	8, 11 and 5
TLR Docking	TLR3 and TLR4	TLR3, TLR7, TLR8	TLR4-MD2	Not explicitly tested	Ephrin B2 receptor
Immune Simulation	Robust humoral (IgG, IgM) and cellular (IFN-γ, IL-2) responses, memory cells	Strong immune response, memory B/T-cell induction, high IFN-γ/IL-2 levels	Higher antibody titers	humoral/cellular response	IgG/IgM, memory B-cells
Population Coverage	89.3%, with >92% for South Asia	Not explicitly mentioned	Not explicitly mentioned	99.74%	88.3%
Expression System	E. coli (pET-29a(+))	pcDNA™3.1/V5-His-TOPO1	E. coli (pET28(a)+)	mRNA-based	E. coli (pET-28a(+)
Adjuvant Used	50S ribosomal protein L7/L12	Cholera toxin (CT) adjuvant	Resuscitation-promoting factor E (RpfE) (TLR4 agonist)	B-defensin (TLR4 agonist) + MITD sequence (enhances MHC presentation)	50S ribosomal L7/L12
Structural Validation	94.2% residues in favored regions (Ramachandran)	90.3% residues in favored regions (Ramachandran)	90.3% favored (Ramachandran)	Not explicitly mentioned	95.9% favored

* Corresponding Author: Shumaila Zulfiqar <shumaila.zulfiqar@kinnaird.edu.pk>
†These authors contributed equally and share first authorship

Instructions for Authors

Manuscript Writing

The manuscript may contain a Title, Abstract, Keywords, INTRODUCTION, MATERIALS AND METHODS, RESULTS, DISCUSSION (or RESULTS AND DISCUSSION), CONCLUSIONS, ETHICAL STATEMENT (if applicable), ACKNOWLEDGEMENTS, CONFLICT OF INTEREST and REFERENCES, *and any other information that the author(s) may consider necessary*.

Title (Bold and font size 16): The title should be expressive, concise, and informative to the entire readership of the journal. It may include common terms, to make it more identifiable when people search online. Please avoid the use of long pervasive terms and non-standard or obscure abbreviations, acronyms, or symbols.

Abstract (font size 10, max 250 words)**:** Must be self-explanatory**,** stating the rationale, objective(s), methodology, main results, and conclusions of the study. Abbreviations, if used, must be defined on the first mention in the Abstract as well as in the main text. Abstracts of review articles may have a variable format.

Keywords (font size 10)**:** Provide five to eight keywords consisting of words and phrases that are closely associated with the topic depicting the article.

INTRODUCTION (font size 11)**:** Provide a clear and concise statement of the problem, citing relevant recent literature, and objectives of the investigation. Cite references in the text by number in square brackets**,** the reference must be cited in a proper English sentence [1]. or "... as previously described [3, 6–8]". For a single author: Bednorz [2] investigated the environmental pollution ... When there are only two authors: Bednorz and Allan [2] investigated the environmental pollution ... and for three or more authors: Bednorz *et al.* [2] investigated the environmental pollution ..; and list them in the REFERENCES section, in the order of citation in the text.

MATERIALS AND METHODS (font size 11)**:** Provide an adequate account of the procedures or experimental details, including statistical tests (if any), concisely but sufficiently enough to replicate the study. Relevant references to methodology must be cited.

RESULTS (font size 11)**:** Be clear and concise with the help of appropriate Tables, Figures, and other illustrations. Data should not be repeated in Tables and Figures but must be supported with statistics. The data presented in Tables and Figures must be elaborated in the main text.

DISCUSSION (font size 11)**:** Provide interpretation of the RESULTS in the light of previous relevant studies, citing published references.

CONCLUSIONS (font size 11)**:** Briefly state the implication of your study findings, and carefully address the study questions. Confine your conclusions according to the objectives of your study and the aspects covered in the abstract. Discuss both positive and negative findings.

ETHICAL STATEMENT (font size 10)**:** The statement of ethical approval by an appropriate ethics committee or review board must be included in the manuscript (if applicable), as per the Journal's policy.

ACKNOWLEDGEMENTS: (font size 10)**:** In a brief statement, acknowledge the financial support and other assistance.

CONFLICT OF INTEREST (font size 10)**:** State if there is any conflict of interest.

REFERENCES (font size 10)**:** References must be listed in numerical order as listed in the main text. Only published (and accepted for publication) journal articles, books and book chapters, conference proceedings, online reports, a degree thesis, and materials available on the website qualify for REFERENCES. Give online link/doi for published articles.

Declaration: Provide a declaration that: (i) the results are original, (ii) the same material is neither published nor under consideration for publication elsewhere, (iii) approval of all authors has been obtained, and (iv) in case the article is accepted for publication, its copyright will be assigned to the *Pakistan Academy of Sciences*. Authors must obtain permission to reproduce, where needed, copyrighted material from other sources and ensure that no copyrights are infringed upon.

Manuscript Formatting

Manuscripts must be submitted in Microsoft Word (Latest Version .doc or .docx format); pdf files are not acceptable. Figures can be submitted separately in TIFF, GIF, JPEG, EPS, or PPT. Manuscripts, in *Times New Roman*, 1.15 spaced (but use single-space for Tables, long headings, and long captions of tables and figures). The Manuscript sections must be numbered, i.e., **1. INTRODUCTION, 2. MATERIALS AND METHODS,** and so on… (a) **Title** of the article **(**Capitalize the initial letter of each main word, font-size 16, **bold**), max 160 characters (no abbreviations or acronyms), depicting article's contents; (b) Author's complete name (font size 12, **bold**), and professional affiliation (i.e., each author's Department, Institution, Mailing address, and Email and Contact number, but no position titles) (font size 12); (c) Indicate the corresponding author with *; and (d) **Short running title**, max 50 characters (font size 10).

Headings and Subheadings (font size 11): All flush left

LEVEL-1: **ALL CAPITAL LETTERS; Bold**

Level-2: **Capitalize Each First Letter (**Except prepositions**); Bold**

Level-3: Capitalize the first letter only (Sentence case)***; Bold, Italic***

Level-4: *Run-in head*; *Italics*, *in the normal paragraph position. Capitalize the first letter only and end in a colon (i.e., **:**)*

A list of REFERENCES must be prepared as under:

a. Journal Articles *(Name of journals must be stated in full)*

1. J. Rashid, A. Ahsan, M. Xu, I. Savina, and F. Rehman. Synthesis of cerium oxide embedded perovskite type bismuth ferrite nanocomposites for sonophotocatalysis of aqueous micropollutant ibuprofen. *RSC Advances* 13(4): 2574-2586 (2023). DOI: 10.1039/d2ra07509a

2. A. Fayyaz, N. Ali, Z.A. Umar, H. Asghar, M. Waqas, R. Ahmed, R. Ali, and M.A. Baig. CF-LIBS based elemental analysis of Saussurea simpsoniana medicinal plant: a study on roots, seeds, and leaves. *Analytical Sciences* 40(3): 413-427 (2024). DOI: 10.1007/s44211-023-00480-9

3. W. Bialek and S. Setayeshgar. Cooperative sensitivity and noise in biochemical signaling. *Physical Review Letters* 100: 258-263 (2008). https://doi.org/10.1103/PhysRevLett.100.258101

b. Books

4. W.R. Luellen (Ed.). Fine-Tuning Your Writing. *Wise Owl Publishing Company, Madison, WI, USA* (2001).

5. U. Alon and D.N. Wegner (Eds.). An Introduction to Systems Biology: Design Principles of Biological Circuits. *Chapman & Hall/CRC, Boca Raton, FL, USA* (2006).

c. Book Chapters

6. M.S. Sarnthein, J.E. Smolen, and J.D. Stanford. Basal sauropodomorpha: historical and recent phylogenetic developments. In: The Northern North Atlantic: A Changing Environment. P.R. Schafer and W. Schluter (Eds.). *Springer, Berlin, Germany* pp. 365-410 (2000).

7. S. Brown and L.A. Boxer. Functions of Europhiles. In: Hematology, (4^{th} ed). W.J. Williams, E. Butler, and M.A. Litchman (Eds.). *McGraw Hill, New York, USA* pp. 103-110 (1991).

d. Reports

8. M.D. Sobsey and F.K. Pfaender. Evaluation of the H_2S method for Detection of Fecal Contamination of Drinking Water. Report No.-WHO/SDE/WSH/02.08. *Water Sanitation and Health Programme, WHO, Geneva, Switzerland* (2002).

e. Online References

These should specify the full URL for reference, please check again to confirm that the work you are citing is still accessible:

9. UNESCO. Global Education Monitoring Report 2024/5: Leadership in education–Lead for learning. *United Nations Educational, Scientific and Cultural Organization, Paris, France* (2024). https://digitallibrary.un.org/record/4066661?ln=en&v=pdf

10. L.M. Highland and P. Bobrowsky. The landslide handbook–A guide to understanding landslides. Circular 1325. *US Geological Survey, Reston, Virginia* (2008).

    https://pubs.usgs.gov/circ/1325/pdf/C1325_508.pdf

f. Conference Proceedings

11. M. Khalid, A.B. Majid, F. Mansour, and C.R. Smith. Word Representations with Recursive Neural Networks for Morphology. *27^{th} European Conference on Signal Processing, (2^{nd} - 6^{th} September 2021), Madrid, Spain* (2021).

g. A Degree Thesis

12. M. Afzal. Investigation of structural and magnetic properties of nanometallic Fe-Mn Alloys. Ph.D. Thesis. *Quaid-i-Azam University, Islamabad, Pakistan* (2023).

Tables: Insert all tables as editable text, not as images. Number tables consecutively following their appearance in the text. A concise but self-explanatory heading must be given. Tables should be numbered according to the order of citation (like **Table 1.**, **Table 2.** (font size 10)). *Do not* abbreviate the word "Table" to "Tab.". Round off data to the nearest three significant digits. Provide essential explanatory footnotes, with superscript letters or symbols keyed to the data. Do not use vertical or horizontal lines, except for separating column heads from the data and at the end of the Table.

Figures: In the main text write Figure, not Fig. Figures may be printed in two sizes: column width of 8.0 cm or page width of 16.5 cm; In the Figure caption, number them as **Fig. 1.**, **Fig. 2.** Captions to Figures must be concise but self-explanatory (font size 10). Laser-printed line drawings are acceptable. Do not use lettering smaller than 9 points or unnecessarily large. Photographs must be

of high quality. A scale bar should be provided on all photomicrographs. All Figures should have sufficiently high resolution (minimum 300 dpi) to enhance the readability. Figures as separate files in JPG or TIFF format may be provided.

SUBMISSION CHECKLIST

The following list will be useful during the final checking of an article before submission to the journal.

1. Manuscript in MS Word format
2. Cover Letter
3. Novelty Statement
4. Copyright Form
5. Figures in JPG or TIFF format

In case of any difficulty while submitting your manuscript, please get in touch with:

Editor-in-Chief

Pakistan Academy of Sciences
3-Constitution Avenue,
G-5/2, Islamabad, Pakistan
Email: editor@paspk.org
Tel: +92-51-920 7140
Websites: http://www.paspk.org/proceedings/; http://ppaspk.org/

PROCEEDINGS OF THE
PAKISTAN ACADEMY OF SCIENCES: PART B
Life and Environmental Sciences

CONTENTS

Volume 62, No. 4, December 2025 **Page**

PAKISTAN ACADEMY OF SCIENCES, ISLAMABAD, PAKISTAN
HEC Recognized, Scopus Indexed